공학박사학위논문

Development of an assessment technique for subsidence risk in mining areas using strength reduction method

강도감소법을 이용한 광산지역 지반침하 위험지수 산정기법 개발

2016년 8월

서울대학교 대학원

에너지시스템공학부

전 병 규

Development of an assessment technique for subsidence risk in mining areas using strength reduction method

강도감소법을 이용한 광산지역 지반침하 위험지수 산정기법 개발

지도교수 전 석 원

이 논문을 공학박사학위논문으로 제출함
2016년 6월

서울대학교 대학원
에너지시스템공학부
전 병 규

전병규의 박사학위논문을 인준함
2016년 7월

위 원 장 송 재 준 (인)

부 위 원 장 전 석 원 (인)

위 원 송 원 경 (인)

위 원 최 성 웅 (인)

위 원 민 기 복 (인)

ABSTRACT

Development of an assessment technique for subsidence risk in mining areas using strength reduction method

Byungkyu Jeon

Department of Energy Systems Engineering

The Graduate School

Seoul National University

Mine development leads to inevitable environmental consequences resulting in so called ‘mine hazards’, which occur extensively over a long period of time across a large area. They can cause serious social and economic troubles both during operation and after closing of a mine. In particular, ground subsidence needs to be carefully managed because it is difficult to predict the location, scale, and time of its occurrence. Mine subsidence prediction methods have been developed by many researchers for the past several decades. Those methods usually focus on predicting the ground movement over mined cavities having well-defined geometry. However, more interests are taken in ‘risk assessment of mine subsidence’ and ‘potential locations of high risk of subsidence’ rather than the ground movement itself in most mine development and reclamation projects. This is

because of that the need for monitoring and reclamation of ground subsidence is highly dependent on the surface utility and other circumstances. The overall assessment of mine subsidence risk is of great importance in most cases.

The aim of this study is to develop a risk assessment method of ground subsidence in mining areas considering the effect of mined cavities and rock mass conditions. The strength reduction technique which is often used in the slope stability analysis was employed to calculate the factor of safety on ground subsidence in mining areas. Then a relationship between the risk of subsidence and the factor of safety was obtained. FLAC2D was used to implement the strength reduction technique considering five variables, i.e. the depth, width, height, angle of cavity and rock mass condition, in the analysis. A numerical prediction model for subsidence was derived from regression analysis. In addition, new techniques were suggested to estimate the influence area of subsidence at the ground surface and to evaluate the interaction among multiple cavities. Finally, in order to validate the developed approach in this study, risk assessment analysis was performed on actual mine sites. Most subsidence traces surveyed in the mining sites well matched the subsidence risk contour map which was obtained in the prediction model analysis.

Keywords : Mining subsidence, Risk assessment, Numerical simulation, FLAC2D, Strength reduction method, Regression analysis.

Student Number : 2007-30285

CONTENTS

LIST OF TABLES

LIST OF FIGURES

1. Introduction

1.1 Motivation

Mining development leads to inevitable mine-related damages, such as ground subsidence, soil pollution, and acid mine drainage. These damages occur extensively over a long period and across a large area, and they can cause serious social and economic problems both during operation and after closing. In particular, ground subsidence needs to be carefully managed because it is difficult to predict the location, scale, and time of its occurrence.

In Korea, the mining right holder or mining lessee has a responsibility to prevent and restore the ground subsidence in their mining areas. This duty is specified by legislation governing the mining industry: the *Mining Industry Act* (Act No. 11690, 2013) and the *Mining Damage Prevention and Restoration Act* (Act No. 13080, 2015).

However, it is hard to expect that the people responsible for preventing mining damage would take proper measures for prevention and restoration of ground subsidence due to the dwindling size of companies in the domestic mining industry. Figure 1.1 shows the number of metal and non-metal operating mines according to the annual sales. About 55 percent of the mines have an annual turnover of less than one hundred million won.

Furthermore, the management of subsidence is often neglected after the closing of mines, even though the occurrence of subsidence might increase. Table 1.1 presents the status of mines in Korea. About 98.5 percent of coal

mines, 96.4 percent of metal mines, and 77.7 percent of non-metal mines have been closed. As a result, numerous mines exist all over the country without any subsequent management, which exacerbates the risk of subsidence.

Table 1.1 Present status of mines in Korea (MIRECO, 2014).

(Unit: EA)

Mine type / State	Coal mine	Metal mine	Non-metal mine	Total
Operating mine	6	56	531	593
Pause mine	0	21	101	122
Abandoned mine	394	2,089	2,198	4,681
Total	400	2,166	2,830	5,396

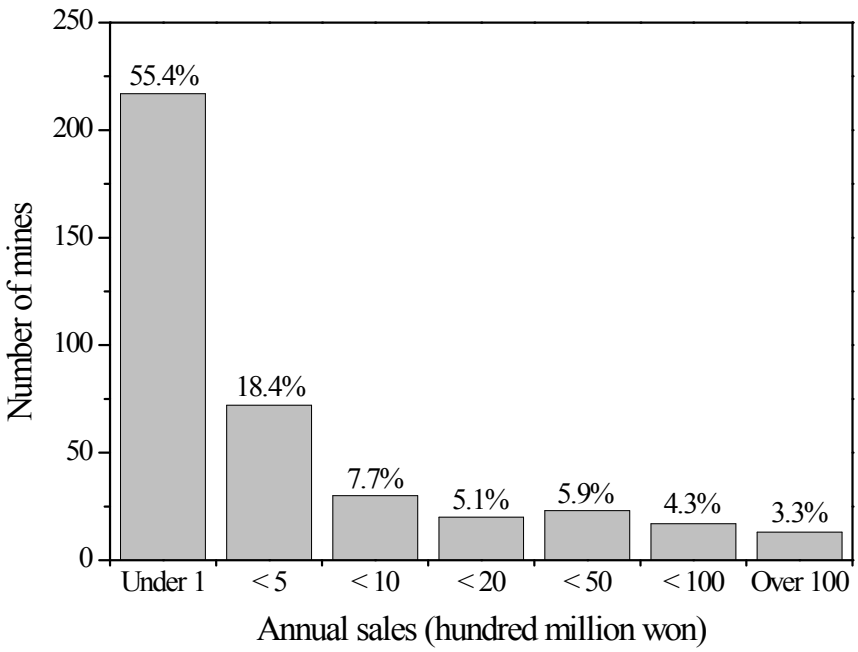

Figure 1.1 Number of metal and non-metal operating mines in Korea according to the annual sales (KOSIS, 2014).

In order to promote mine damage prevention projects and minimize mine damage, the government established the Mine Reclamation Corporation (MIRECO) in 2005, which was formerly the Coal Industry Rationalization Corporation (CIRC). The MIRECO has the goal of completing the mine damage prevention projects for abandoned mines in 20 years (Ministry of Environment, 2009; Jeon and Jeon, 2014). The MIRECO invested 805.6 billion won in reclamation projects in the period from 1995 to 2014, as shown in Table 1.2. The subsidence prevention projects account for about 10 percent of the total budget.

Unfortunately, it is not economically feasible to carry out a subsidence prevention project in every abandoned mine. As shown in Table 1.2, the average cost of the project is about 200 million won per site. At present, the MIRECO selects the sites for the subsidence prevention project each year in accordance with a priority list which is based on the presence or absence of the major facilities surrounding the mines, such as roads, railroads, and settlements. However, if a subsidence occurs, which can cause severe damage to the facilities, the site will be managed immediately, although that is low on the priority list.

For economic efficiency, therefore, it is necessary to determine subsidence risk levels of abandoned mines and to execute the ground stabilization project preferentially according to the risk level. In order to prioritize the mines by risk, appropriate methods for the prediction and assessment of subsidence risk in mine areas are required.

Table 1.2 Budget execution for mine damage prevention projects performed by the MIRECO (MIRECO, 2007; 2008a; 2009; 2010; 2011; 2012a; 2013; 2014).

(Unit: Million Won)

Year	Subsidence prevention†	Water treatment	Forest restoration	Others‡	Total
1995	1,121(5)	7	3,397	2,295	6,820
1996	5,018(7)	323	4,643	2,900	12,884
1997	803(4)	3,302	6,538	1,892	12,535
1998	3,750(1)	3,116	6,149	1,456	14,471
1999	3,359(3)	4,526	5,828	1,604	15,317
2000	3,815(7)	1,243	3,523	1,325	9,906
2001	4,544(8)	1,796	3,884	2,130	12,354
2002	3,252(7)	1,188	2,644	2,845	9,929
2003	1,205(8)	4,167	2,188	3,596	11,156
2004	2,989(13)	4,744	4,685	3,348	15,766
2005	5,860(20)	5,518	6,405	5,012	22,795
2006	4,255(16)	6,228	4,834	6,640	21,957
2007	3,187(25)	10,853	7,533	58,427	80,000
2008	5,686(37)	8,534	9,780	70,523	94,523
2009	3,685(35)	4,009	13,250	53,130	74,074
2010	12,478(41)	3,252	3,587	59,709	79,026
2011	8,646(41)	9,451	1,995	61,912	82,004
2012	6,797(46)	13,941	3,701	57,561	82,000
2013	5,029(55)	15,041	2,311	65,619	88,000
2014	2,769(40)	10,997	1,553	66,681	82,000
Total	83,993(403)	106,008	93,594	521,965	805,560

†The number of project sites is indicated in the bracket.

‡Others include projects of waste debris release prevention, tailing release prevention, soil improvement, dust prevention, abandoned facility withdrawal, aftercare management, and technology development.

Mine subsidence prediction methods have been developed by many researchers for the past several decades, and they can be roughly divided into four categories: graphical method, profile function method, influence function method, and numerical method (Whittaker and Reddish, 1989; Bahuguna et al., 1991; Brady and Brown, 2004; Harrison, 2011).

Graphical method is based on the data gathered from a large number of actual field measurements. This method category consists of a series of tables, charts, and graphs from which a prediction of subsidence can be made. The best-known method is that developed by the National Coal Board (NCB) for use in the coalfields of the United Kingdom.

Profile function method predicts the complete subsidence profiles at the ground surface by using mathematical formulae that can be defined according to the mining geometry and site conditions. There are various types of such equations suggested by many studies (Whittaker and Reddish, 1989; Diez and Alvarez, 2000; Torano et al., 2000; Asadi et al., 2004). Such approaches are relatively easy to use because the equation can determine the subsidence profiles directly.

Influence function method is used to estimate the total subsidence and strain at any point of the surface by calculating the amount of influence exerted by infinitesimal elements of an extraction area. In addition, the principle of superposition is used to calculate the overall ground movement. This approach has an advantage of being applicable to complex mine geometry and various types of mining situations (Sutherland and Munson, 1984; Ren et al., 1989; Lin et al., 1992; Yi and Cheng, 2009).

Numerical method is based on the principles of mechanics and the

assumptions of constitutive models to be applicable to the overlying strata (i.e., surrounding rock mass). Several numerical techniques are useful for predicting the induced displacements and stresses in the analysis domain, such as the Finite Element Method (Yao et al., 1993, Ren and Li, 2008), Discrete Element Method (Choi and Kim, 2003; Keilich et al., 2006; Lee and Choi, 2011), Finite Difference Method (Lloyd et al., 1997; Alejano et al., 1999; Han et al., 2007; Shahriar et al., 2009; Xu et al., 2013), and hybrid code (Caudron et al., 2006; Vyazmensky et al., 2007 and 2010).

The widely used methods mentioned above usually focus on predicting the vertical displacement and strain at the ground surface. Additionally, the quantitative values estimated from these methods are used for evaluating the stability of surface structures, which means that the prediction and estimation of ground movement mainly follow such methods. For the subsidence prevention project, however, an assessment of the potential risk of subsidence occurrence is preferred, rather than an evaluation of ground movement, because of the limited budget. In other words, the project should make a decision over which areas to prioritize.

In recent years, several studies have been conducted to assess the subsidence risk in mining areas. Bekendam (2004) suggested a method for the assessment of stability and subsidence over shallow abandoned room-and-pillar limestone mines by using the safety factor, which is the ratio of the pillar strength and the mean vertical pillar stress. Kim et al. (2006) selected nine major factors that can cause ground subsidence (depth of drift, topography, slope gradient, groundwater level, permeability, RMR, lineaments, geology, and land use) and assessed ground subsidence hazard

by using the Geographic Information System (GIS). Malinowska and Hejmanowski (2010) carried out a risk assessment of building damage on mining terrains with an influence function method that calculates the deformation of the ground and categorized the mining areas into five groups according to the magnitude of expected deformations. Jung et al. (2014) developed a simple and quantitative method for subsidence susceptibility estimation, which uses only two pieces of information (the depth of gangway and topographic features).

Although these approaches have the advantage of being able to evaluate the relative risk of subsidence in mining areas, the effect of the features of cavity and rock mass conditions have not been considered. Fundamentally, the subsidence related with the underground mining arises from the mined cavities, whose shape and size could affect the subsidence profiles on the ground surface. In addition, the rock mass conditions influence the growth of subsidence because the initial failure in the vicinity of a cavity propagates through the surrounding rock mass and reaches the surface, which may be considered a general development process of the mining subsidence. Consequently, the assessment of subsidence risk should deal with the features of mined cavity and rock mass conditions as the primary factors, even though there are many affecting factors such as elapsed time, mining method, and surface topography.

1.2 Research objectives

As discussed in the previous section, the selection and application of suitable methods for evaluation of subsidence risk are essential in the subsidence prevention project. The main purpose of this thesis is to develop an assessment technique for prediction and evaluation of subsidence risk in mining areas. This approach is based on numerical simulation results that considered characteristics of the surrounding rock mass and mined cavity.

The major objectives of this study include:

(1) *To execute numerical simulation to identify the effect of selected factors on subsidence.* Ground profile of rock mass, and shape and size of mined cavity, were selected as the main factors. In addition, the strength reduction method was applied in the simulation using commercial FDM software, FLAC2D.

(2) *To analyze the simulation result and to derive an assessment technique.* Statistical analyses, such as correlation and regression analyses, were carried out to make an equation that represents the simulation result and evaluates the subsidence risk. Furthermore, the limit angle, also called the angle of draw, was analyzed to identify the influencing area on the ground surface. The effect of multi-cavity was also discussed, which is essential for applying the technique on the complicated orebody mines.

(3) *To verify the developed technique by applying it to actual cases.* The technique was applied to three actual mine sites by comparing the subsidence risk areas calculated by the proposed technique with field data of subsidence traces.

1.3 Outline of dissertation

This dissertation consists of six chapters. Chapter 2 introduces the subsidence prediction methods that are used widely. In Chapter 3, the methodology and assumptions of numerical simulation are explained, and the simulation results are given. Chapter 4 deals with the statistical analyses and the development procedure of the subsidence risk assessment technique. Chapter 5 presents the methodology and applications of the developed technique. Finally, Chapter 6 summarizes the major findings obtained in this study and the limitations of the proposed technique.

2. Subsidence prediction methods

2.1 Introduction

Whittaker and Reddish (1989) defined “subsidence” as a surface point sinking to a lower level, and it can include a structure settling into the ground or the ground itself lowering and carrying the structure with it, or even a surface layer collapsing into an underground cavity. Brady and Brown (2004) defined “subsidence” as the lowering of the ground surface following underground extraction of an orebody, produced by almost all types of underground mining. Harrison (2011) defined the “phenomenon of subsidence” as an inevitable consequence of the underground extraction of any resource, which might be solid, liquid, or gas. Moreover, he defined “subsidence” as encompassing the complete range of surface effects associated with the mining of minerals.

Eventually, the mining subsidence involves a movement of the ground surface caused by the mining operations. The creation of any subsurface opening perturbs the stress state in the surrounding rock mass; then ground movement, such as deformation and displacement, is produced by the perturbation. The stress change can cause the collapse of the rock around the mined void; then, the ground movement associated with the collapse propagates to the surface. In general, the “subsidence” not only refers to vertical displacement on the surface but also horizontal movement induced by the lateral shift of ground.

According to Brady and Brown (2004), subsidence can be divided into

two types: continuous and discontinuous. Continuous subsidence, also known as trough type, involves the formation of a smooth surface subsidence profile that is free of step changes. This type of subsidence is usually associated with the extraction of thin, horizontal or flat-dipping orebodies overlain by weak, non-brittle sedimentary strata. On the other hand, discontinuous subsidence is characterized by large surface displacements over a limited surface area, and the formation of steps or discontinuities in the surface profile. This type of subsidence may develop suddenly or progressively. Figure 2.1 illustrates the forms of continuous and discontinuous subsidence.

Discontinuous subsidence mainly involves the geological conditions of surrounding rock mass, such as weak overburden materials, regularly jointed rock mass, and structural features such as a dyke or a fault. Due to the wide range of circumstances leading to discontinuous subsidence, there is no generic method for predicting or analyzing the phenomenon. Instead, the principles of geomechanics must be applied on a case-by-case basis (Harrison, 2011). For example, the limiting equilibrium analysis may be useful in estimating ultimate collapse conditions when a case of discontinuous subsidence is dominated by a clearly defined discontinuity of rock.

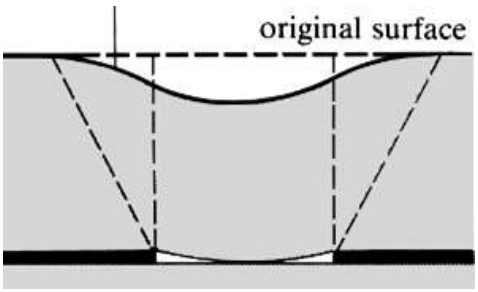

(a) Continuous subsidence

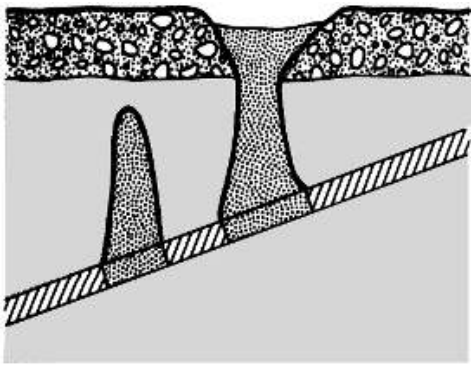

(b) Crown hole

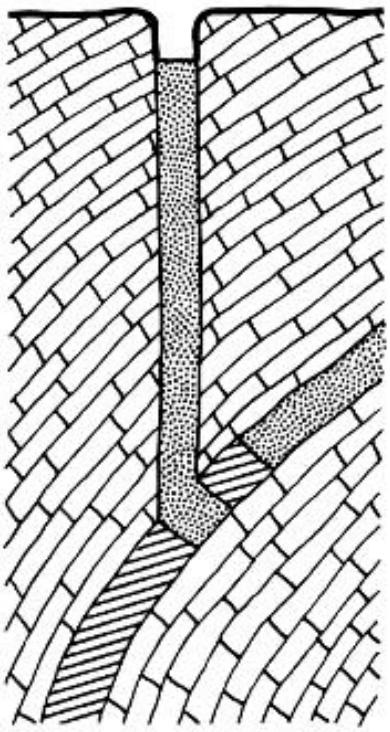

(c) Chimney caving

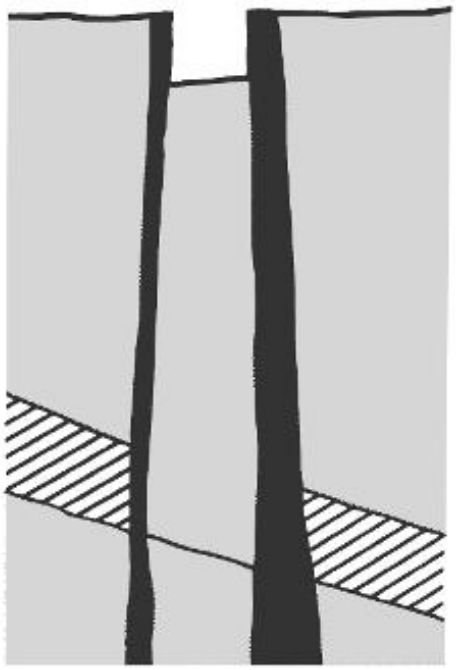

(d) Plug subsidence

Figure 2.1 Types of continuous and discontinuous subsidence: (a) Trough subsidence over a longwall extraction, (b) Crown hole, (c) Chimney caving, and (d) Plug subsidence (after Brady and Brown, 2004).

On the contrary, subsidence profiles on the surface related with continuous subsidence can be estimated from several subsidence prediction methods: graphical method, profile function method, influence function method, and numerical method. Because the continuous subsidence results in a smooth and continuous profile, some parameters for defining the profile curve can be used commonly in the prediction methods. Figure 2.2 shows a typical subsidence profile generated from an extraction of flat orebody and its defining parameters.

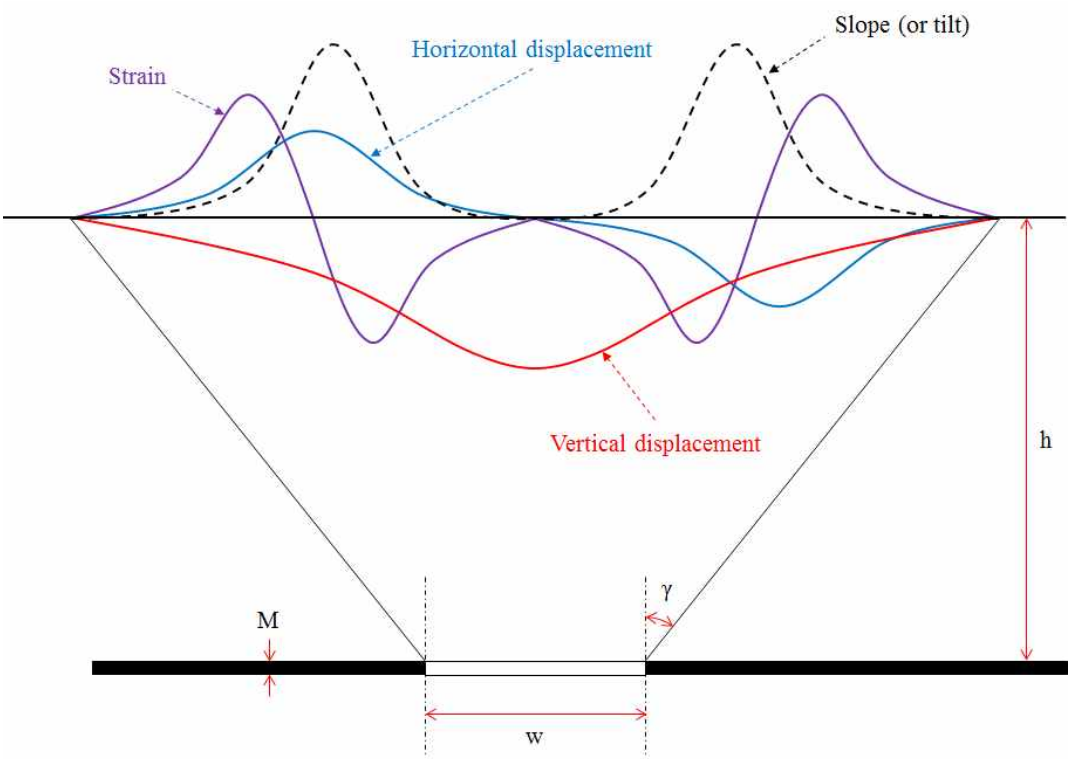

Figure 2.2 Terminology and typical curves of subsidence profile: M is extraction height, w is panel width, h is mining depth, and γ is angle of draw (also referred to limit angle) (after NCB, 1975).

Table 2.1 Factors affecting mine subsidence (after Harrison, 2011).

Factor	Description
Extraction thickness	The thicker the material extracted, the larger the amount of possible surface subsidence.
Mining depth	The magnitude and time to onset of subsidence are dependent on mining depth.
Inclination of extraction horizon	The subsidence profile is shifted in a downdip direction with both the limit angle and the horizontal strains increased downdip and reduced updip.
Degree of extraction	Lower extraction ratios tend to both reduce and delay the onset of subsidence.
Mined area	The critical width of a mined void must be extracted in all direction if maximum subsidence is to develop.
Method of working	The amount of subsidence is controlled by the degree of caving induced by the mining method together with the amount of support.
Extraction rate	Surface subsidence follows the face as it progresses, and so to minimize the effect of strain and tilt on surface structures.
Competence of surrounding materials	The mechanical behavior of the rock adjacent to the mined void directly affects the initiation of subsidence.
In-situ stress state	High horizontal stresses may foster formation of an arch in the material overlying a mined void, thereby attenuating subsidence.
Geological discontinuities	The existence of discontinuities may increase and localize subsidence potential so strongly that the effects fo the other parameters can be discounted.
Near-surface geology and surface topography	The nature of any near-surface and unconsolidated rocks affects subsidence development.
Hydrogeology	Deformation of the strata around mined areas may alter hydraulic gradients, and rocks may be weakened by changes in saturation.
Elapsed time	Subsidence does not occur instantaneously but over a period of time, especially in room and pillar mine.

In general, there are four parameters used to define the extent of the surface movements: displacement, tilt, curvature, and strain. The displacement is divided into two components: vertical and horizontal displacement. The tilt and curvature are calculated from the first and second derivatives of the subsidence profile curve, respectively. The strain is determined by calculating the horizontal change in length of a section of a subsidence profile. These parameters are required to assess the possible damage to surface structures.

The magnitude and areal extent of subsidence are affected by many geological and mining parameters (Harrison, 2011). Table 2.1 lists the main factors affecting the mining subsidence. Consequently, the various subsidence prediction methods utilize these factors to estimate the key subsidence parameters. The main concepts and features of the various methods are explained in the following section.

2.2 Methods for prediction of ground movement

The primary purpose of predicting the ground movement is to assess the stability of structures on the mining terrains directly. Because the various structures, such as buildings, roads, and railways, have some maximum permissible limit to maintain their safety, the ground movement, such as vertical and horizontal displacement, should be estimated to prevent any destruction of the facilities.

2.2.1 Graphical method

Graphical method is based on observed data and uses normalized

parameters to develop charts from which a prediction of subsidence can be made. The most comprehensive and widely used graphical method is the empirical method developed by the National Coal Board (NCB) in the United Kingdom (National Coal Board, 1975). This method is based on observations at around 200 sites in several coal fields. The subsidence data were mainly collected during the period from 1950 to 1965 and were rationalized by the NCB. This method has been employed extensively throughout UK coalfields and has served as an excellent means of assessing the anticipated response of the surface to underground coal mining operations (Whittaker and Reddish, 1989).

This method consists of some charts and nomograms for predicting the maximum subsidence and subsidence profile. Three mining parameters, seam extraction height (M), extraction width (W), and extraction depth (h) were taken into account in this method. Figure 2.3 shows the relationship of subsidence to extraction width and depth, and this nomogram is used to determine the maximum subsidence (S). Then, the subsidence profile can be drawn from data obtained from Figure 2.4.

Because most of the observations used in this method were gathered from UK coalfields, the charts and nomograms are only available for similar circumstances. However, many of the concepts developed by the NCB have been found to be applicable elsewhere and have been used in other locally developed empirical methods (Brady and Brown, 2004).

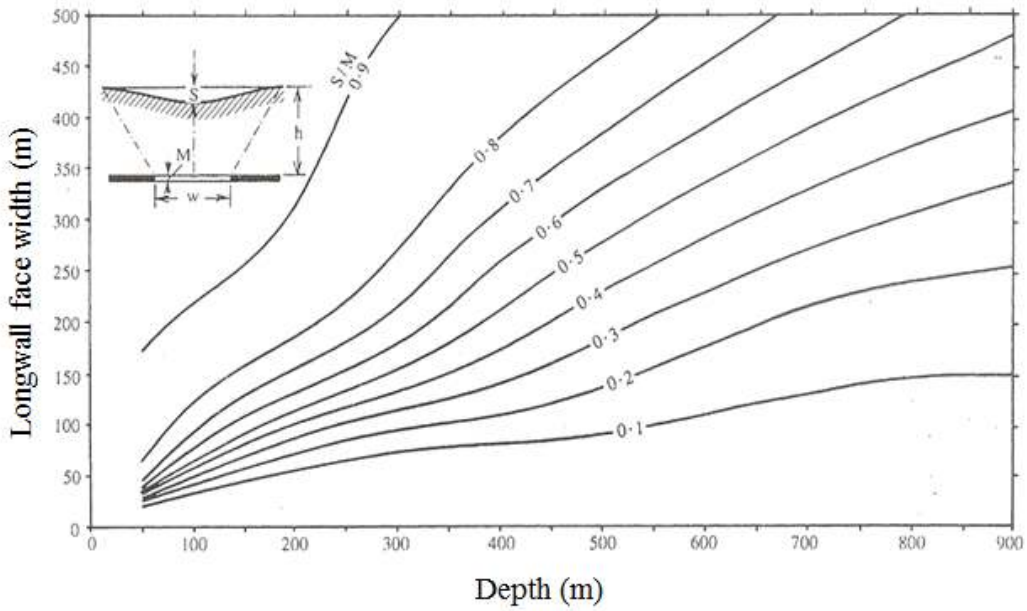

Figure 2.3 Relationship of subsidence to extraction width and depth (after NCB, 1975).

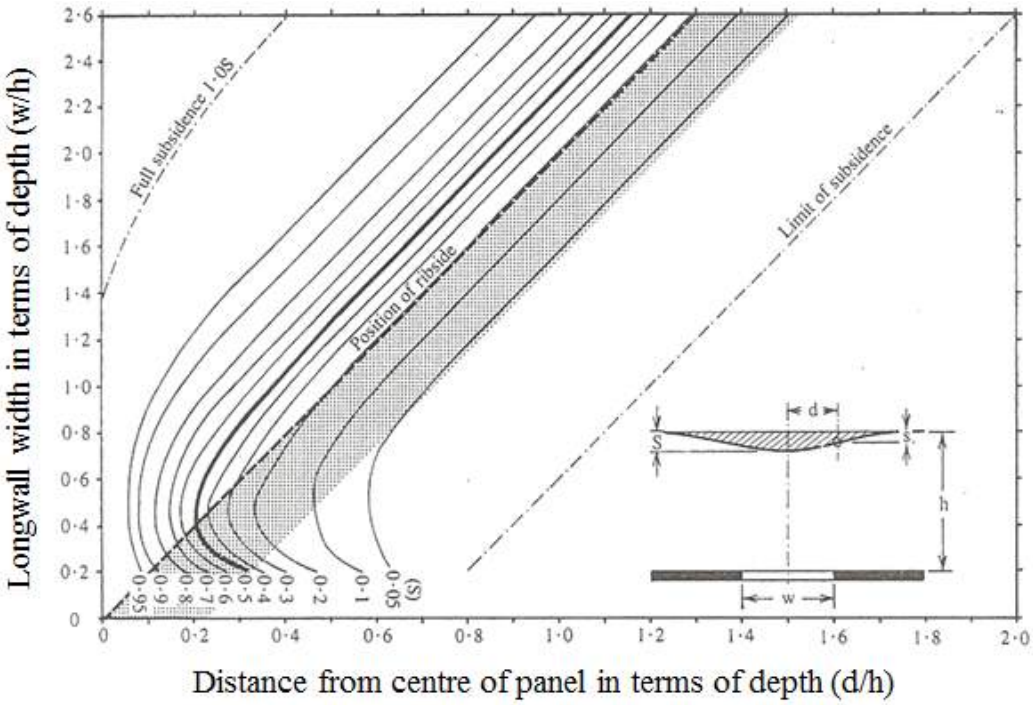

Figure 2.4 Design graph for prediction of subsidence profiles (after NCB, 1975).

2.2.2 Profile function method

Profile function method predicts the subsidence profiles by using some equations that are defined from the mining geometry and site conditions. This method type is relatively easy to use and apply to new situations because the equations can be calibrated by matching the observed data. For this reason, the profile function method is widely used for prediction of the ground movement.

The subsidence profile is expressed as equation (2.1).

$$s = f(S_{\max}, R, x) \tag{2.1}$$

where $S_{\max}$ is the maximum value of subsidence induced by extraction; R is the critical radius of extraction which might be affected by the site conditions; and x is the distance from the origin which can be used as the transition point or the center of extracted void.

In general, the maximum value of subsidence is calculated by multiplying the extracted seam height (M) by a subsidence factor (a). Figure 2.5 shows the terminology and definition of parameters used in the profile function method, and some of commonly used profile functions are listed in Table 2.2. These profile functions, developed decades ago, have been successfully applied in horizontal or moderately inclined coal seams.

Table 2.2 Commonly used profile functions in horizontal coal seam (after Whittaker and Reddish, 1989).

Transition point based functions	Face center based functions
Hyperbolic function $s = (S/2)\left\{1 - \tanh\left(\frac{2x}{R}\right)\right\}$	Polish profile function $s = S\exp\left(-\frac{S}{R^2 c}x^2\right)$
Exponential function $s = S\exp\left(-0.5\left(\frac{x+R}{R}\right)^2\right)$	Hungarian profile function $s = S\exp\left(-\frac{x^2}{2d^2}\right)$
Donets trigonometrical function $s = (S/2)\left\{1 - \frac{x}{R} - \frac{1}{\pi}\sin\left(\frac{\pi x}{R}\right)\right\}$	Niederhofer's method $s = S\left\{1 - \left(\frac{x}{p}\right)^2\right\}^2$
Trigonometrical function $s = S\sin^2\left(\frac{\pi}{4}\left(\frac{x}{R} - 1\right)\right)$	Indian profile function $s = S\exp\left(-\frac{nx^2}{p^2 - x^2}\right)$

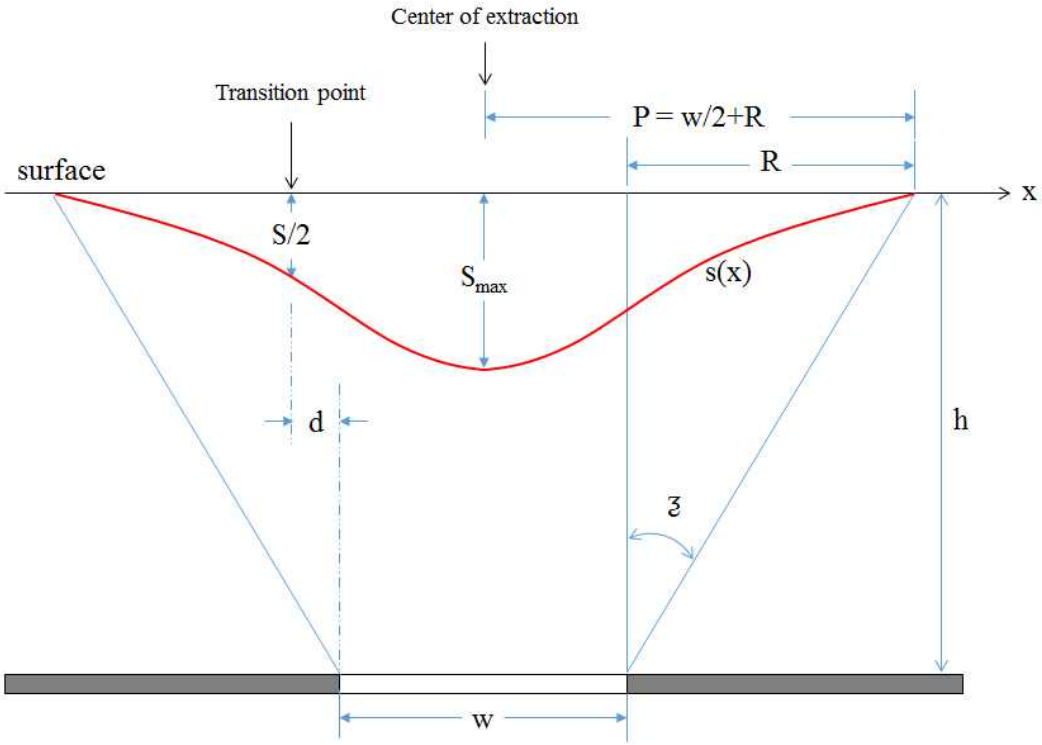

Figure 2.5 Basic subsidence profile function s(x) in horizontal coal seam (after Whittaker and Reddish, 1989).

In recent years, several studies have been carried out to develop profile functions that can be applied to steeply inclined coal seams. Diez and Alvarez (2000) proposed a new profile function by using the exponential function and the principle of superposition as given by equation (2.2). In addition, Torano et al. (2000) applied this profile function to estimate the strain at the surface.

$$z(x) = D_1 e^{-\left(\frac{x - x_{01}}{B_1}\right)^2} + D_2 e^{-\left(\frac{x - x_{02}}{B_2}\right)^2} + D_3 e^{-\left(\frac{x - x_{03}}{B_3}\right)^2} \qquad (2.2)$$

where x is horizontal distance from a point to the origin of coordinates, and $z(x)$ is the vertical movement at that point. $x_{0\,i}$, D_i, and B_i are the coefficients.

Asadi et al. (2004) proposed a new profile function to predict the surface subsidence over longwall panel in the inclined seams as given by equation (2.3).

$$S(x) = S_{\max}\left[c\exp\left(-f\left(\frac{-x}{R_1}\right)^g\right) + d\exp\left(-p\left(\frac{x}{R_2}\right)^q\right)\right] \qquad (2.3)$$

where $S(x)$ is the subsidence; x is the distance from the point of maximum subsidence of movement trough; and f, g, p, and q are the constants obtained experimentally.

In addition, this profile function has been verified by application to field data in Parvada (Asadi et al., 2004) and Negin (Asadi et al., 2005) coal mines in Iran.

Profile function method can predict the subsidence profile by using only an equation, even if very little measured data is available for matching the profile curve. However, the profile function may not match exactly the shape of that given by measured data and, consequently, introduce an error.

2.2.3 Influence function method

Basically, influence function method is based on the principle of superposition and an assumption that an infinitesimal part of extraction area influences on the surface within a conical-shaped area. As shown in Figure 2.6, a small element of extraction affects movement of the surface, and the effect is expressed as a function of distance from the center of element. Equation (2.4) is the standard form of an influence function.

$$K_Z = f(r) \tag{2.4}$$

where K_Z is the magnitude of influence of dA on P, and r is horizontal distance between position of P and the infinitesimal element dA.

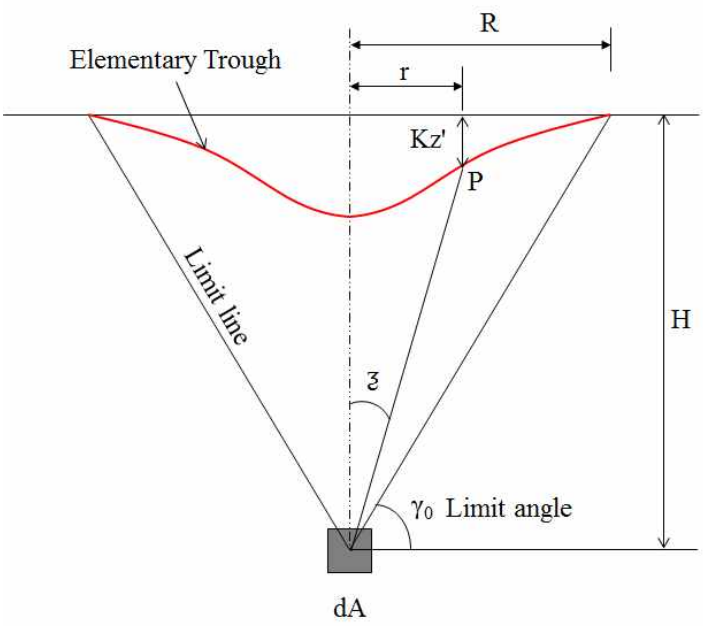

(a) extraction based

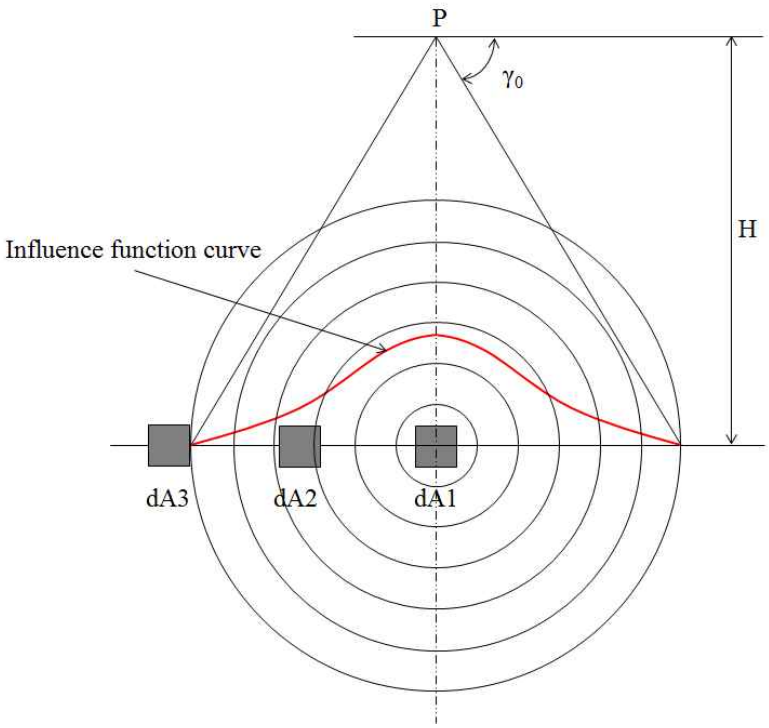

(b) surface point based

Figure 2.6 Basic concept of influence function method (after Ren et. al., 1987).

In addition, the extraction of an element, A, induces a ground movement in a surface point, and the total subsidence is calculated by equation (2.5) in accordance with the superposition. If the area of influence is assumed to be circular, full subsidence is expressed by equation (2.6).

$$s = \iint_A K_Z(r)dA \tag{2.5}$$

$$S = 2\pi \int_0^R rK_Z(r)dr \tag{2.6}$$

According to Whittaker and Reddish (1989), a major advantage of influence functions is their ability to predict subsidence movements at any point above extractions of any practical shape. The major drawback is that they are considerably more difficult to apply than are profile functions, and much more difficult to check and calibrate.

To simplify the application of influence functions, a circular-shaped net of influence area, which consists of sufficient rings and sectors, was used at each surface point. In addition, the influence function methods have been successfully applied to various conditions, such as for multi-seam extraction (Sutherland and Munson, 1984; Ren et al., 2014), for calculation of principal strains (Ren et al., 2010), and for inclined seam extraction (Ren et al., 1989; Lin et al., 1992; Yi and Cheng, 2009).

2.2.4 Numerical method

Numerical method is based on the principles of mechanics and the assumptions of constitutive models to apply to the overlying strata. This method uses computer-based numerical modeling to reproduce the subsidence phenomenon by simulating the behavior of the rock mass. This approach could be used to model non-linear and post-yield properties of the material and to consider various types of geological features related to discontinuities and in-situ stresses in the rock mass. Over the past several decades, a wide range of approaches has been developed for the numerical modeling of subsidence. Numerical techniques are available for predicting the induced displacements and stresses in the analysis domain, such as the Finite Element Method (Yao et al., 1993, Ren and Li, 2008), Discrete Element Method (Choi and Kim, 2003; Keilich et al., 2006; Lee and Choi, 2011), Finite Difference Method (Lloyd et al., 1997; Alejano et al., 1999; Han et al., 2007; Shahriar et al., 2009; Xu et al., 2013), and hybrid code (Caudron et al., 2006; Vyazmensky et al., 2007 and 2010). However, the application of numerical methods requires sophisticated software and suitably skilled analysts, although they are powerful and comprehensive in their ability to predict subsidence (Harrison, 2011).

An example of the numerical modeling to be presented here is that of Shahriar et al. (2009). They used the three-dimensional finite difference code FLAC3D to predict the subsidence associated with an inclined shallow coal seam of the Negin coal mine in Iran. The elastoplastic (Mohr-Coulomb) behavior model was used for simulating the surface subsidence, and a horizontal to vertical stress ratio of 1.5 was applied for considering the

in-situ stress of the region.

Figure 2.7 shows the vertical displacement and the angle of draw on both sides of the panel which has 90m of extraction length, 30^0 of dip angle, 62m of dip side depth, 17m of rise side depth, and 1.7m of extraction height. Besides, they had compared the subsidence profile calculated from their numerical model with both the measured value of the site and the curve predicted from profile function method, as shown in Figure 2.8. As a result, they found that the amount of the maximum subsidence was underestimated up to 3 percent in comparison with surveying and profile function, and the position of the maximum subsidence was shifted towards the rise side of the panel.

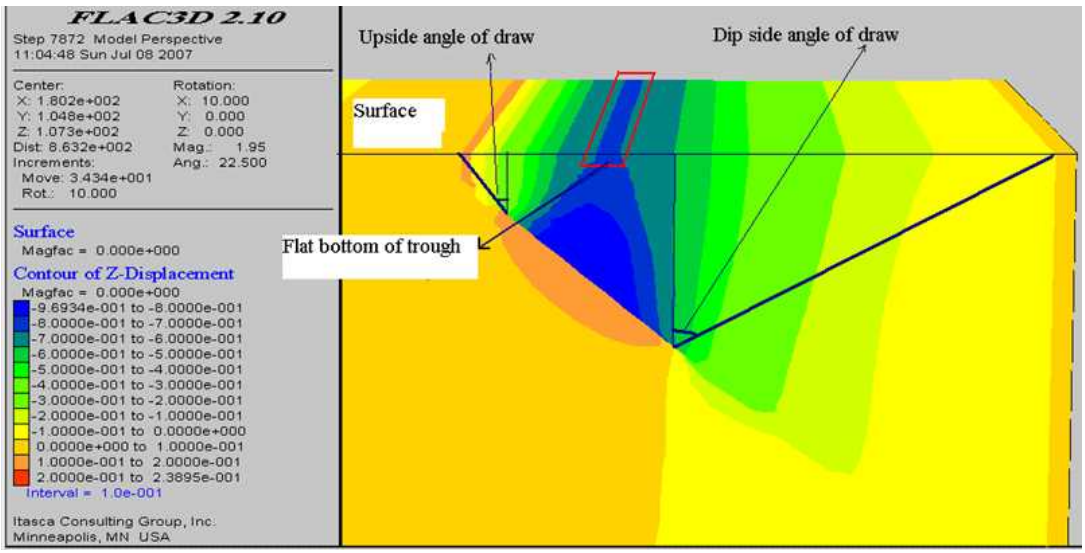

Figure 2.7 Vertical displacement and the angle of draw simulated from FLAC3D model which consists of an inclined plat coal panel (after Shahriar et. al., 2009).

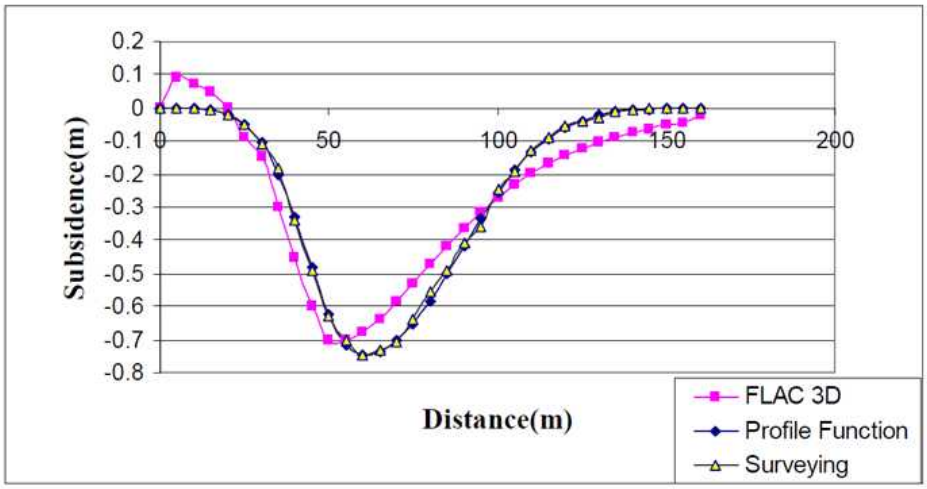

Figure 2.8 Predicted subsidence profiles by FLAC3D and profile function method versus surverying (after Shahriar et. al., 2009).

2.3 Methods for assessment of subsidence hazard

Prediction methods of ground movement, explained in the previous section, were developed and verified for conditions involving flat and horizontal coal seams, which are the conventional mining conditions in Europe. However, the geological structures of orebodies in Korea are more complicated, and the shape and location of mined cavities vary depending on the mining method and geological features. For these conditions, assessment of subsidence hazard may be a more practical approach for use in subsidence prevention project explained in Chapter 1.

Recently, several studies on evaluation and estimation of subsidence hazard have been carried out in Korea. Ryu et al. (2007) suggested a simple method to evaluate subsidence hazard using a diffusion theory. The diffusion model has an analogous relationship with the granular model which

can explain a mechanism of subsidence. In addition, they just used information about geometry of cavity and topography, and applied the method to abandoned metal and coal mines. Figure 2.9 shows the subsidence hazard maps constructed by using the suggested method.

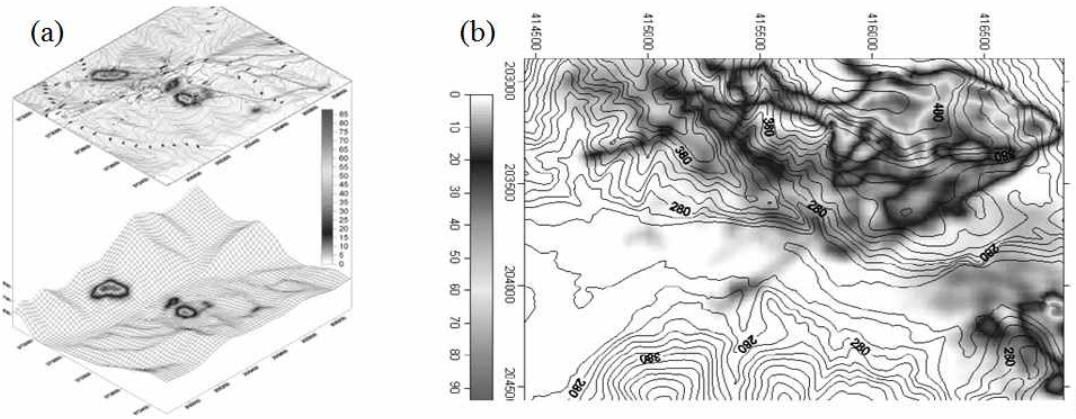

Figure 2.9 Subsidence hazard maps constructed by diffusion theory based method: (a) abandoned metal mine and (b) abandoned coal mine (after Ryu et al., 2007).

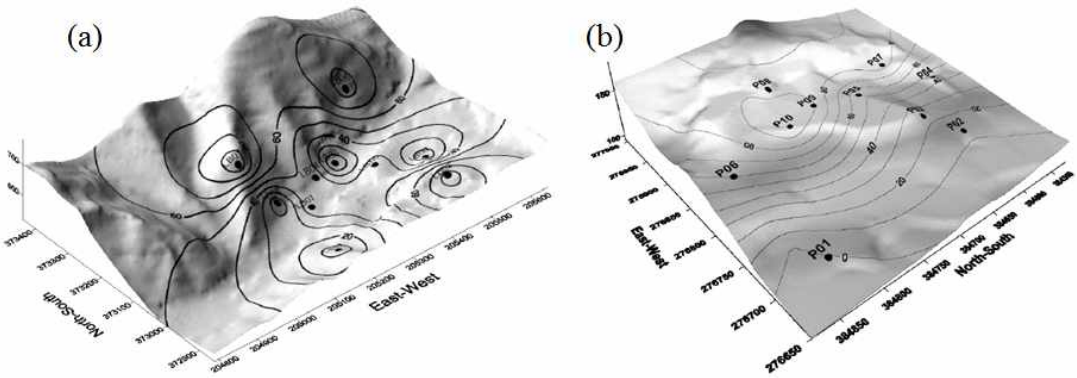

Figure 2.10 Contours of possibility of sinkhole: (a) Kumho mine in Bonghwa, Kyungbook province and (b) Choong-ju mine in Iryu, Choongbook province (after Choi et al., 2009).

Choi et al. (2009) developed a fuzzy reasoning method for estimating the possibility of subsidence occurrence, especially sinkhole type, in abandoned mine area. This method has an advantage in producing the reliable estimation results with a simple performance procedure even when the precise information on the local geology and mining conditions is rare. They used four variables in the model: gallery width (W), the ratio of mining depth to height (H/M), the ratio of pillar width to mining height (P/M), and roof index of rock mass (R). Figure 2.10 shows contours of the possibility of sinkhole predicted by fuzzy reasoning method.

Jung et al. (2010) developed a method for assessing subsidence hazard over abandoned mine areas through an analysis of influential factors. This method is based on compilation and analysis of research articles, documented survey records of Korean coal mine subsidence, results of numerical analyses, and physical model experiments. They selected eight factors of subsidence: mining depth, mining width, mining height (or thickness), dip of cavity, overburden condition, submersion, dynamic load, and rainfall. Then, multi-variable regression analysis and AHP (Analytical Hierarchy Process) were used to evaluate weighting value of each factor. Table 2.3 shows the developed method for estimation of subsidence hazard in Korean coal mines, and Table 2.4 presents the classes of hazard rating and corresponding meaning.

Table 2.3 Subsidence hazard estimation method for Korean coal mines (after Jung et al., 2010).

Category	Item \ Level	Ⅴ	Ⅳ	Ⅲ	Ⅱ	Ⅰ	0
Mining dimension	Depth (m)	<60	60~120	120~200	200~300	>300	-
		25	15	5	2	1	-
	Width (m)	>50	30~50	15~30	5~15	<5	-
		15	12	9	6	3	-
	Height (m) Thickness (m)	>5	3~5	2~3	1~2	<1	-
		12	9	6	3	1	-
	Dip (deg)	>45	35~45	25~35	15~25	<15	-
		12	9	6	3	1	-
Rock	Overburden condition	Very Weak	Weak	Fair	Good	Very Good	-
		20	16	12	8	2	-
Water	Submersion	Cyclic	Dry	Submerged			-
		11	6	2			-
External load	Dynamic load	Rail+Road	Rail	Road	None		-
		5	3	2	0		-
Correction factor	Rainfall (mm/5days)	>400	300~400	200~300	100~200	50~100	<50
		10	8	5	2	1	0

Table 2.4 Classes of hazard rating and corresponding meaning with follow-up measures (after Jung et al., 2010).

Class	Value	Status	Corresponding measures
Ⅰ	0~20	Very stable	None
Ⅱ	20~40	Stable	Usual management
Ⅲ	40~60	Fair	Detailed inspection
Ⅳ	60~80	Unstable	Reinforce/support after inspection
Ⅴ	80~100	Very unstable	Immediate reinforce/support

3. Numerical analysis

In order to develop an assessment technique for subsidence risk, the numerical method, one of the subsidence prediction methods as explained in Chapter 2, was fully implemented. In this study, a commercial FDM code, FLAC2D, was used to assess the subsidence risk in mining areas. The effect of influence factors on mining subsidence was mainly considered, and the results of the numerical analysis were used as the fundamental basis for construction of assessment technique. This chapter presents a definition of a new indicator for representing subsidence risk and explains the strength reduction method for calculating the factor of safety (FOS). In addition, methodologies and results of the numerical analysis are described.

3.1 Definition of subsidence risk level

According to the United Nations (UN/ISDR, 2004), ‘risk’ is defined as a probability of harmful consequences, or expected losses (deaths, injuries, property, livelihoods, economic activity disrupted or environment damaged) resulting from interactions between natural or human-induced hazards and vulnerable conditions. Conventionally, risk is expressed by the notation Risk = Hazards × Vulnerability. In addition, ‘hazard’ is a potentially damaging physical event, phenomenon or human activity that may cause the loss of life or injury, property damage, social and economic disruption or environmental degradation. And, ‘vulnerability’ is the conditions determined by physical, social, economic, and environmental factors or processes, which

increase the susceptibility of a community to the impact of hazards. Therefore, ‘subsidence risk’ was defined as a probability of occurrence of subsidence in mining areas. In this case, a mined cavity could be treated as a hazard, and a rock mass condition could be a vulnerability.

The simplest way to assess the subsidence risk quantitatively is to use a representative indicator. For example, factor of safety (FOS), defined as a ratio of material strength to design load, is a typical index used for describing the capacity of structures. In addition, the FOS has been widely used as an indicator to represent the stability of geotechnical structures such as slopes, tunnels, and pillars of underground mining. In this study, ‘subsidence risk level’ (SRL) was defined as the indicator that represents a probability of occurrence of subsidence in mining areas. The value of SRL was calculated from a simple equation expressed as the reciprocal of the FOS.

$$SRL = \frac{1}{FOS} \times 100(\%) \quad \text{if} \quad FOS \geq 1 \tag{3.1a}$$

$$SRL = 100(\%) \quad \text{if} \quad FOS < 1 \tag{3.1b}$$

Figure 3.1 shows the relationship between SRL and FOS according to equation (3.1). If the FOS equals 1, then the subsidence can occur immediately in the current conditions and the value of SRL is calculated as 100 %. However, if the FOS less than 1, which means that subsidence has already occurred, the upper limit of SRL is set to 100 %. Consequently, the

SRL ranges from 0 % at perfectly stable conditions to 100 % at high-risk conditions.

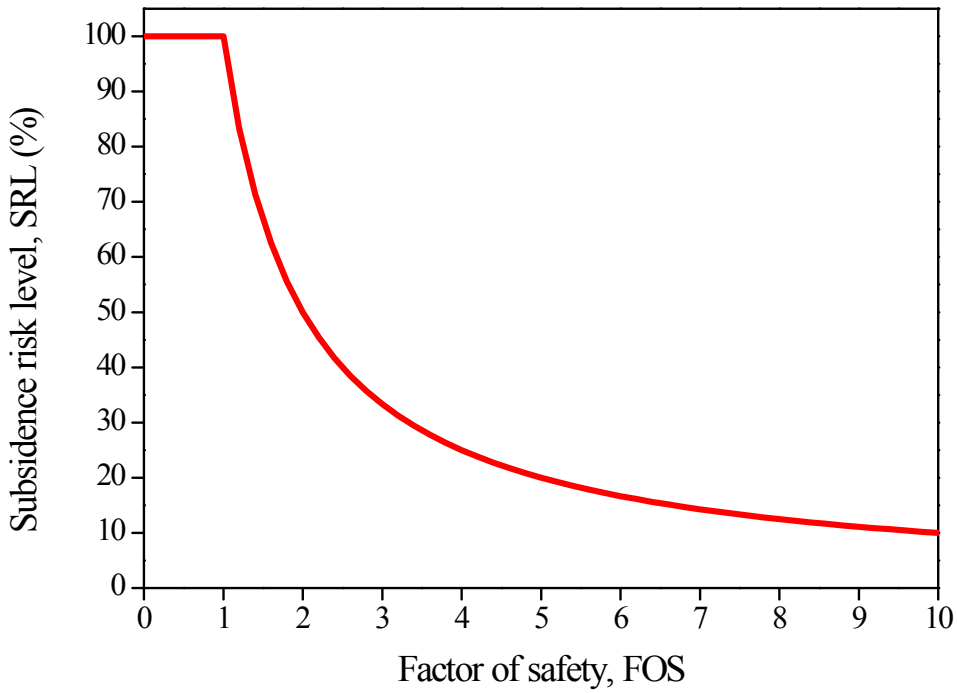

Figure 3.1 Relationship between factor of safety (FOS) and subsidence risk level (SRL) defined in this study.

3.2 Strength reduction method

3.2.1 Introduction

The strength reduction method is useful for evaluating the stability of the various types of geotechnical constructions, especially slope stability, by calculating the FOS, with numerical analyses such as FEM and DEM. In

soil slope, a typical way of computing FOS with FEM or FDM is simply reducing the soil shear strength until collapse occurs, and then the resulting FOS is defined as the ratio of the actual shear strength of soil to the reduced shear strength at failure. This method was used for soil slope stability analysis as early as 1975 by Zienkiewicz et al. (1975), and has been applied by Matsui and San (1992), Ugai and Leshchinsky (1995), Griffiths and Lane (1999), Dawson et al. (1999), Cai and Ugai (2000), Cheng et al. (2007) and many others. In addition, several studies have been carried out to apply a non-linear failure criterion with the technique in order to analyze the stability of rock slopes (Dawson et al. 2000; Hammah et al. 2005; Fu and Liao 2010; Chakraborti et al. 2012).

This method has several advantages over the traditional limit equilibrium methods, of which the most notable is that the former does not require any assumptions about the shape or location of the failure surface. The critical failure surface being found automatically can be a great advantage to efficiency in the safety assessment of underground structures as well as the stability analysis of the slope (Yang and Huang 2009; Huang et al. 2012; Lee et al. 2012). In this study, the mined cavities were regarded as geotechnical structures, and the surrounding rock mass was selected as a target for this method. Therefore, the failure of rock mass and the subsidence on the ground surface could be evaluated directly, rather than assumed.

3.2.2 Application in FLAC

In order to implement the strength reduction method in FLAC2D, there are three important requirements to be determined: (a) selection of failure criterion and reduced shear strength parameters, (b) obvious process of reducing the parameters, and (c) definition of convergence criterion.

a. Failure criterion and reduced parameters

The failure criterion and reduced shear strength parameters of rock mass should be selected. In general, the Mohr-Coulomb (M-C) failure criterion is widely used, and two strength parameters (i.e., cohesion and friction angle) are selected as the target to reduce their strength. Since the criterion represents a linear relationship between normal and shear stress or maximum and minimum principal stress, the FOS can be simply defined as a strength reduction factor (SRF), which is a ratio of original strength to reduced strength of rock mass, as shown in equation (3.2). The simplicity of the M-C model is an advantage for application of the strength reduction method in numerical simulations. The Hoek-Brown (H-B) failure criterion is also applicable in order to take non-linearity of rock mass into account. However, how to utilize the H-B criterion into the method has not been clearly elucidated. Considering its simplicity, the M-C model was applied in this analysis.

$$FOS = SRF = \frac{c_o}{c_r} = \frac{\tan\phi_o}{\tan\phi_r} = \frac{T_o}{T_r} \tag{3.2}$$

where SRF is the strength reduction factor, C is the cohesion, ϕ is the friction angle, and T is the tensile strength. The subscripts ‘o’ and ‘r’ mean the original value and reduced value of its property, respectively.

Furthermore, the tensile strength of rock mass is also considered as the strength property, along with the cohesion and friction angle. Then, three key strength parameters were chosen as the reduced strength parameters. Figure 3.2 show the change of the three parameters of the M-C criterion according to the strength reduction method.

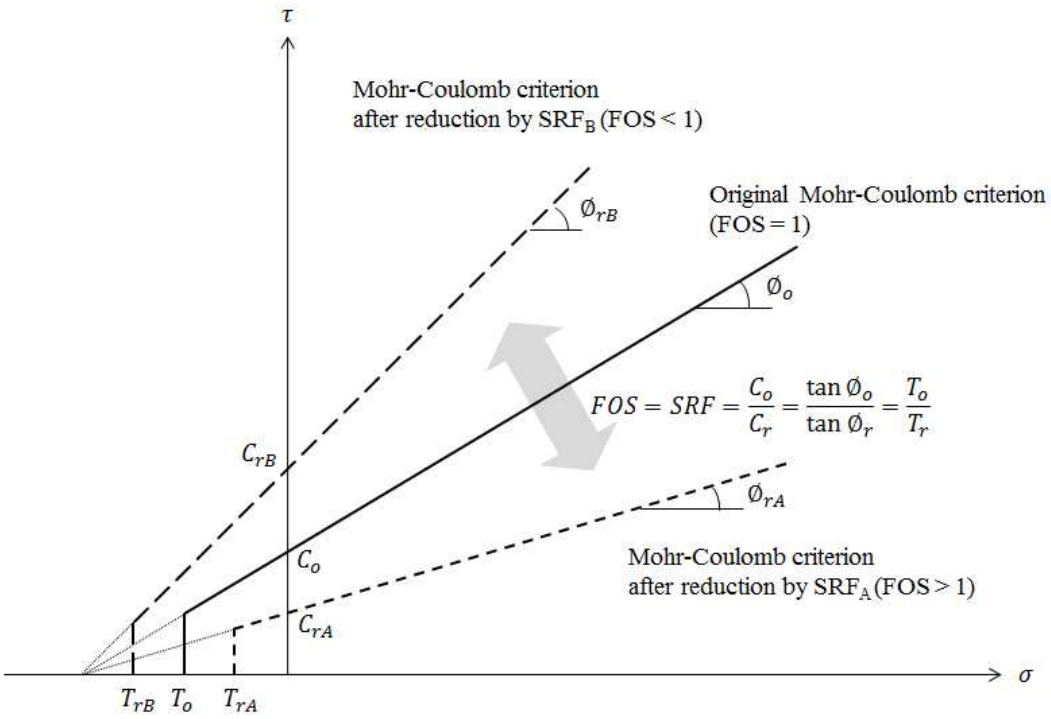

Figure 3.2 Changes in Mohr-Coulomb failure criterion according to strength reduction method. Subscript ‘A’ and ‘B’ describe the case of stable and unstable states in original conditions.

b. Reducing process

An obvious reducing process of selected parameters is needed. The conventional way for determination of the FOS at failure state is to reduce the value of parameters in sequence with a very small interval. That is, the SRF is monotonically increased with the progress of the analysis. In the first step, the initial value of SRF is set to 1. Then, the value of SRF in the second step is slightly increased by an amount specified by the analysis. The increment of SRF between each step decides the resolution of FOS at the final step and dominates the total number of iterations (Figure 3.3(b)).

Another way for the reducing process is a bracketing and bisection approach suggested by Dawson et al. (1999). This method has the advantage of being able to reduce the number of iterations significantly; however, it is inevitable that a numerical model should be alternately failed and stable during the whole analysis as depicted in Figure 3.3(a).

In this study, the conventional approach for the reducing process was used to induce a sequential failure of surrounding rock mass and identify the phenomenon of its propagation. The SRF of current stage is calculated by dividing the SRF of the previous stage by 0.95, such as in equation (3.3), which is expected to achieve accurate results.

$$SRF_N = \left(\frac{1}{0.95}\right)^{N-1} \tag{3.3}$$

where SRF_N is the strength reduction factor of the N^{th} iteration.

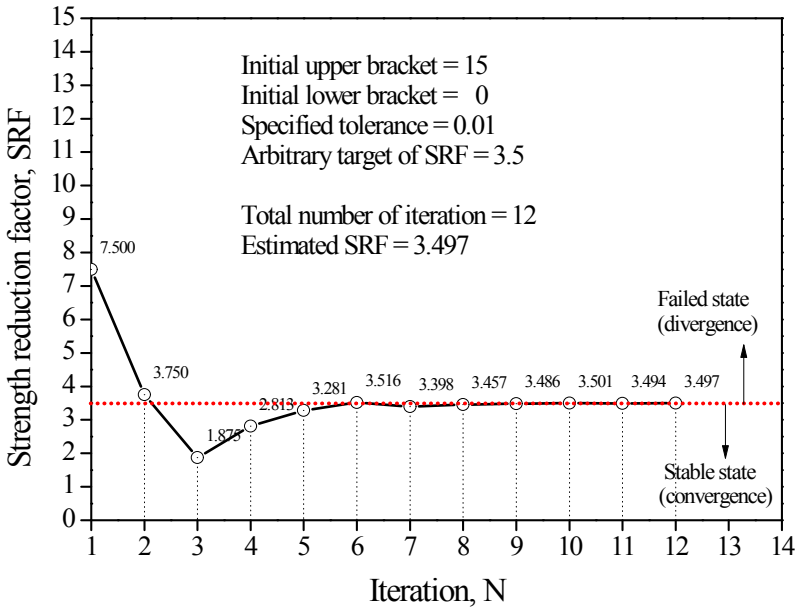

(a) Bracketing and bisection method (suggested by Dawson et. al. 1999)

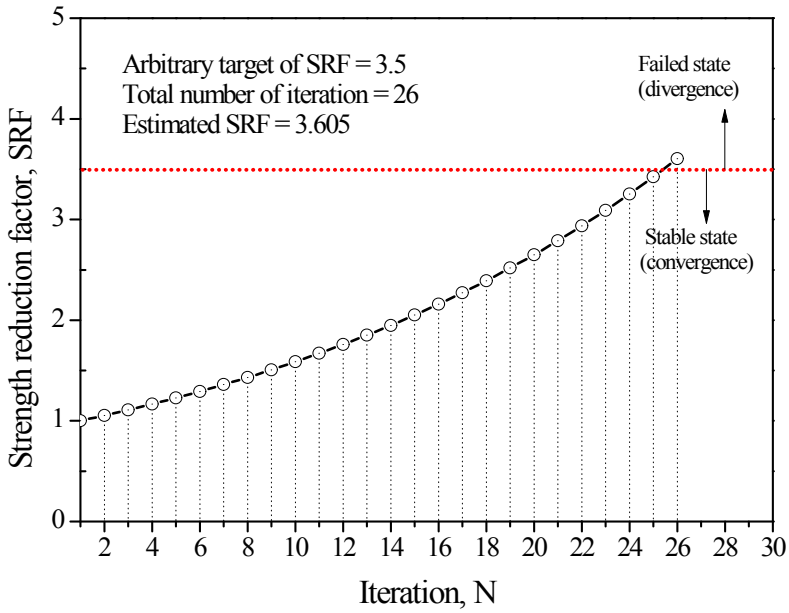

(b) Conventional method used in this study

Figure 3.3 Reducing process for calculation of FOS using strength reduction method: (a) bracketing and bisection method and (b) monotonically increasing method.

c. Definition of convergence criterion

The strength reduction method requires a definition of the convergence criterion to decide the failure state, which also means termination of iterations in the reducing process. Previous studies have selected and defined several kinds of convergence criterions, such as displacement (Ugai and Leshchinsky 1995; Griffith and Lane 1999), shear strain (Matsui and San 1992), and unbalanced force ratio (Dawson et al. 1999), to decide the failure state in numerical models.

In the present analysis, the unbalanced force ratio (UFR) was selected as a convergence criterion because FLAC does not perform the numerical calculation (i.e., solving process) when the UFR is smaller than a specific value defined by users. The unbalanced force ratio in FLAC is defined as the ratio of the net force acting on a grid-point to the mean absolute value of force exerted by each surrounding zone (Itasca Consulting Group, 2011). In FLAC, the value of 0.001 is set for a critical UFR by default, and Dowson et. al. (1999) successfully carried out the stability analysis of geotechnical structures with the value. In addition, a maximum limit of solving steps should be decided to prevent the infinite loop of solving process. The value of limit steps is usually related with the strength parameters applied for the model and the number of mesh points. In this study, the value of 40,000 is set for the maximum limit steps by considering the model size and properties of analysis domain.

Once the solving process is continually executed under a given SRF, it will be terminated when the UFR decreases to 0.001 or the total number of solving steps reaches 40,000. At the end of the solving, the SRF is updated

and the parameters are reduced by Equation (3.3) if the UFR is smaller than 0.001; otherwise, the SFR is finally decided as the FOS of the numerical model. Figure 3.4 shows a flow chart explaining how to find a FOS of a given condition. In addition, if the termination of solving occurs immediately after the first iteration, it means that the FOS is less than or equal to 1. In this case, the original value of the strength parameter is increased fourfold to restart the solving process with an abundant initial value, because the SRF in this process is monotonically increased, and then the whole process is repeated.

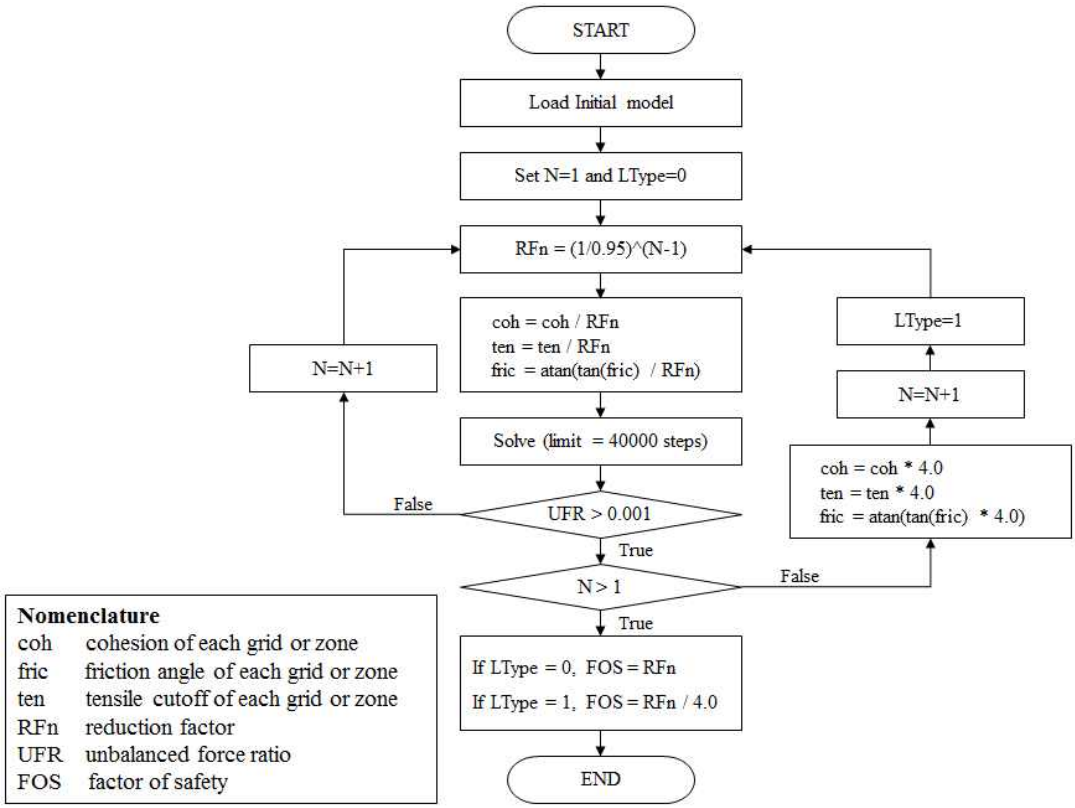

Figure 3.4 Flow chart for calculation of FOS in numerical simulations.

3.3 Design of numerical model

3.3.1 Selection of main factors

In order to construct the numerical model and evaluate the FOS, it is necessary to preferentially select the factors causing the subsidence. There are many factors affecting mine subsidence such as extraction thickness, mining depth, degree of extraction, method of working, competence of surrounding materials, and in-situ stress (Harrison 2011).

However, it is not possible to consider all the affecting factors to evaluate the FOS. Jung et al. (2010) determined a relative importance of influential factors on subsidence and arranged the factors in order of priority: mining depth, overburden condition, mining width, mining height, dip of orebody, submersion, rainfall, and external load. Choi and Kim (2007) extracted the main factors related to the subsidence by using PCA (principle component analysis) and found that the depth of gangway, RMR (rock mass rating), and geology are the significant factors in abandoned coal mine.

In this study, only two categories of factors were selected as the main factors on subsidence: the geometrical feature of the mined cavity and the nature of the surrounding rock mass. Since the subsidence initiates from the collapse of the mined cavity and propagates through the rock mass, the shapes, dimensions, and locations of the mined cavity and the strength of overlying rock mass are the most effective factors (Jeon et al. 2012).

3.3.2 Cavity model

Unlike the relatively flat and continuative characteristics of coal seams in Europe and elsewhere, Korean coal seams have steeply inclined and very complicated structures. These features make it difficult to obtain accurate information about the mined cavity because of the multiple mining levels and the various coal-extraction volumes. Therefore, a simplification was made for the quantification of the mined cavity. As shown in Figure 3.5, a mined cavity was simplified as a parallelepiped that could be slanted towards its dip-direction. The shape and size of the cavity are determined by the height (H), thickness (T), inclination (I), and width (W). The depth (D) of cavity is calculated from the vertical distance between the top of cavity and surface. Although the simplified cavity model has a three-dimensional shape, only a vertical cross section that contains the dip-direction vector was considered in order to reduce the computational time here because a significant number of iterations are required to find the FOS at a given condition. Consequently, the width of cavity (W) was excluded from the numerical analysis, and the two-dimensional model with an infinite length of cavity was generated.

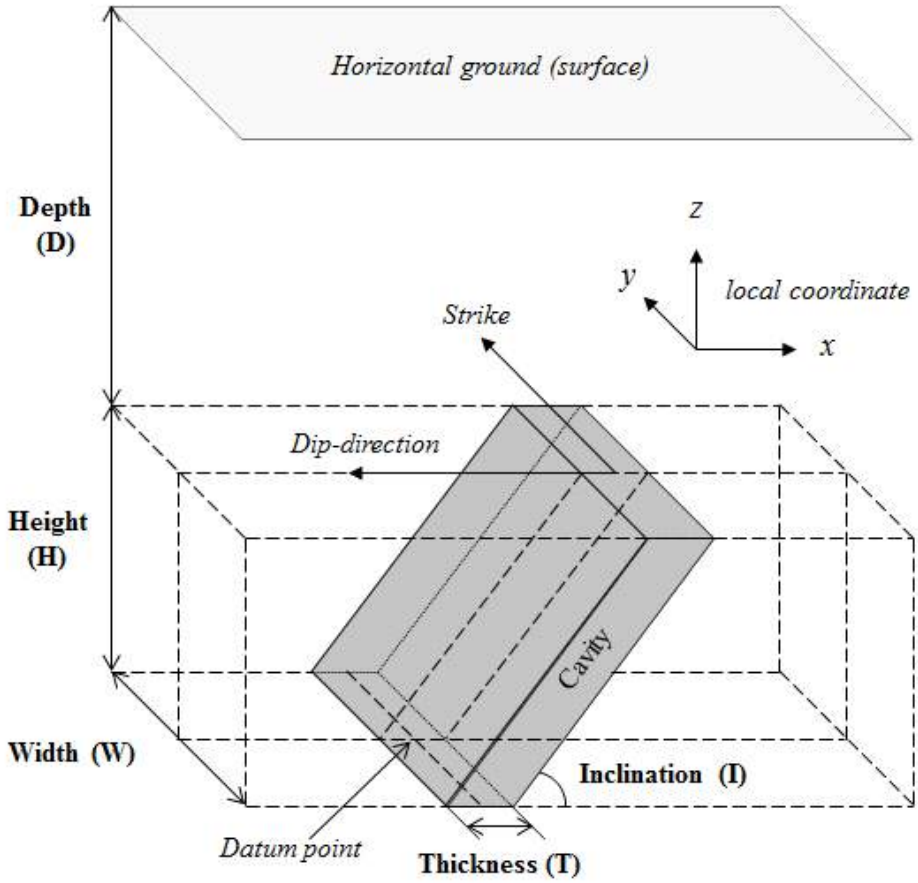

Figure 3.5 Simplified cavity model used in the numerical models.

3.3.3 Rock mass model

There are many kinds of affecting factors associated with rock mass such as the mechanical behavior of the rock, in-situ stress state, geological discontinuities, near-surface geology, and surface topography. Although each factor affects the subsidence, it is difficult to consider all factors in the risk assessment of mine subsidence. In the mine subsidence prediction methods mentioned in Chapter 2, the influence of rock mass on subsidence has been

applied as a comprehensive factor. For example, in influence function methods, a subsidence factor is considered a site constant; it depends on geological conditions, treatment of the goaf area, and the mining method (Ren et al. 1987). The application of the subsidence factor is very useful to achieve highly accurate prediction by choosing a suitable value from field measurement or experience.

In reality, the rock mass properties vary in different geological layers, but they are not usually well defined. The geological condition at shallow depth is typically weak, and it gets better as the depth increases. Accordingly, the mined cavities at the depth greater than a particular value may not contribute to the ground subsidence at the surface. In addition, the volume expansion, an important concept for the analysis of the ground subsidence due to the collapse of the mined cavities, is not easy to implement in the continuum analysis such as FLAC because the failure of an element and separation of adjacent elements is not allowed in the analysis (Jeon et. al., 2012).

In this study, a rock mass type (R) was defined as a factor that represents the surrounding rock mass conditions and expressed by a numeric value. The rock mass type is created from four basic assumptions: (i) the ground surface is flat and horizontal; (ii) the rock mass is horizontally layered; (iii) the rock mass consists of soil, and weathered, weak, fair, and hard rock; and (iv) the rock mass becomes stronger with increase in depth. Figure 3.6 shows the numerical models generated by the rock mass type along with the depth. For example, when the rock mass type equals 1, its numerical model is sequentially composed of 5 m of soil, 5m of weathered

rock, 5m of weak rock, 5m of fair rock, and 60m of hard rock. The mechanical properties of each layer used in this model are listed in Table 3.1, and the values were obtained from the geotechnical survey reports performed at abandoned mines in Gangwon Province, Korea.

Table 3.1 Mechanical properties of layered rock mass models.

Layer	Density (kg/m^3)	Young's modulus (Pa)	Cohesion (Pa)	Friction angle (°)	Poisson's ratio	Tensile strength (Pa)
Soil	1820	1.98×10^7	6.00×10^3	30.4	0.34	6.87×10^3
Weathered rock	2067	2.17×10^8	1.33×10^5	31.3	0.32	1.50×10^5
Weak rock	2540	2.35×10^9	3.38×10^5	34.6	0.24	3.55×10^5
Fair rock	2633	3.50×10^9	5.73×10^5	39.0	0.22	5.47×10^5
Hard rock	2638	9.14×10^9	1.44×10^6	42.4	0.19	1.27×10^6

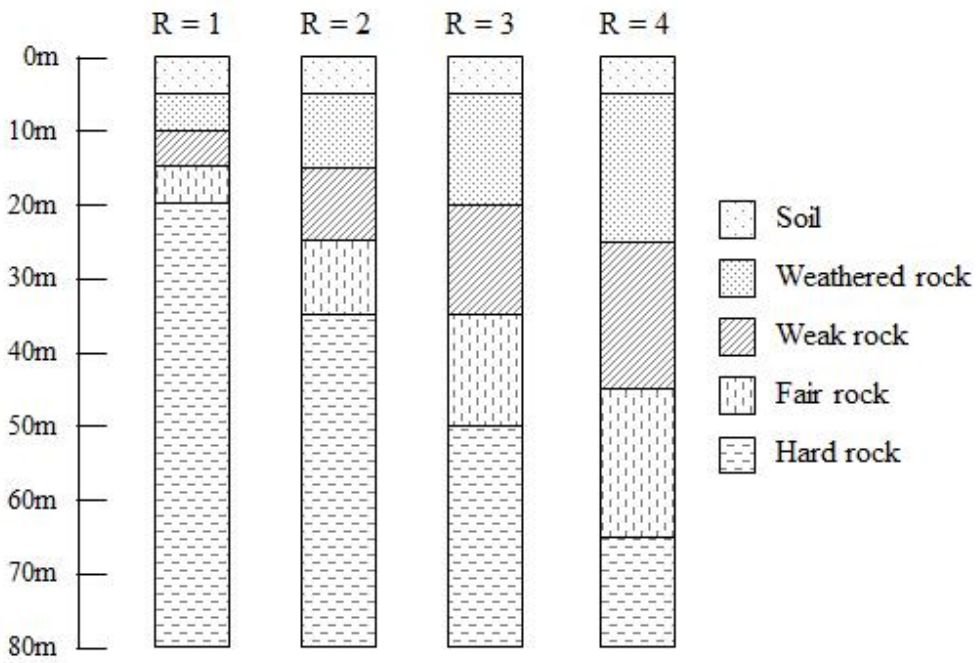

Figure 3.6 Four types of rock mass models used in numerical model.

3.3.4 Analysis domain

A rectangular-shaped numerical model, 160 m of width and 80 m of height, was generated as shown in Figure 3.7. Both flank sides and bottom boundaries were restricted along x and y directions in displacement respectively, and the upper boundary was kept free for representing the ground surface. As a result, the rock mass type (R) and the four factors related to the mined cavity, height (H), thickness (T), inclination (I), and depth (D), were chosen as the parameters to calculate the FOS and SRL. Each variable has four different values; 1, 2, 3 and 4 for rock mass type, 10, 20, 30 and 40 m for depth, 5, 10, 15 and 20 m for height, 2, 3, 4 and 5 m for thickness, 45, 60, 75 and 90° for inclination. Accordingly, 1024 ($=4^5$) cases of numerical models were designed in total.

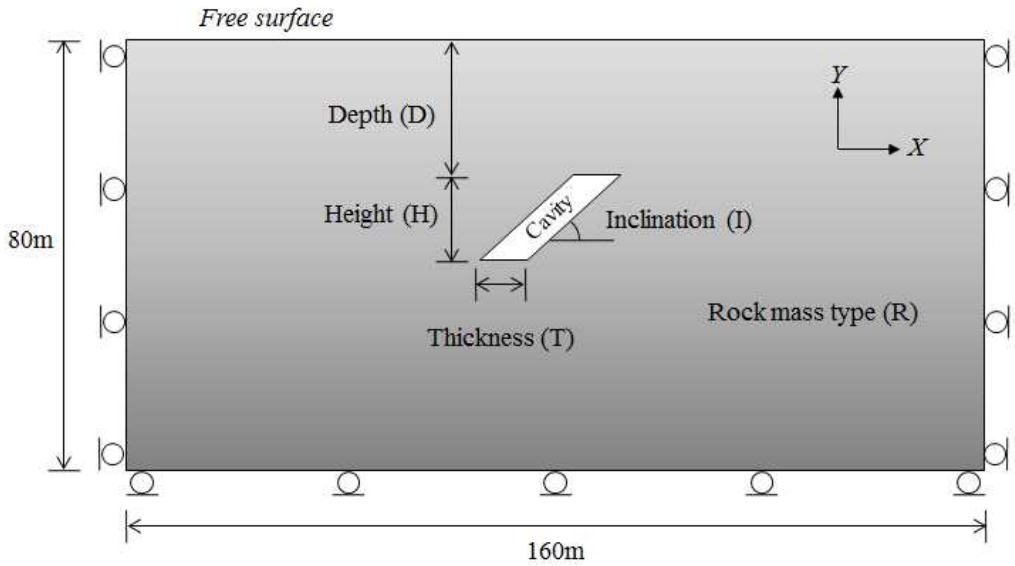

Figure 3.7 Definition of five variables and dimension of numerical models used in FLAC2D.

3.4 Results of numerical simulation

Based on the numerical models, the FOS for each of the 1024 cases was computed. Total compilation of the simulation results are listed in Table 3.2, 3.3, 3.4, and 3.5. The average, minimum, and maximum values of FOS are calculated as 3.253, 0.277, and 10.586, respectively. The distribution of the FOS follows a skewed histogram, such as that shown in Figure 3.8. About 70 percent of all cases are computed to range from 1.0 to 3.0. Meanwhile, 20 cases are calculated under the critical state. As explained in Subsection 3.1, a critical state is defined when the FOS equals unity, which divides the failed and stable state at a given condition.

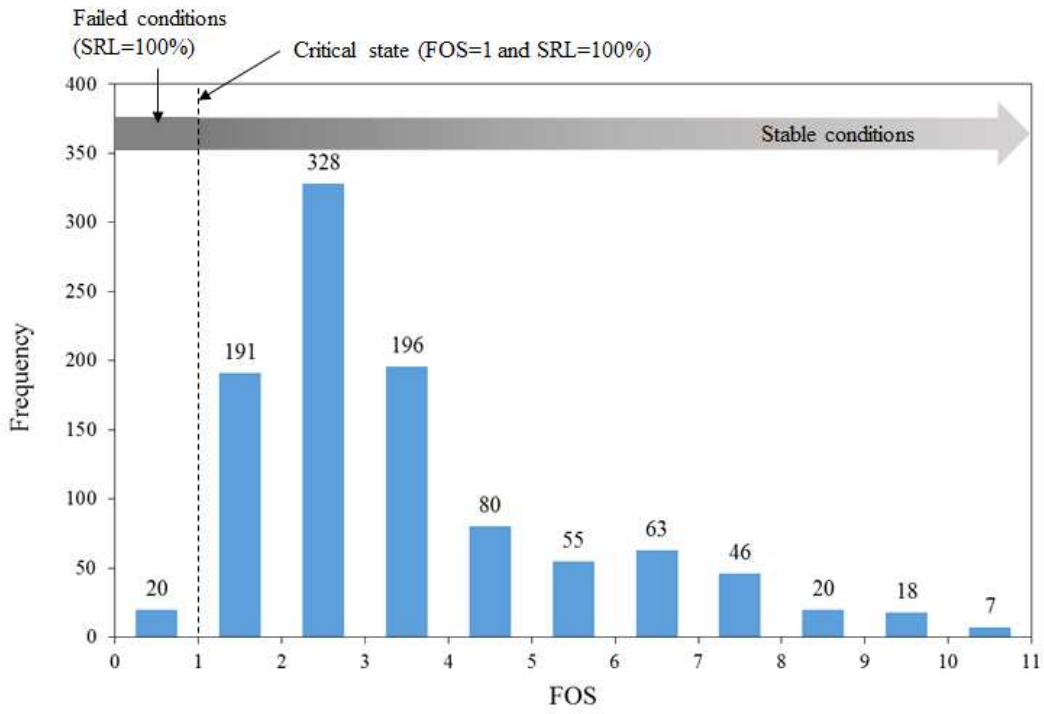

Figure 3.8 Distribution of FOS calculated from numerical simulations.

Figure 3.9 shows the distribution of magnitude of displacement vector when the rock mass type (R) and depth (D), height (H), thickness (T) and inclination (I) of cavity are 3, 30m, 10m, 3m and 45°, respectively. From these results, it was found that the movement of surrounding rock mass occurs initially at the vicinity of the roof of the cavity, which means the collapse of the cavity causes the initiation of subsidence. Then, the movement propagates through the rock mass and reaches the surface. In this case, the FOS was calculated to 2.392 because the convergence criterion explained in Subsection 3.2.2 was satisfied when the iteration number equals 18. In addition, the profile of horizontal and vertical displacement on the surface are shown in Figure 3.10. The absolute value of the horizontal and vertical displacement are increased in accordance with the strength reduction process. Especially, the points of zero horizontal displacement and maximum subsidence were slightly shifted from the center of cavity because the inclination of cavity was set to 45°.

In order to comprehend the effect of five factors on surface movement, the horizontal and vertical displacement were normalized by the absolute value of maximum vertical displacement as shown in Figures 3.11, 3.12, 3.13, 3.14, and 3.15. In each case, the contour plot is representing the magnitude of normalized displacement vector when its original value is larger than 10 mm. From these results, it was found that the FOS increases with the depth (D) and inclination (I) of cavity, but decreases with the increase of the rock mass type (R) and the height (H) and thickness (T) of cavity.

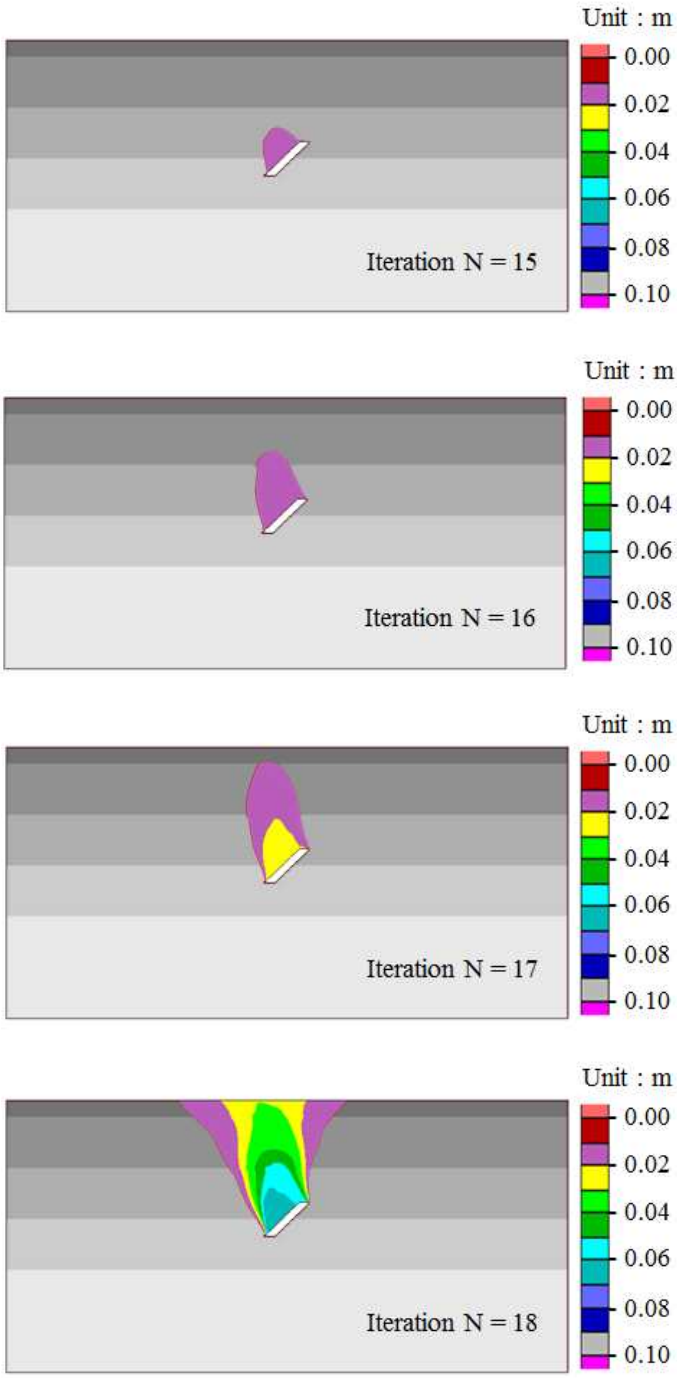

Figure 3.9 Contour of magnitude of displacement vector according to increase of iteration number when R, D, H, T and I were 3, 30m, 10m, 3m and 45°, respectively.

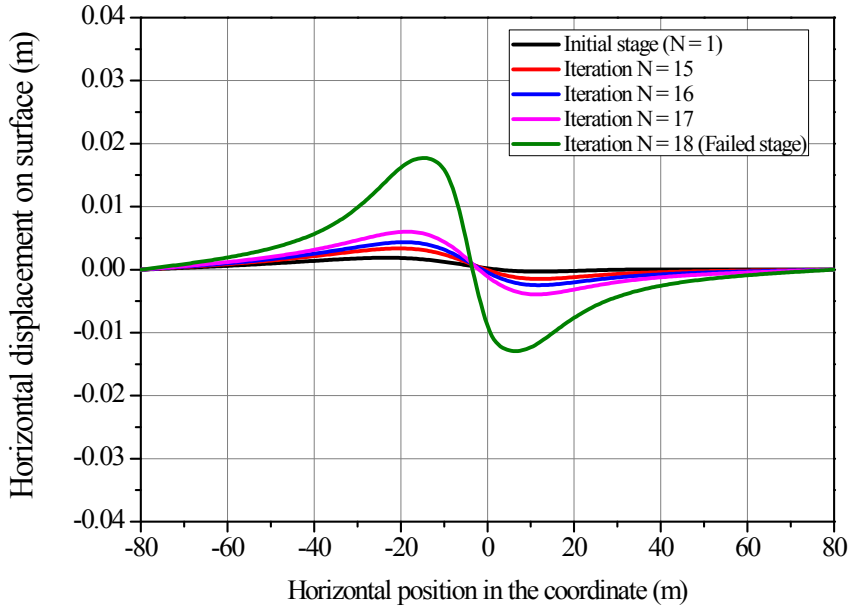

(a) Horizontal displacement

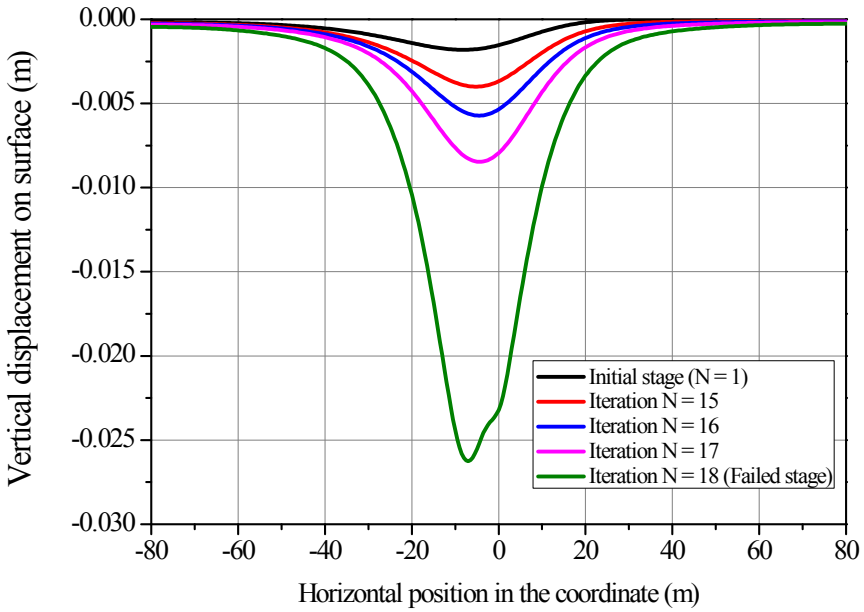

(b) Vertical displacement

Figure 3.10 Changes of horizontal and vertical displacement according to increase of iteration number when R, D, H, T and I were 3, 30m, 10m, 3m and 45°, respectively.

Table 3.2 FOS calculated from numerical simulations in the case of Rock mass type 1.

R=1	D	10m				20m				30m				40m			
T	H / I	5m	10m	15m	20m	5m	10m	15m	20m	5m	10m	15m	20m	5m	10m	15m	20m
2m	45°	2.650	2.051	1.948	1.360	6.338	4.426	3.605	2.936	9.553	6.338	4.904	3.995	9.076	7.023	5.434	4.426
	60°	3.425	2.790	2.790	2.518	7.781	6.021	4.904	4.205	10.06	7.781	6.338	5.162	9.553	7.781	6.338	5.434
	75°	3.995	3.605	3.605	3.605	8.622	7.023	6.021	5.434	10.59	8.191	7.023	6.338	10.06	7.781	6.672	6.021
	90°	4.426	4.205	4.205	4.205	9.076	7.781	7.023	6.338	10.59	8.622	7.392	6.338	10.06	8.191	7.023	6.021
3m	45°	2.392	1.948	1.851	1.360	5.720	4.205	3.425	2.936	9.076	6.338	4.659	3.795	8.622	6.672	5.162	4.205
	60°	3.091	2.650	2.650	2.392	7.023	5.720	4.659	3.995	9.553	7.392	6.021	5.162	9.076	7.392	6.338	5.434
	75°	3.605	3.425	3.425	3.425	7.781	6.672	5.720	5.162	10.06	8.191	7.023	6.021	9.553	7.781	6.672	5.720
	90°	3.795	3.795	3.795	3.795	8.191	7.392	6.672	6.021	10.06	8.191	7.023	6.338	9.553	7.781	6.672	6.021
4m	45°	2.158	1.670	1.758	1.292	5.434	3.995	3.254	2.790	8.191	6.021	4.659	3.795	8.622	6.338	5.162	4.205
	60°	2.790	2.518	2.518	2.392	6.338	5.162	4.426	3.995	9.076	7.023	5.720	4.904	9.076	7.023	6.021	5.162
	75°	3.091	3.091	3.091	3.091	7.023	6.338	5.720	4.904	9.553	7.781	6.672	6.021	9.076	7.392	6.338	5.720
	90°	3.254	3.254	3.254	3.254	7.392	7.023	6.672	6.021	9.553	8.191	7.023	6.338	9.076	7.781	6.672	6.021
5m	45°	2.051	1.758	1.670	1.292	4.904	3.795	3.254	2.790	7.781	5.720	4.426	3.605	8.191	6.338	4.904	4.205
	60°	2.518	2.392	2.392	2.158	5.720	4.904	4.426	3.795	8.622	7.023	5.720	4.904	8.622	7.023	6.021	5.162
	75°	2.650	2.650	2.650	2.650	6.338	6.021	5.434	4.904	9.076	7.392	6.672	5.720	8.622	7.392	6.338	5.720
	90°	2.650	2.650	2.650	2.650	6.672	6.338	6.338	5.720	9.076	7.781	6.672	6.021	9.076	7.392	6.338	5.720

Table 3.3 FOS calculated from numerical simulations in the case of Rock mass type 2.

R=2	D	10m				20m				30m				40m			
T	H / I	5m	10m	15m	20m	5m	10m	15m	20m	5m	10m	15m	20m	5m	10m	15m	20m
2m	45°	2.051	1.507	1.166	1.053	3.425	2.392	1.851	1.670	4.659	3.605	3.091	2.518	7.392	5.162	4.205	3.425
	60°	2.518	2.158	1.758	1.670	3.995	3.091	2.650	2.518	5.162	4.426	3.995	3.605	8.191	6.338	5.162	4.426
	75°	2.790	2.650	2.272	2.158	4.205	3.605	3.254	3.254	5.434	5.162	4.659	4.426	8.622	7.023	6.021	5.434
	90°	2.936	2.936	2.650	2.650	4.205	3.795	3.425	3.425	5.434	5.434	5.162	4.904	8.622	7.023	6.021	5.434
3m	45°	1.851	1.432	1.108	1.053	3.091	2.272	1.851	1.670	4.426	3.425	2.936	2.518	7.023	5.162	3.995	3.254
	60°	2.272	2.051	1.670	1.587	3.605	2.936	2.518	2.518	4.904	4.205	3.795	3.425	7.781	6.021	5.162	4.426
	75°	2.650	2.518	2.158	2.158	3.995	3.425	3.091	3.091	5.162	4.904	4.426	4.205	8.191	6.672	5.720	5.162
	90°	2.790	2.650	2.650	2.650	3.995	3.605	3.425	3.425	5.162	5.162	4.904	4.659	8.191	6.672	6.021	5.434
4m	45°	1.758	1.360	1.108	0.663	2.936	2.272	1.758	1.670	3.995	3.425	2.790	2.392	6.338	4.904	3.795	3.254
	60°	2.158	1.851	1.670	1.587	3.425	2.790	2.392	2.392	4.426	4.205	3.605	3.254	7.392	5.720	4.904	4.205
	75°	2.392	2.272	2.051	2.051	3.605	3.254	2.936	2.936	4.659	4.659	4.426	3.995	7.781	6.338	5.720	5.162
	90°	2.518	2.518	2.518	2.518	3.795	3.605	3.254	3.254	4.904	4.904	4.659	4.659	7.781	6.672	5.720	5.434
5m	45°	1.587	1.292	1.053	0.463	2.790	2.158	1.670	1.587	3.795	3.254	2.790	2.392	6.021	4.659	3.795	3.091
	60°	1.948	1.758	1.587	1.507	3.254	2.650	2.272	2.272	4.205	3.995	3.605	3.254	6.672	5.720	4.659	4.205
	75°	2.272	2.158	2.051	1.948	3.425	3.091	2.790	2.790	4.426	4.426	4.205	3.995	7.023	6.021	5.434	4.904
	90°	2.392	2.392	2.392	2.392	3.605	3.425	3.091	3.091	4.659	4.426	4.426	4.426	7.392	6.338	5.720	5.162

Table 3.4 FOS calculated from numerical simulations in the case of Rock mass type 3.

R=3	D	10m				20m				30m				40m			
T	H / I	5m	10m	15m	20m	5m	10m	15m	20m	5m	10m	15m	20m	5m	10m	15m	20m
2m	45°	2.051	1.228	0.440	0.307	2.650	1.851	1.360	1.228	3.425	2.518	2.051	1.670	4.205	3.091	2.650	2.392
	60°	2.518	1.670	1.507	1.360	3.091	2.392	1.851	1.670	3.795	3.091	2.650	2.272	4.659	3.605	3.425	3.091
	75°	2.790	2.051	1.948	1.851	3.425	2.790	2.392	2.158	3.795	3.425	3.091	2.650	4.904	3.795	3.795	3.605
	90°	2.936	2.272	2.272	2.158	3.605	2.936	2.518	2.518	3.995	3.605	3.091	2.790	4.904	3.995	3.995	3.795
3m	45°	1.851	1.166	0.323	0.307	2.518	1.758	1.360	1.166	3.254	2.392	1.948	1.587	3.995	2.936	2.650	2.272
	60°	2.272	1.587	1.507	1.292	2.936	2.272	1.851	1.670	3.605	2.936	2.518	2.158	4.426	3.605	3.254	2.936
	75°	2.650	1.948	1.948	1.758	3.091	2.650	2.272	2.158	3.605	3.254	2.936	2.650	4.659	3.795	3.605	3.605
	90°	2.790	2.158	2.158	2.158	3.254	2.790	2.392	2.392	3.795	3.425	3.091	2.790	4.659	3.795	3.795	3.795
4m	45°	1.758	1.108	0.487	0.307	2.272	1.670	1.292	1.108	3.091	2.392	1.948	1.587	3.795	2.936	2.518	2.272
	60°	2.158	1.507	1.432	1.292	2.650	2.158	1.758	1.670	3.425	2.936	2.392	2.158	4.205	3.425	3.254	2.936
	75°	2.392	1.851	1.851	1.758	2.936	2.518	2.158	2.051	3.425	3.091	2.790	2.650	4.426	3.605	3.605	3.425
	90°	2.518	2.051	2.051	2.051	2.936	2.650	2.392	2.392	3.605	3.254	2.936	2.790	4.426	3.795	3.605	3.605
5m	45°	1.587	1.053	0.323	0.307	2.158	1.587	1.292	1.108	2.936	2.272	1.851	1.507	3.605	2.790	2.518	2.158
	60°	1.948	1.432	1.360	1.228	2.518	2.051	1.670	1.587	3.254	2.790	2.392	2.051	3.995	3.254	3.091	2.790
	75°	2.272	1.758	1.758	1.670	2.650	2.392	2.051	2.051	3.254	3.091	2.790	2.518	4.205	3.425	3.425	3.254
	90°	2.392	2.051	1.948	1.948	2.790	2.518	2.272	2.272	3.425	3.091	2.936	2.650	4.205	3.605	3.605	3.605

Table 3.5 FOS calculated from numerical simulations in the case of Rock mass type 4.

R=4	D	10m				20m				30m				40m			
T	H / I	5m	10m	15m	20m	5m	10m	15m	20m	5m	10m	15m	20m	5m	10m	15m	20m
2m	45°	2.051	1.228	0.292	0.292	2.272	1.670	1.360	1.053	3.091	2.158	1.587	1.360	3.254	2.518	2.051	1.758
	60°	2.518	1.670	1.292	1.166	2.518	2.158	1.758	1.507	3.605	2.650	2.158	1.948	3.605	2.936	2.518	2.272
	75°	2.790	2.051	1.587	1.587	2.650	2.392	2.158	1.948	3.795	2.936	2.518	2.392	3.605	3.254	2.936	2.650
	90°	2.936	2.272	1.851	1.851	2.650	2.518	2.272	2.051	3.795	3.091	2.518	2.518	3.795	3.254	2.936	2.650
3m	45°	1.851	1.166	0.307	0.277	2.158	1.670	1.292	1.053	2.936	2.051	1.587	1.360	3.091	2.518	2.051	1.670
	60°	2.272	1.587	1.228	1.166	2.392	2.051	1.758	1.507	3.254	2.518	2.051	1.851	3.425	2.936	2.518	2.158
	75°	2.650	1.948	1.587	1.587	2.518	2.272	2.051	1.851	3.605	2.790	2.392	2.272	3.425	3.091	2.790	2.518
	90°	2.790	2.158	1.758	1.758	2.518	2.392	2.272	2.051	3.605	2.936	2.518	2.392	3.605	3.254	2.936	2.650
4m	45°	1.758	1.108	0.307	0.277	1.948	1.587	1.228	0.397	2.790	2.051	1.587	1.292	2.936	2.392	1.948	1.670
	60°	2.158	1.507	1.166	1.166	2.272	1.948	1.670	1.432	3.091	2.518	2.051	1.851	3.254	2.790	2.392	2.158
	75°	2.392	1.851	1.507	1.507	2.392	2.158	2.051	1.851	3.254	2.790	2.392	2.272	3.254	3.091	2.790	2.518
	90°	2.518	2.051	1.758	1.758	2.392	2.272	2.158	2.051	3.425	2.790	2.392	2.392	3.425	3.091	2.790	2.650
5m	45°	1.587	1.053	0.292	0.277	1.851	1.507	1.228	0.358	2.650	1.948	1.507	1.292	2.936	2.272	1.948	1.670
	60°	1.948	1.507	1.166	1.108	2.158	1.851	1.587	1.432	2.936	2.392	1.948	1.758	3.091	2.650	2.392	2.051
	75°	2.272	1.758	1.507	1.432	2.158	2.051	1.948	1.758	3.091	2.650	2.272	2.158	3.254	2.936	2.650	2.392
	90°	2.392	2.051	1.758	1.758	2.272	2.158	2.158	1.948	3.254	2.650	2.392	2.272	3.254	2.936	2.790	2.518

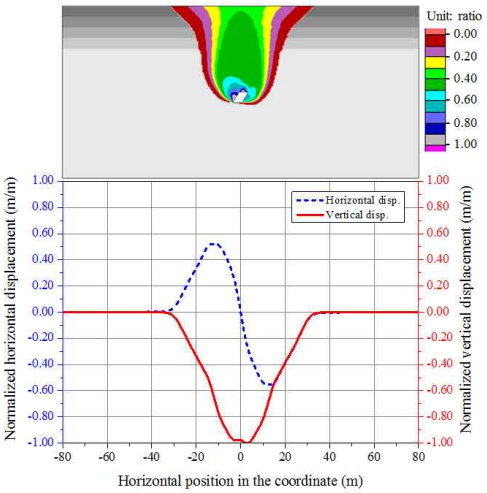

(a) R = 1

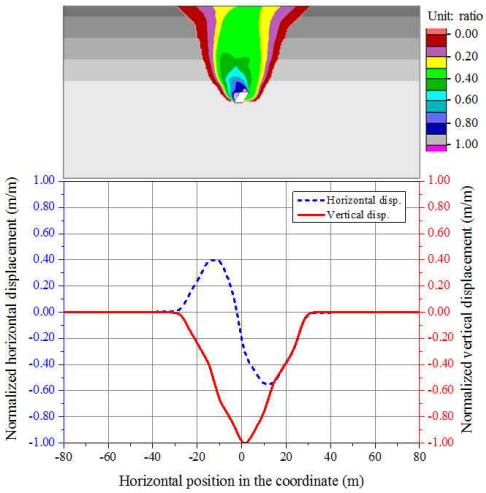

(b) R = 2

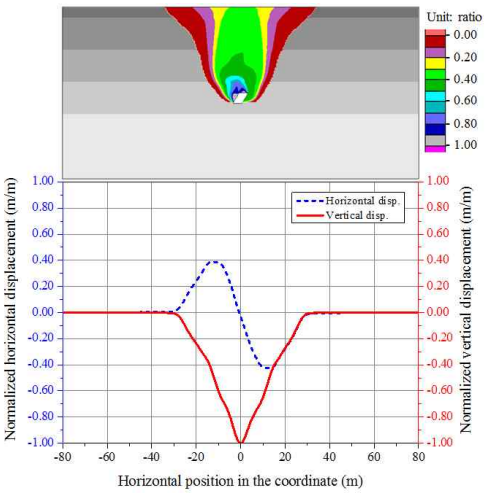

(c) R = 3

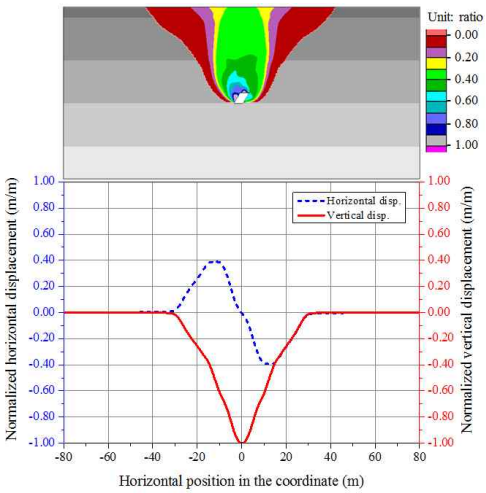

(d) R = 4

Figure 3.11 Normalized vertical and horizontal displacement according to change of the rock mass type (R) when D, H, T and I were fixed to 40m, 5m, 4m and 60°, respectively. The FOSs were calculated as (a) 9.076, (b) 7.392, (c) 4.205, and (d) 3.254.

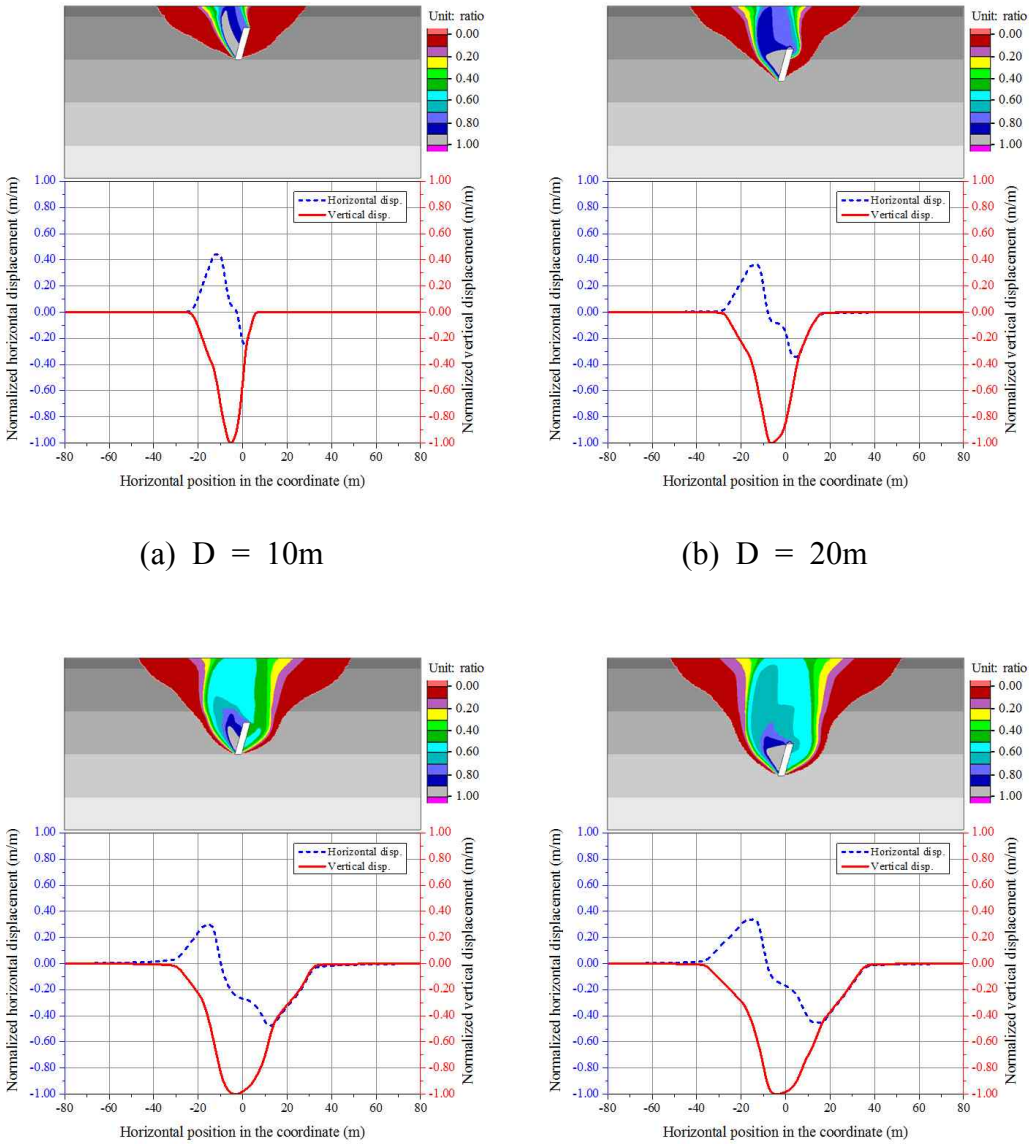

(a) D = 10m (b) D = 20m

(c) D = 30m (d) D = 40m

Figure 3.12 Normalized vertical and horizontal displacement according to change of the depth of cavity (D) when R, H, T and I were fixed to 4, 15m, 3m and 75°, respectively. The FOSs were calculated as (a) 1.587, (b) 2.051, (c) 2.392, and (d) 2.790.

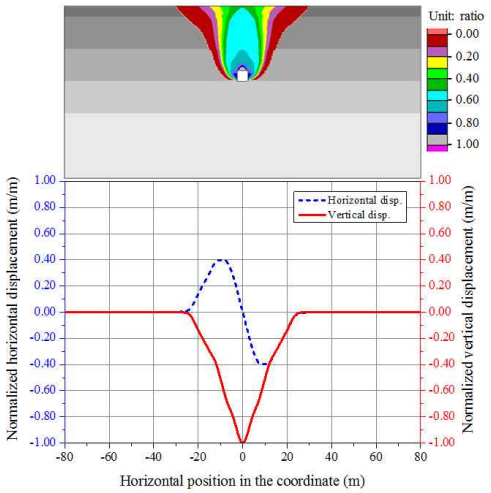

(a) H = 5m

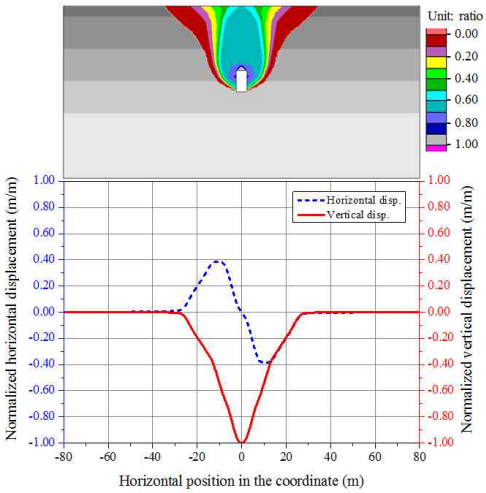

(b) H = 10m

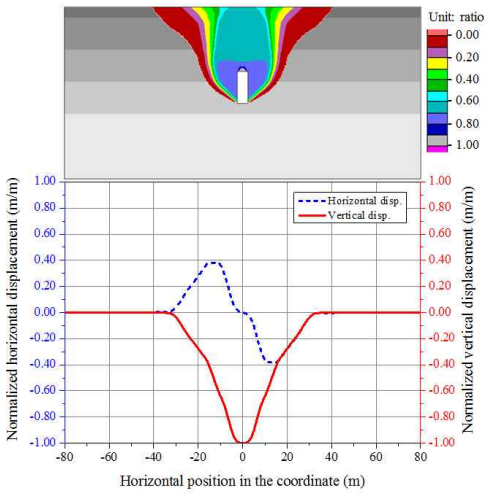

(c) H = 15m

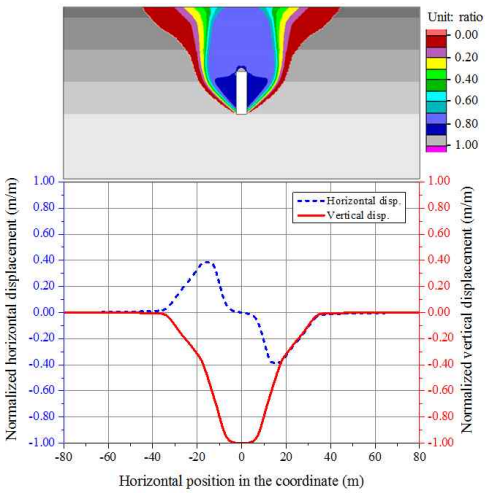

(d) H = 20m

Figure 3.13 Normalized vertical and horizontal displacement according to change of the height of cavity (H) when R, D, T and I were fixed to 3, 30m, 5m and 90°, respectively. The FOSs were calculated as (a) 3.425, (b) 3.091, (c) 2.936, and (d) 2.650.

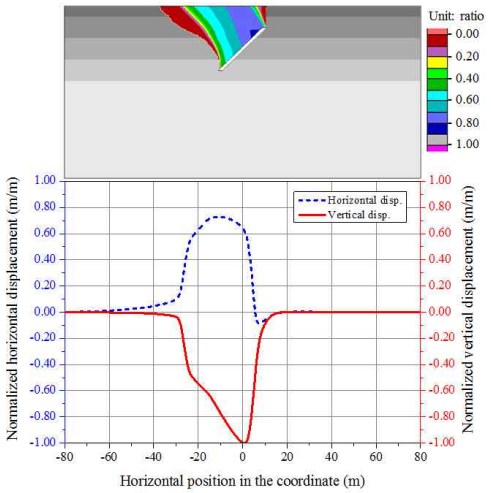

(a) T = 10m

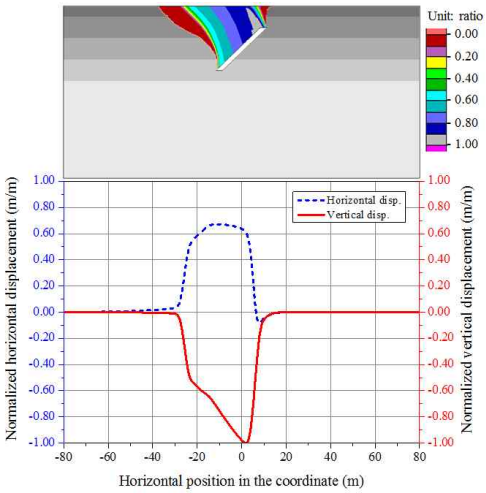

(b) T = 20m

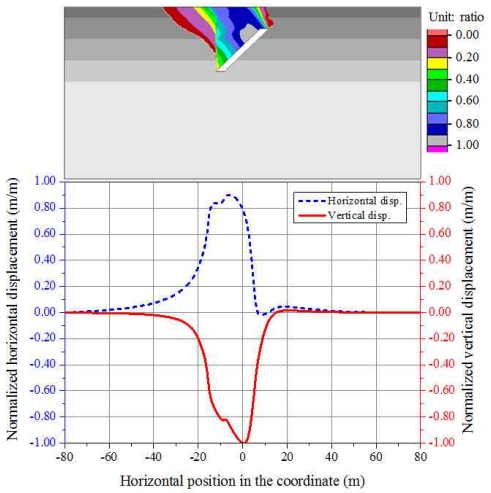

(c) T = 30m

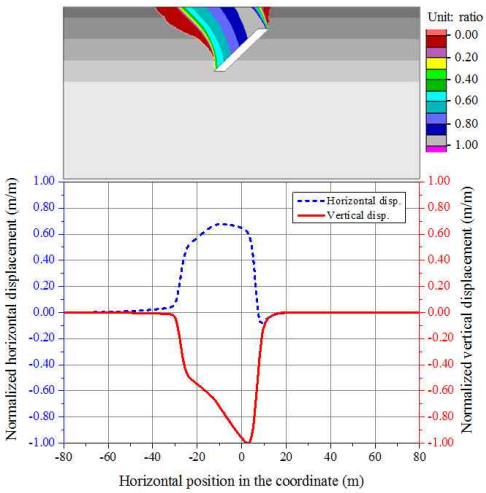

(d) T = 40m

Figure 3.14 Normalized vertical and horizontal displacement according to change of the thickness of cavity (T) when R, D, H and I were fixed to 2, 10m, 20m and 45°, respectively. The FOSs were calculated as (a) 1.053, (b) 1.053, (c) 0.663, and (d) 0.463.

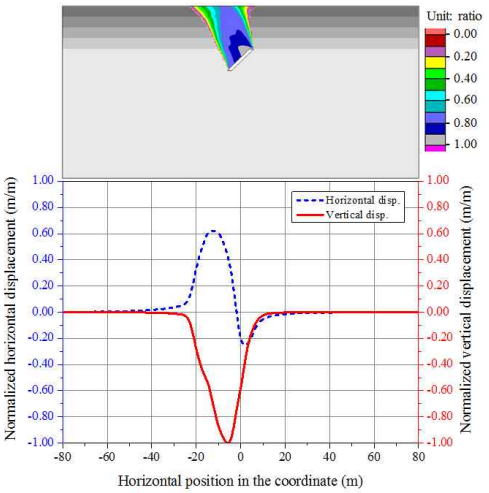

(a) I = 45°

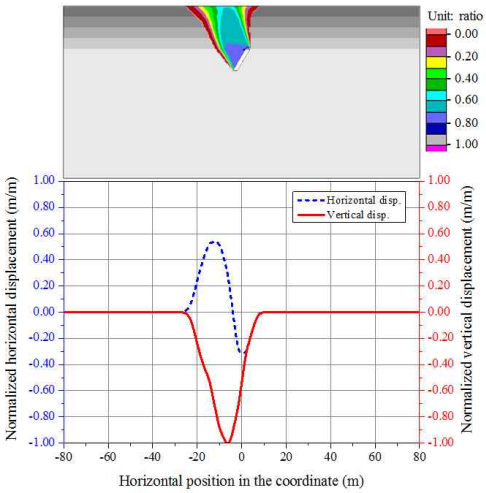

(b) I = 60°

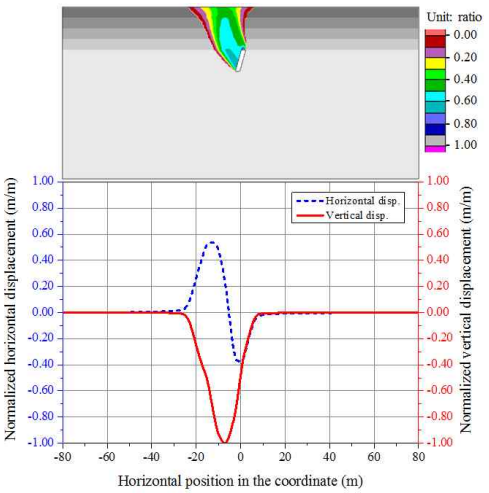

(c) I = 75°

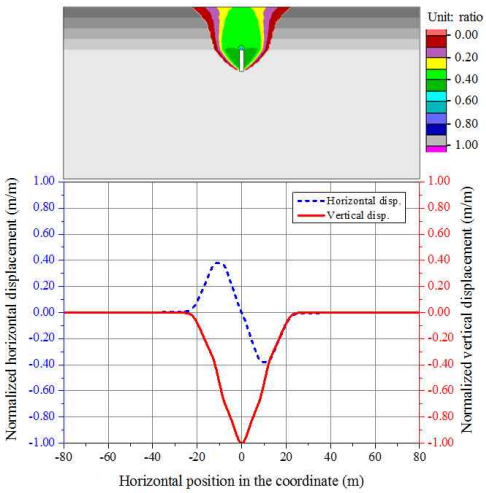

(d) I = 90°

Figure 3.15 Normalized vertical and horizontal displacement according to change of the inclination of cavity (I) when R, D, H and T were fixed to 1, 20m, 10m and 2m, respectively. The FOSs were calculated as (a) 4.426, (b) 6.021, (c) 7.023, and (d) 7.781.

4. Assessment of subsidence risk

This chapter deals with the development process of assessment technique for subsidence risk based on the results of numerical simulations. This chapter consists of three main subjects: (ⅰ) the method for evaluation of FOS and SRL using by regression analysis, (ⅱ) the assumption and technique for estimation of influence area on surface, and (ⅲ) the method for consideration of interaction effect between multiple cavities.

4.1 Determination of subsidence risk level

To construct the assessment method for the SRL, an analysis of the FOS is essential because the SRL is calculated from the FOS by using the simple equation as introduced in Section 3.1. In addition, a commercial statistic software, SPSS, was used.

4.1.1 Effect of influence factors on FOS

In order to check the relationship between the FOS and influence factors, a descriptive statistic analysis was performed. The standard deviation, average, minimum and maximum values, and 25^{th} and 75^{th} percentiles are listed in Table 4.1 to 4.5. These results also can be represented by a box-plot as depicted in Figure 4.1(a) to 4.5(a). The top and bottom of the boxes indicate the 25^{th} and 75^{th} percentile values, respectively, and the maximum and minimum values are marked at top and bottom of the vertical lines, respectively. The dotted line was created by curve fitting of its mean

values. In addition, the standard deviations of each case are plotted by a histogram, as shown in Figure 4.1(b) to 4.5(b).

From the fitting lines, it was revealed that the FOS increases with the depth and inclination of cavity, whereas the FOS decreases with the increase of the rock mass type and height and thickness of cavity. The reasons for this relationship might be deduced as follows. First, the FOS is in inverse proportion to the rock mass type because a larger R value represents relatively weak conditions of rock mass in this study (Figure 4.1). Second, the FOS increases with the depth of cavity because the assumption explained in Section 3.3.2 was applied and the amount of rock mass between the cavity and surface was enlarged (Figure 4.2). Third, the increases of the height and thickness of cavity reduce the FOS because the product of the two variables means the area of cavity in 2-dimensional cases (Figure 4.3 and 4.4). Finally, the FOS increases with the inclination of cavity because the horizontal width of cavity (i.e., horizontal distance between two ends of cavity) becomes smaller when the value of its inclination is higher (Figure 4.5).

Table 4.1 Statistical results of the FOS according to the change of rock mass type (R).

R	Statistics of FOS					
	S.D.	Mean	Min.	25%	75%	Max.
1	2.257	5.596	1.292	3.652	7.023	10.586
2	1.688	3.736	0.463	2.392	4.904	8.622
3	0.930	2.576	0.307	1.948	3.254	4.904
4	0.731	2.184	0.277	1.758	2.650	3.795

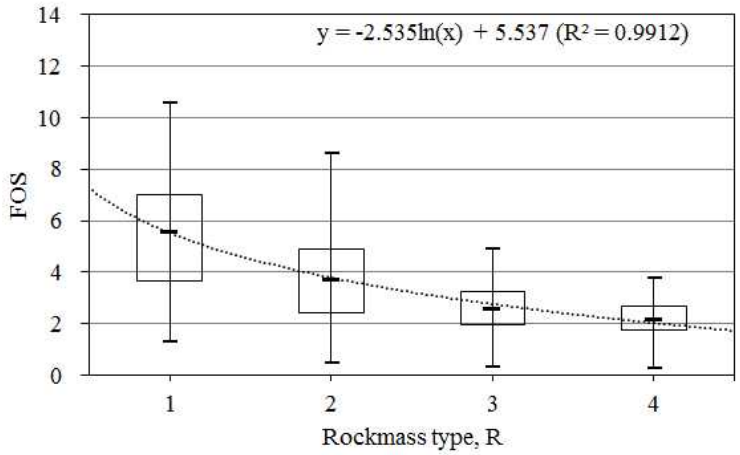

(a) box-plot

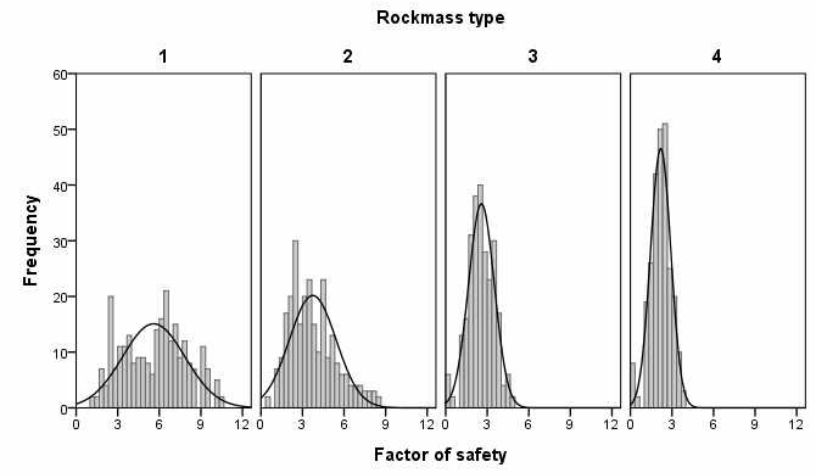

(b) histogram

Figure 4.1 Relationship between the FOS and rock mass type.

Table 4.2 Statistical results of the FOS according to the change of depth of cavity (D).

D	Statistics of FOS					
	S.D.	Mean	Min.	25%	75%	Max.
1	0.820	2.024	0.277	1.507	2.518	4.426
2	1.702	3.171	0.358	2.051	3.605	9.076
3	2.097	4.131	1.292	2.650	4.904	10.586
4	2.033	4.766	1.670	3.091	6.338	10.056

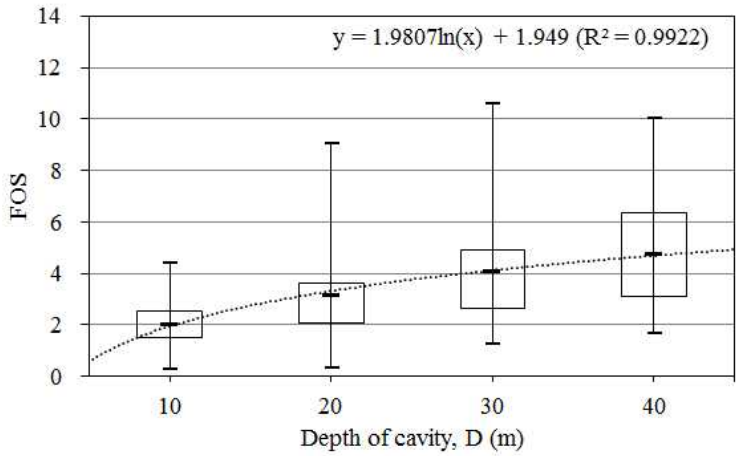

(a) box-plot

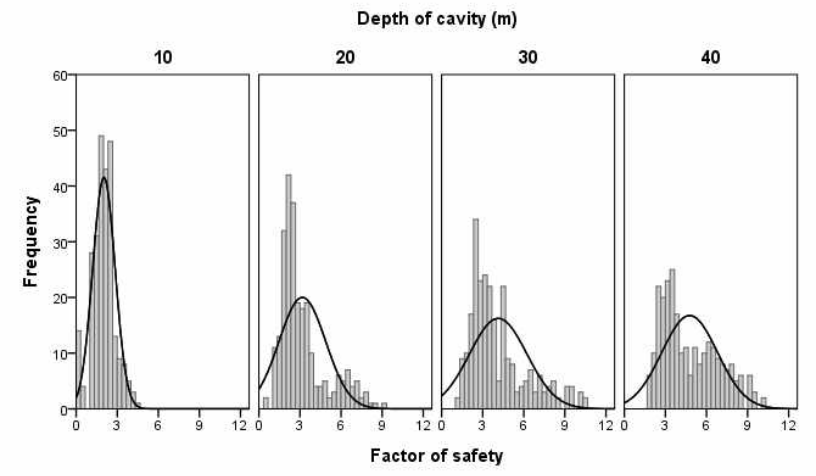

(b) histogram

Figure 4.2 Relationship between the FOS and depth of cavity.

Table 4.3 Statistical results of the FOS according to the change of height of cavity (H).

H	Statistics of FOS					
	S.D.	Mean	Min.	25%	75%	Max.
1	2.425	4.422	1.587	2.650	5.434	10.586
2	1.966	3.647	1.053	2.158	4.843	8.622
3	1.713	3.166	0.292	1.948	4.205	7.392
4	1.523	2.856	0.277	1.692	3.795	6.338

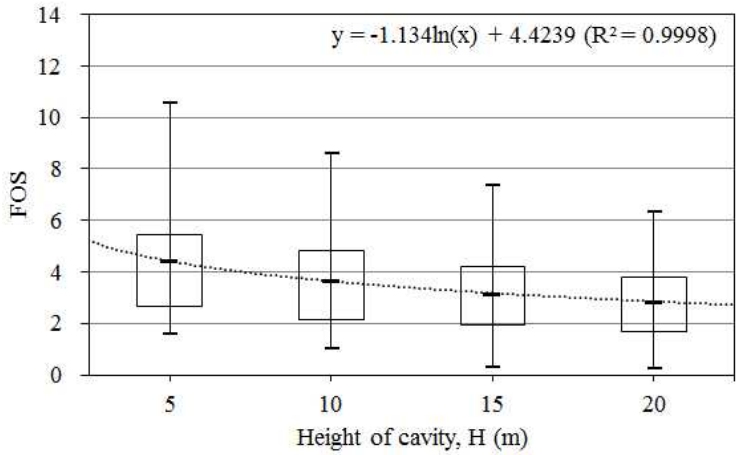

(a) box-plot

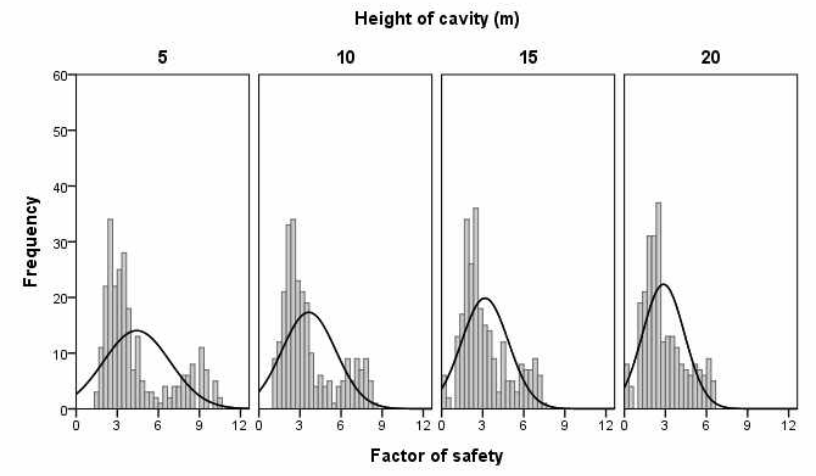

(b) histogram

Figure 4.3 Relationship between the FOS and height of cavity.

Table 4.4 Statistical results of the FOS according to the change of thickness of cavity (T).

T	Statistics of FOS					
	S.D.	Mean	Min.	25%	75%	Max.
1	2.156	3.769	0.292	2.272	4.843	10.586
2	2.050	3.601	0.277	2.158	4.601	10.056
3	1.967	3.440	0.277	2.051	4.426	9.553
4	1.883	3.281	0.277	1.974	4.205	9.076

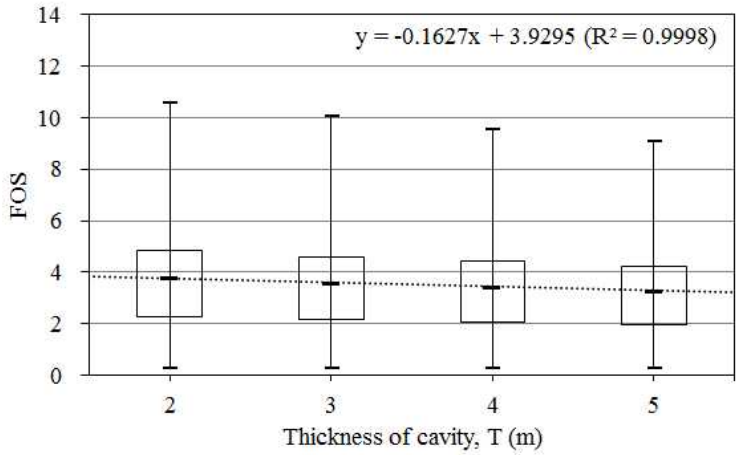

(a) box-plot

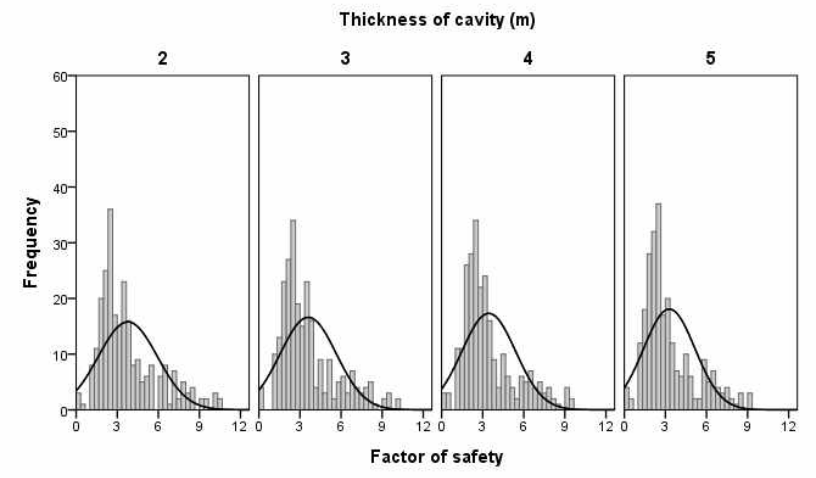

(b) histogram

Figure 4.4 Relationship between the FOS and thickness of cavity.

Table 4.5 Statistical results of the FOS according to the change of inclination of cavity (I).

I	Statistics of FOS					
	S.D.	Mean	Min.	25%	75%	Max.
1	1.839	2.720	0.277	1.587	3.425	9.553
2	1.934	3.413	1.108	2.051	4.371	10.056
3	2.009	3.870	1.432	2.392	5.098	10.586
4	2.036	4.088	1.758	2.518	5.434	10.586

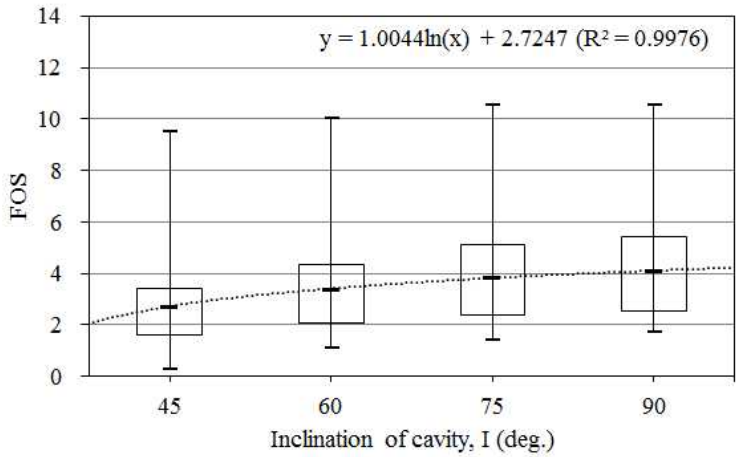

(a) box-plot

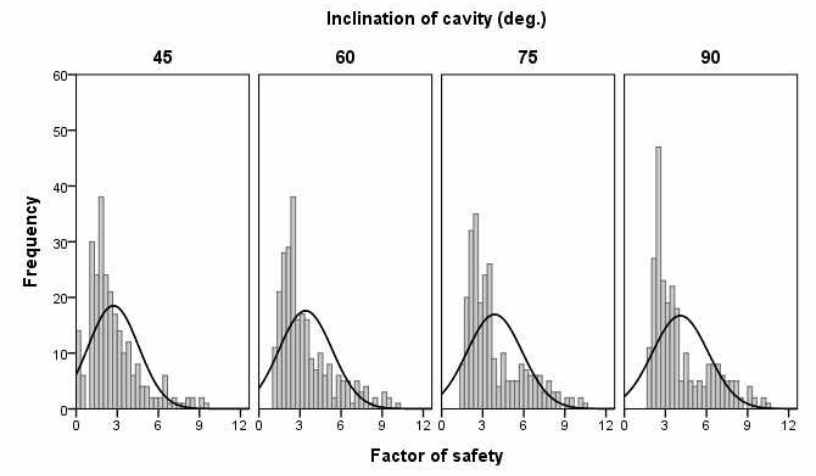

(b) histogram

Figure 4.5 Relationship between the FOS and inclination of cavity.

4.1.2 Regression analysis

Regression analysis was performed to construct an assessment model that can quantitatively estimate the value of FOS based on the numerical simulations. In general, regression analysis is divided into two basic equation models: linear and non-linear.

The linear regression model is simple and useful when the relationship between the independent and dependent variables is linear. Prior to the linear regression analysis, a correlation analysis was carried out to check a linearity of the FOS and five factors. Among generally used correlation methods, such as Pearson, Kendall and Spearman, the Pearson correlation coefficient is selected in this study because it is widely used to measure the degree of linear relationships. The correlation coefficients between the FOS and influence factors are shown in Table 4.6.

Table 4.6 Correlation coefficient between FOS and influence factors.

Variables	Pearson correlation coefficient					
	1	2	3	4	5	6
1. Rock mass type	1					
2. Depth of cavity	.000	1				
3. Height of cavity	.000	.000	1			
4. Thickness of cavity	.000	.000	.000	1		
5. Inclination of cavity	.000	.000	.000	.000	1	
6. FOS	-.630*	.508*	-.286*	-.090*	.252*	1

*Correlation is significant at the 0.01 level (2-tailed)

As a result, the FOS has a strong relationship with the rock mass type, a medium one with the depth of cavity, and weak ones with the other factors. These relationships were similar with the relative importance of influential factors derived by Jung et al. (2010), even if the most influential factor is the mining depth in their study. A reason for this difference might be concluded that the numerical model used in this model consists of the layered rock mass.

However, the interpretation just represents the strength of association between two variables; it does not account for the effect of influence factors on the FOS. A linear regression analysis can be more helpful to understand the effect. The basic equation of the linear regression model is defined as equation (4.1), and each coefficient was calculated as listed in Table 4.7.

$$FOS = c_0 + c_1 R + c_2 D + c_3 H + c_4 T + c_5 I \quad (4.1)$$

where c_i are coefficients of the linear model; R is the rock mass type used in this study; D is the depth of cavity in meters; H is the height of cavity in meters; T is the thickness of cavity in meters; and I is the inclination of cavity in degrees.

A coefficient of determination, which can be used for an indicator of fitness of regression model in statistic and denoted as R^2 or r^2, was calculated as 0.810. However, the linear regression model is unsuitable for representing the numerical simulations because the scatter-plot does not correspond to a 1:1 straight line, as shown in Figure 4.6.

Table 4.7 Estimated value of coefficients for linear regression model.

Coefficient	Estimated value	Std. Error	95% Confidence Interval	
			Lower bound	Upper bound
c0	3.886	0.179	3.534	4.237
c1	-1.140	0.025	-1.188	-1.091
c2	0.092	0.002	0.087	0.097
c3	-0.104	0.005	-0.113	-0.094
c4	-0.163	0.025	-0.211	-0.114
c5	0.030	0.002	0.027	0.034

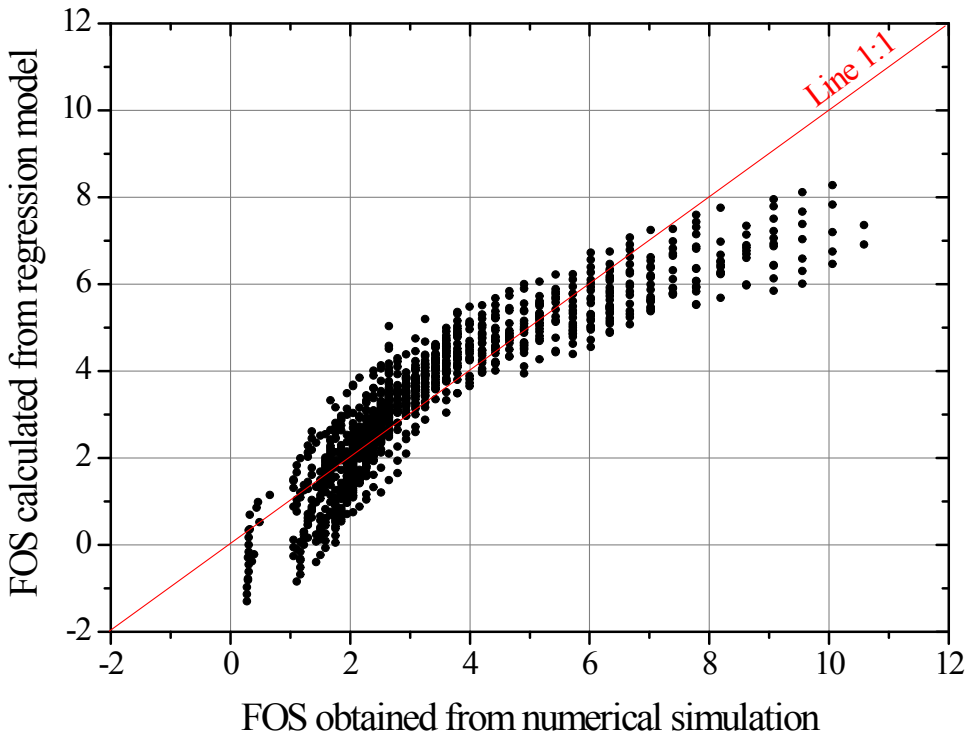

Figure 4.6 Scatter-plot of FOS obtained from numerical simulation and FOS calculated from linear regression model.

In addition, a non-linear regression analyse was carried out to improve the fitness of the linear regression model. Each independent variable was formulated by a power-law function, and the dependent variable was defined by a combination of the independent variables as expressed in equation (4.2).

$$FOS = c_0 \times R^{c_1} \times D^{c_2} \times H^{c_3} \times T^{c_4} \times I^{c_5} \quad (4.2)$$

where c_i are coefficients of the non-linear model; R is the rock mass type used in this study; D is the depth of cavity in meters; H is the height of cavity in meters; T is the thickness of cavity in meters; and I is the inclination of cavity in degrees.

The coefficient of determination (r^2) was calculated as 0.917, and six coefficients for each variable were estimated as shown in Table 4.8. Figure 4.7 shows the scatter-plot of FOS estimated from the non-linear regression model and FOS obtained from the numerical simulation. The results show that non-linear regression model is more suitable than the linear model in this case.

Table 4.8 Estimated value of coefficients for non-linear regression model.

Coefficient	Estimated value	Std. Error	95% Confidence Interval	
			Lower bound	Upper bound
c0	0.284	0.026	0.234	0.334
c1	-0.678	0.009	-0.696	-0.661
c2	0.608	0.011	0.586	0.63
c3	-0.313	0.008	-0.33	-0.297
c4	-0.146	0.013	-0.172	-0.121
c5	0.471	0.018	0.435	0.508

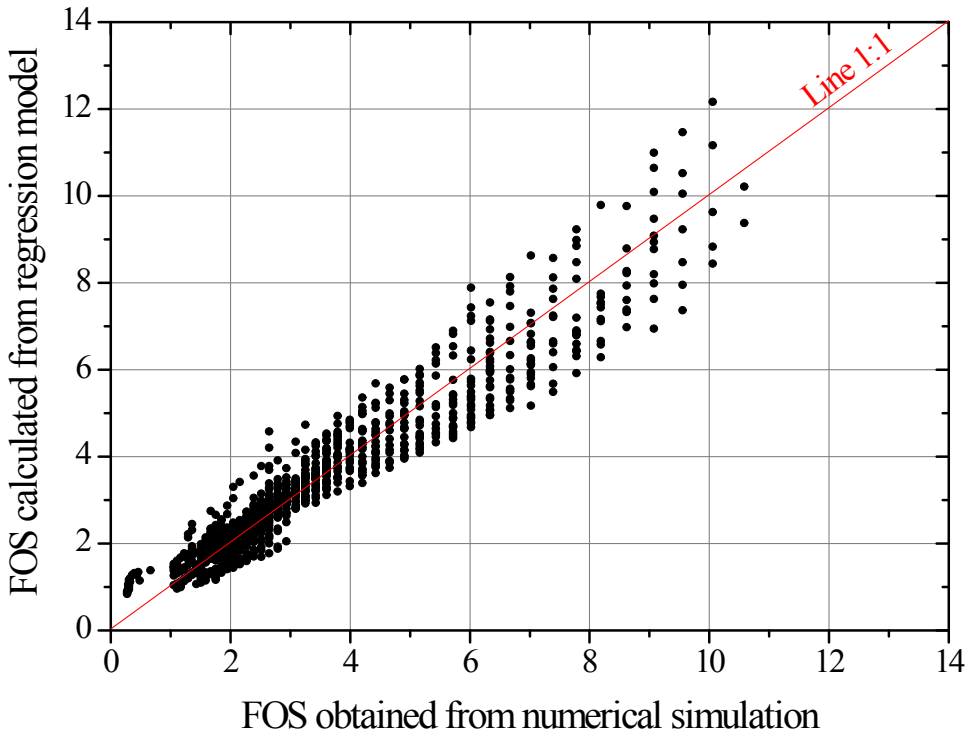

Figure 4.7 Scatter-plot of FOS obtained from numerical simulation and FOS calculated from non-linear regression model.

However, the non-linear regression model, as shown in equation (4.2), has two limitations in applying to practical cases. One is that the FOS is calculated as '0' when a cavity is horizontal, which means the inclination (I) is set to zero, because the equation is expressed in the multiplication of the independent variables. The other is that the definition of the height (H) and thickness (T) of cavity, explained in Subsection 3.3.2, may be confusable when a cavity is horizontal or gently inclined as shown in Figure 4.8.

In order to solve these problems, two ancillary variables were defined as shown in Figure 4.9, and they can also represent the shape of a cavity in the same way that the H and T define it. A cross section of a cavity was simplified as a parallelogram as mentioned in Subsection 3.3.2, which consists of two axes; major (long) and minor (short). The length of major and minor axes of a cavity were denoted by 'L' and 'S' in this study. In addition, the inclination (I) of cavity was defined by an angle between the major axis (L) and the horizon.

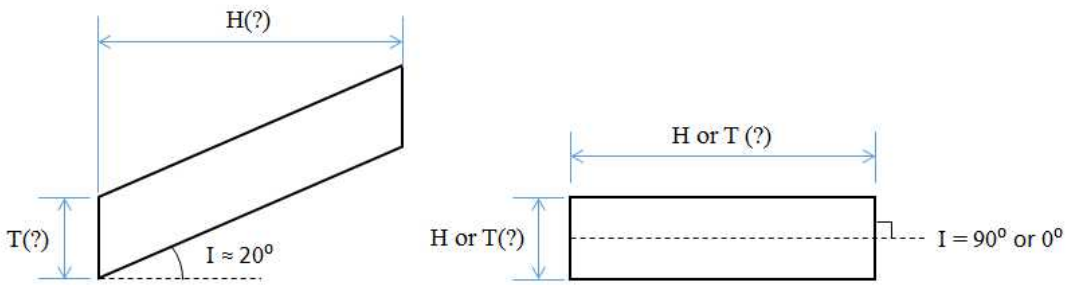

Figure 4.8 Illustrates confusions about a definition of height (H), thickness (T), and inclination (I) of a cavity which is gently inclined or horizontal.

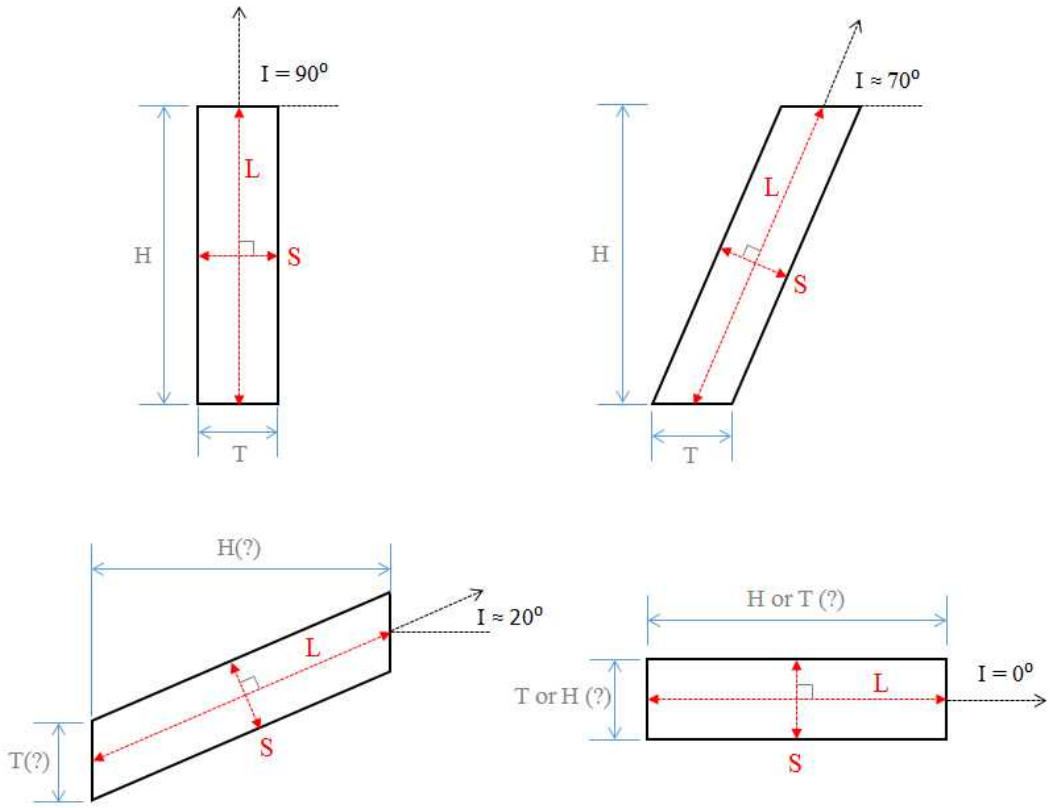

Figure 4.9 Two ancillary variables defining a shape of cavity according to the major and minor axes. L and S are the length of major and minor axes, respectively.

A non-linear regression model was derived by replacing the variables of H and T with the alternative variables of L and S, such as equation (4.3). The coefficient of determination was calculated as 0.916, and the estimated coefficients of each variable are listed in Table 4.9.

$$FOS = c_0 \times R^{c_1} \times D^{c_2} \times L^{c_3} \times S^{c_4} \times \exp(c_5 I) \qquad (4.3)$$

where R is the rock mass type defined in this study; D is the depth of

cavity; L is the length of major axis of cavity; S is the length of minor axis of cavity; I is the inclination of cavity; and c_i are coefficients.

Table 4.9 Estimated value of coefficients for non-linear regression model modified by considering the major and minor axes of a cavity.

Coefficient	Estimated value	Std. Error	95% Confidence Interval	
			Lower bound	Upper bound
c0	1.420	0.071	1.280	1.560
c1	-0.678	0.008	-0.695	-0.662
c2	0.609	0.009	0.591	0.626
c3	-0.317	0.011	-0.339	-0.295
c4	-0.137	0.013	-0.163	-0.112
c5	0.006	0.000	0.005	0.006

Because the FOS is dimensionless, the variables of L and S could be normalized by the variable of D as shown in equation (4.4), thereby the number of constants was reduced. The coefficient of determination was calculated as 0.911, and the estimated coefficients of each variable are listed in Table 4.10.

$$FOS = c_0 \times R^{c_1} \times \left(\frac{D}{L}\right)^{c_2} \times \left(\frac{D}{S}\right)^{c_3} \times \exp(c_4 I) \tag{4.4}$$

where R is the rock mass type defined in this study; D is the depth of cavity in meters; L is the length of major axis of cavity in meters; S is the length of minor axis of cavity in meters, I is the inclination of cavity in degrees; and c_i are coefficients.

Table 4.10 Estimated value of coefficients for non-linear regression model modified by considering the major and minor axes of a cavity and normalized by the depth of cavity.

Coefficient	Estimated value	Std. Error	95% Confidence Interval	
			Lower bound	Upper bound
c0	1.905	0.064	1.779	2.030
c1	-0.679	0.009	-0.697	-0.661
c2	0.347	0.008	0.332	0.363
c3	0.211	0.010	0.191	0.230
c4	0.006	0.000	0.005	0.007

Figure 4.10 shows the scatter-plot of FOS estimated from the non-linear regression model (Eq. 4.4) and FOS obtained from the numerical simulation. Most of the dots are distributed around 1:1 line, which means that the equation can be suitable to estimate the FOS of numerical simulation.

In order to validate an applicability of the regression model for the horizontal or gently inclined cavity, 48 cases of additional numerical simulation were carried out because the equation was generated from the results when the inclination of cavity is more than 45°. The additional simulation consists of three different inclination; 0°, 15°, and 30°. The blue empty dots in Figure 4.10 indicate the results of the additional simulations. As a result, equation (4.4) was selected as a final regression model for estimation of the FOS.

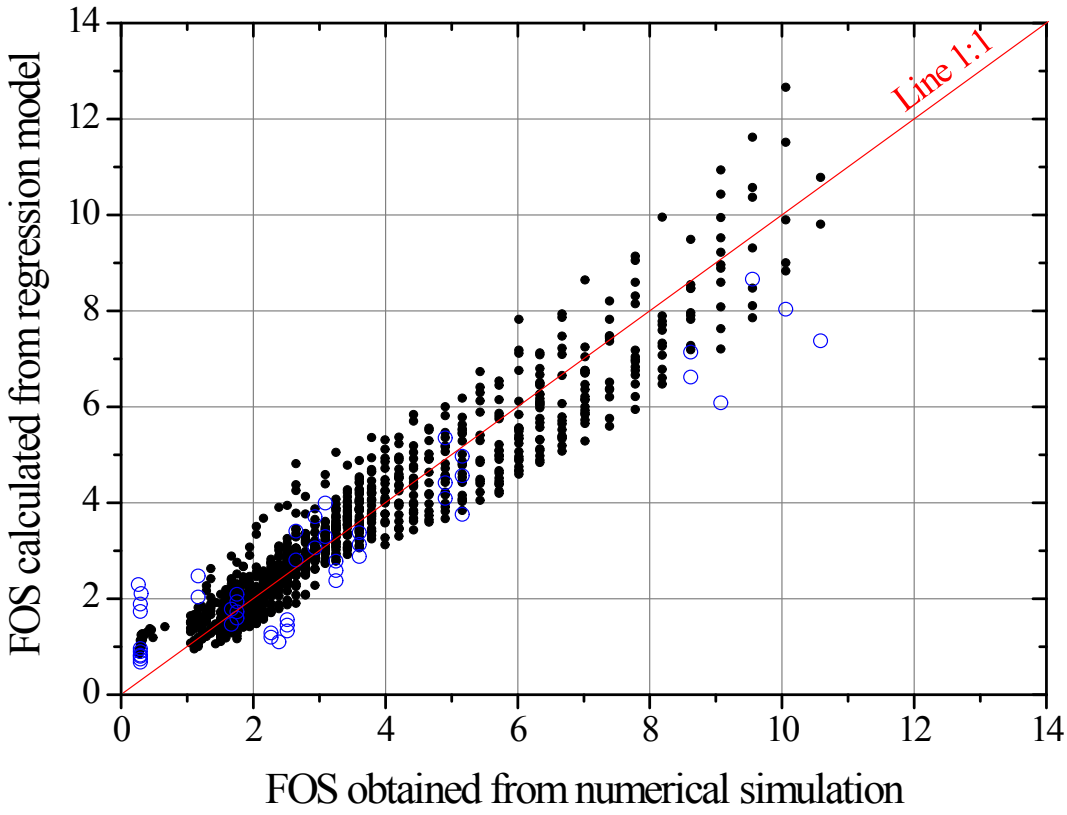

Figure 4.10 Scatter-plot of FOS obtained from numerical simulation and FOS calculated from final non-linear regression model: Black solid dots represent the cases when the inclination of cavity is more than 45°, and blue empty dots represent the cases when the inclination is less than 45°.

4.2 Determination of influence area

The values of FOS and SRL estimated from the final regression model indicate only a risk level, but do not provide information about the range of hazardous areas. In order to identify the subsidence risk area on the surface, the assessment of the influence area induced by the mined cavity is essential.

4.2.1 Definition of limit angle and influence area

In general, the influence area is defined by limit angle, sometimes referred to as angle of draw, and the angle has various ranges according to the inclination of cavity and rock mass conditions (Ren and Li, 2008; Harrison, 2011).

In this study, the influence area was defined as a range of surface whose amount of displacement vector is greater than 10 mm. As shown in Figure 4.11, the position of P1 is determined as a point where the absolute value of displacement vector firstly became larger than 10 mm by calculating from the left boundary. Likewise, the P2 is the right end of the influence area. Therefore, there are two limit angles according to the dip direction of the inclined cavity. One is downward limit angle (θ_1), defined by an angle between a vertical line and a line connecting the toe of the cavity and point P1. The other is upward limit angle (θ_2), defined by an angle between a vertical line and a line connecting the top right corner of the cavity and point P2.

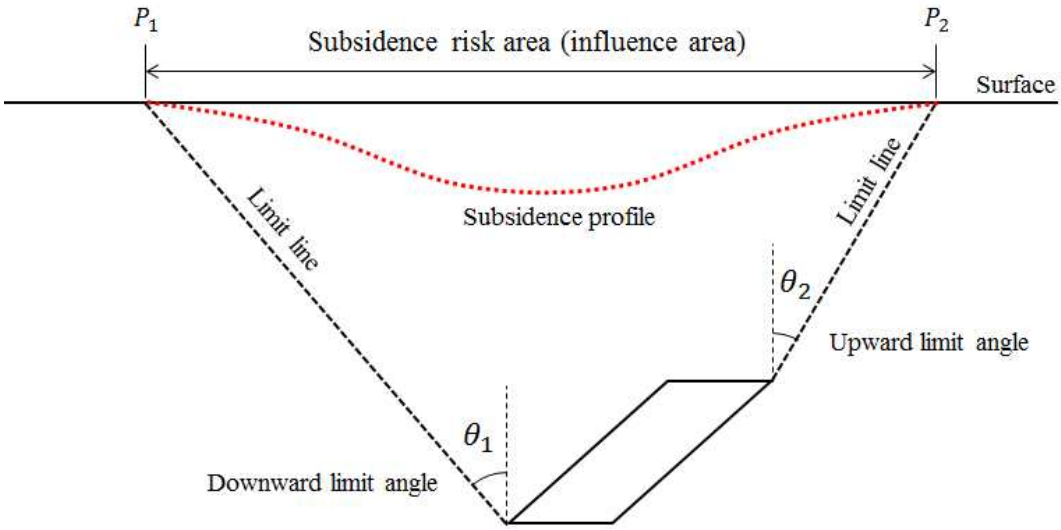

Figure 4.11 Schematic diagram explaining the definition of limit angles.

In order to extend the cross-sectional concept to a three-dimensional case, a projection technique was used. Figure 4.12 illustrates the cavity model and result of its projection. As described in Subsection 3.3.2, the simplified cavity model has an additional parameter, the width of cavity (W), although it was not included in the numerical simulation. The inclined parallelepiped cavity can be projected on the horizontal surface as shown in Figure 4.10(b). The points S1, S4, S5, and S6 could be calculated by applying the downward and upward limit angles, but others require an additional limit angle that defines the angle between $\overline{f'f}$ and $\overline{fS_7}$ in Figure 4.12(a). In this study, the additional angle was replaced by the upward limit angle (θ_2) because this numerical simulation is in two-dimensional.

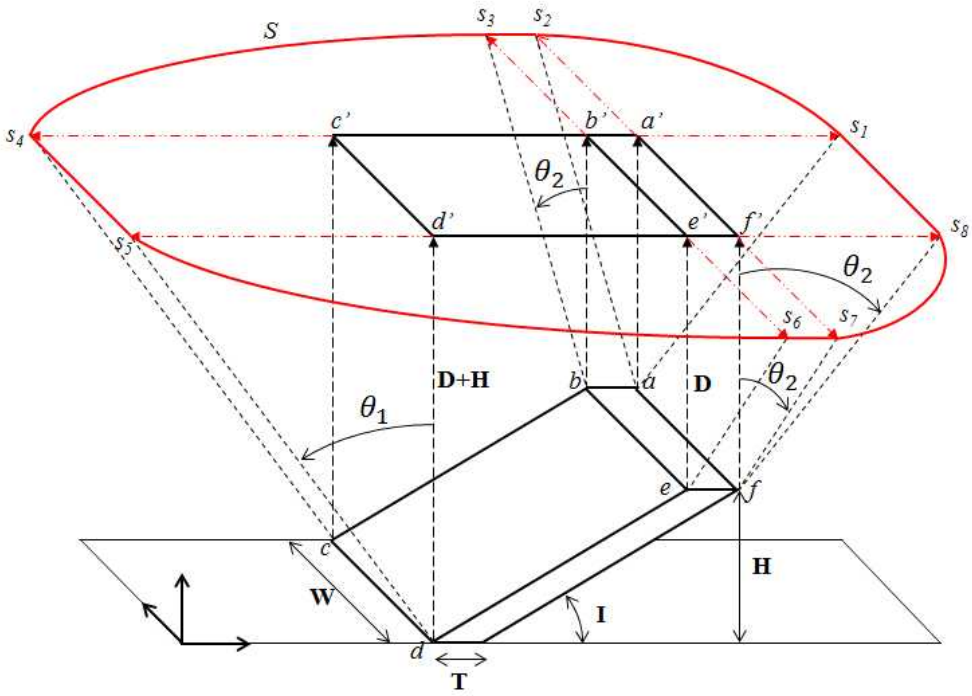

(a) Three-dimensional view

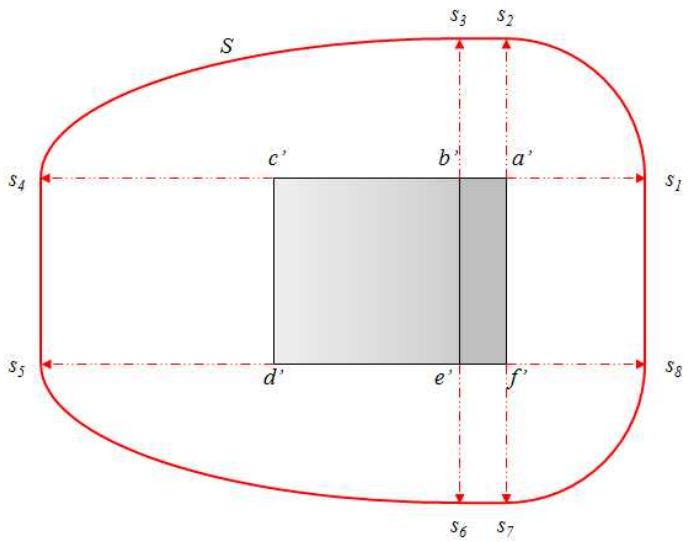

(b) Top view

Figure 4.12 Schematic diagram explaining the determination of subsidence risk area by using a projection technique.

4.2.2 Results and analysis

Figure 4.13 shows the simulation results of four cases according to the change of inclination of cavity. In this case, the downward limit angle (θ_1) slightly increases with increasing the inclination of cavity, but the upward limit angle (θ_2) is highly dependent on the change of inclination of cavity. In particular, it could be considered that the upward limit angle is neglected when the inclination reaches 90°, because the vertical and horizontal displacement are symmetric with respect to the center axis of cavity.

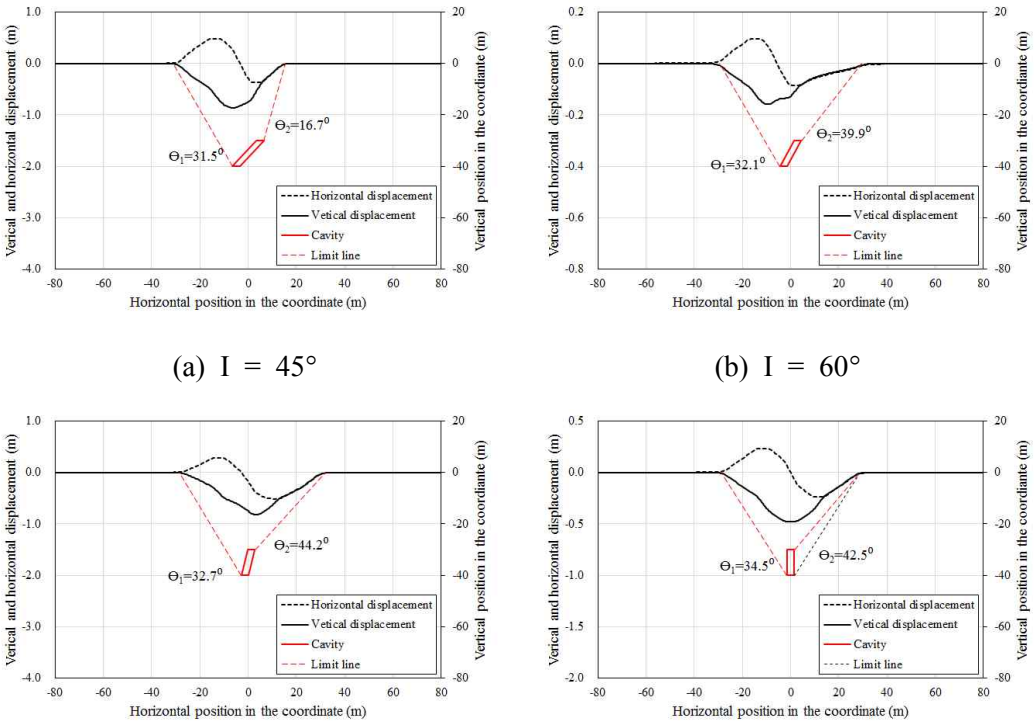

(a) I = 45° (b) I = 60°

(c) I = 75° (d) I = 90°

Figure 4.13 Calculated downward and upward limit angles (θ_1 and θ_2) according to the change of inclination of cavity (I) when R, D, H and T were fixed to 1, 30m, 10m, 3m, respectively.

In general, it is expected that the range of subsidence influence area is much wider than the space of cavity, especially in a continuous subsidence phenomenon, which means that the values of two limit angles are positive, such as shown in Figure 4.11. In this study, however, an abnormal ground movement was detected in a few cases. Figure 4.14 shows the results of unusual cases, and they can be divided into three categories.

The first is a set of cases that the upward limit angle (θ_2) is negative. As shown in Figure 4.14(a), the overall movement of surrounding rock mass is in the direction of the normal vector of the inclined cavity. The second is a set of cases that the collapse of cavity occurs partially at the roof of the cavity. The collapsed zone is formed in a limited depth which consists of relatively weak rock mass (Figure 4.14(b)). The last is a set of cases that the influence area is very narrow, especially in a vertical cavity. As shown in Figure 4.14(c), the ground movement is generated at a limited area when the cavity is vertical and shallow, and the surrounding rock mass is weak.

Overall, these abnormal types of subsidence mainly involve the vulnerable circumstances, such as weak overburden conditions. Although these results can not represent the entire of discontinuous subsidence phenomenon, the abnormal subsidence can be regarded as a particular case of the discontinuous subsidence.

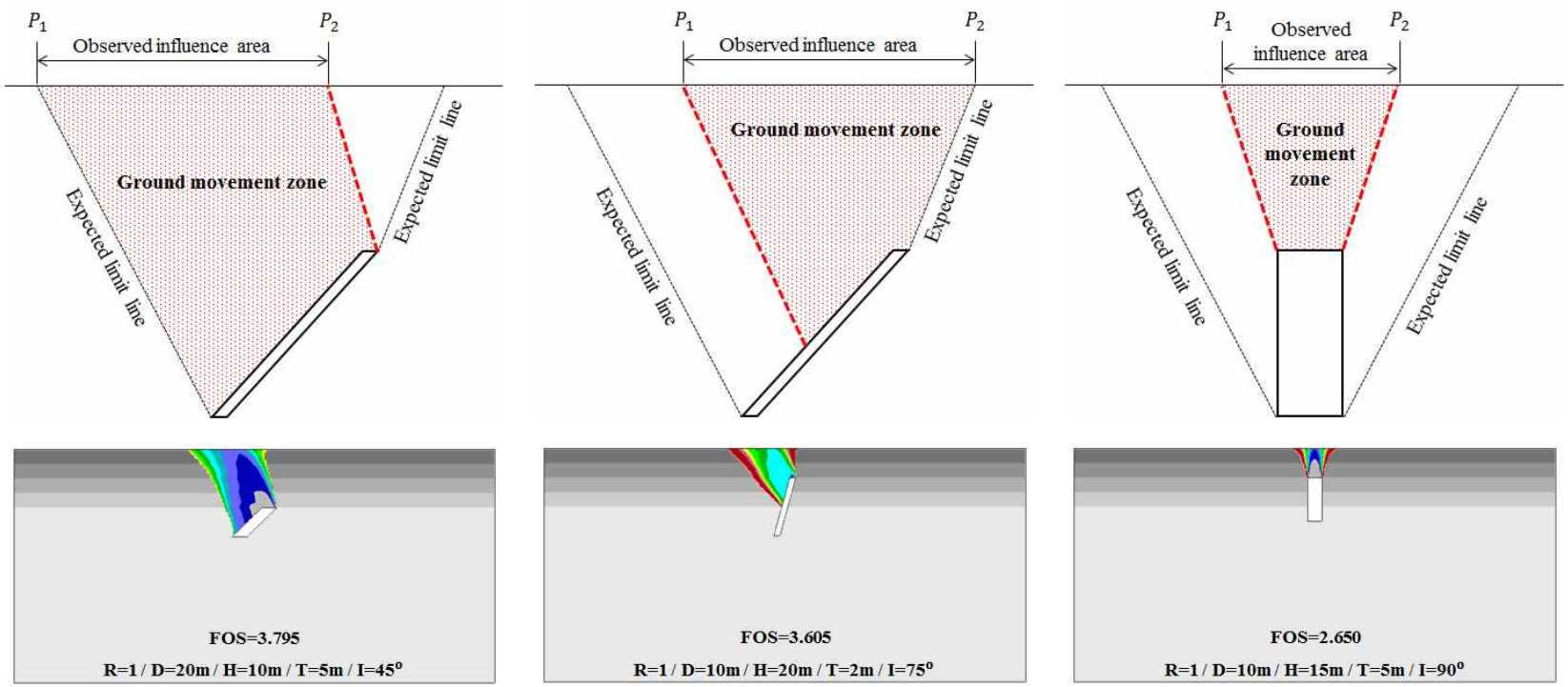

(a) A negative limit angle (b) A partially collapsed zone (c) A narrow zone

Figure 4.14 Illustration of abnormal ground movement in the numerical simulations and corresponding results. The type of ground movement (i.e., collapsed zone) is divided into three categories: (a) a case of negative limit angle, (b) a case of partially collapsed zone, and (c) a case of narrow zone.

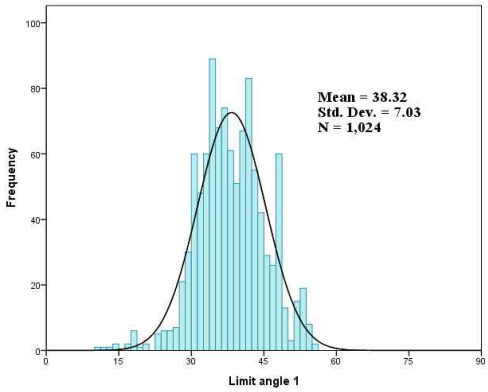

(a) Total

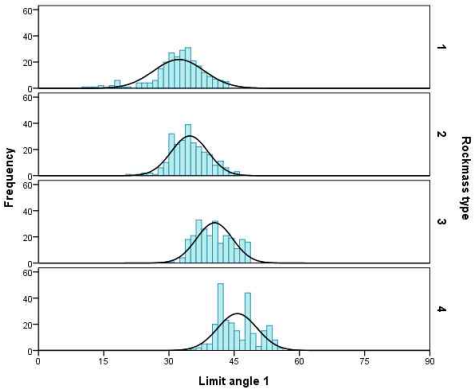

(b) Rock mass type

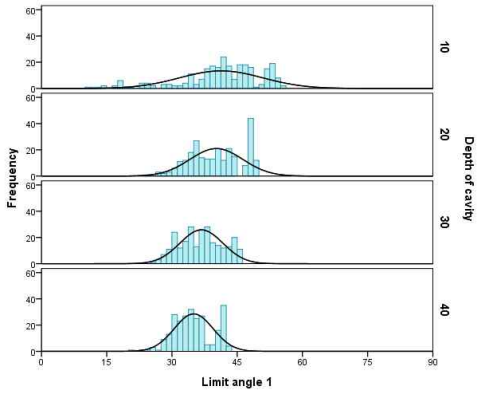

(c) Depth of cavity

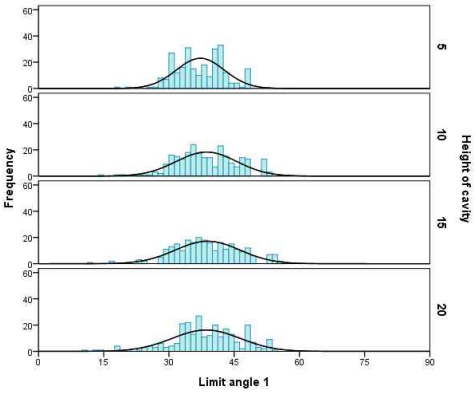

(d) Height of cavity

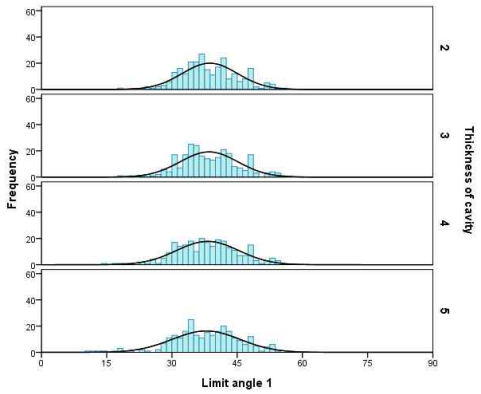

(e) Thickness of cavity

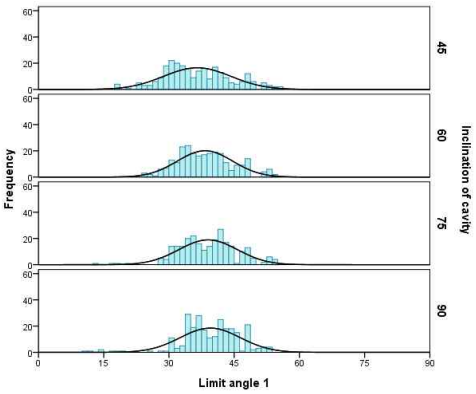

(f) Inclination of cavity

Figure 4.15 Histogram of downward limit angle (θ_1) according to the change of influence factors.

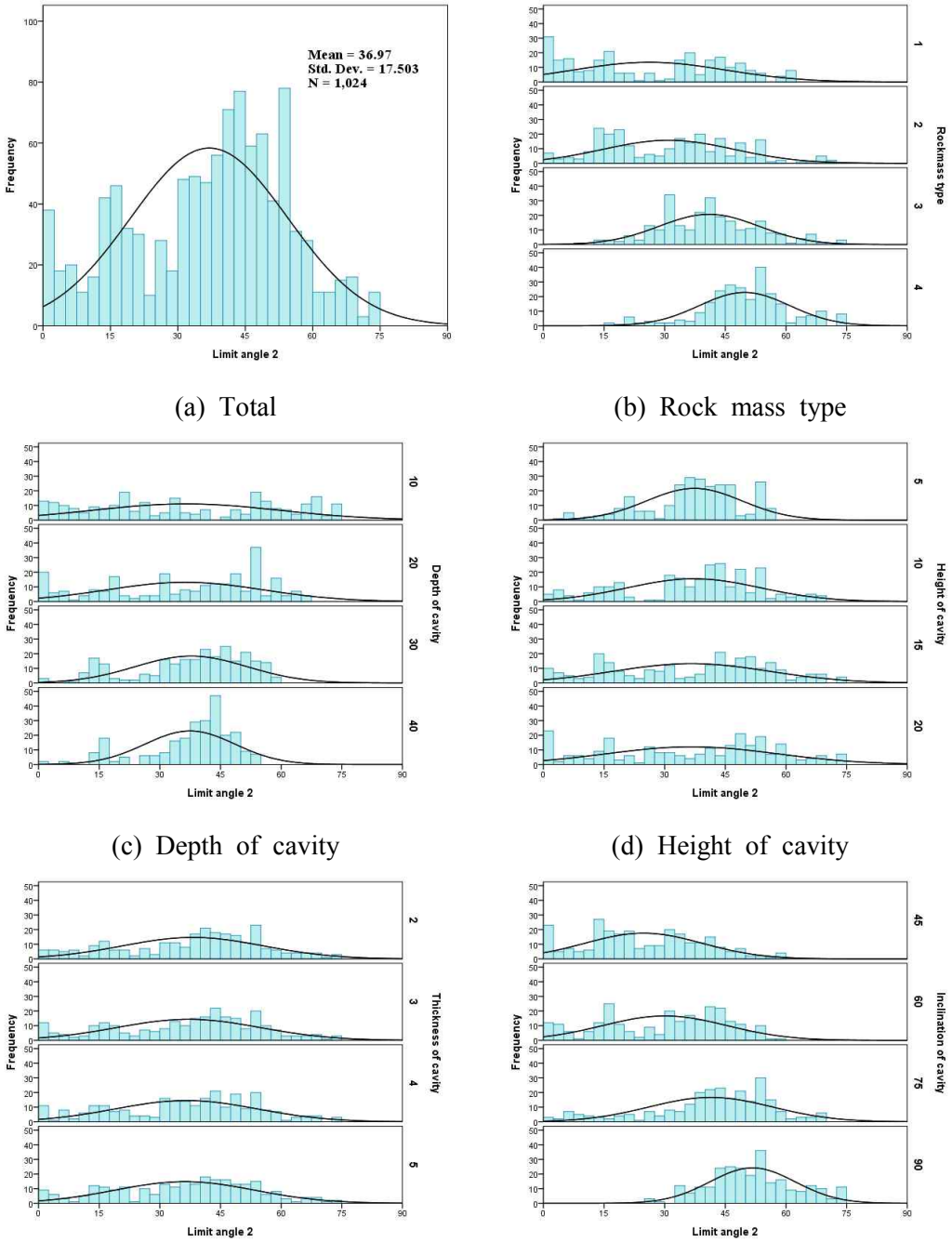

(a) Total

(b) Rock mass type

(c) Depth of cavity

(d) Height of cavity

(e) Thickness of cavity

(f) Inclination of cavity

Figure 4.16 Histogram of upward limit angle (θ_2) according to the change of influence factors.

Even though there are some unexpected cases, this study used full results for assessing the influence area. Figure 4.15 and 4.16 present the relationship of the limit angles with the five factors by drawing a histogram. The average and standard deviation were analyzed by 38.32 and 7.03, respectively, for the downward limit angle (θ_1), and 36.97 and 17.50, respectively, for the upward limit angle (θ_2), as shown in Figures 4.15(a) and 4.16(a), respectively. The effect of influence factors could be analyzed as follows.

Firstly, the rock mass type (R) significantly affects both downward and upward limit angles. The angles increase with increasing value of R. In other words, it was found that the influence area on surface widens by increasing of the rock mass type because the overall strength of the surrounding rock mass conditions in this study is relatively weak when the value of R is larger.

Secondly, the inclination of cavity (I) also affects the two limit angles similarly with the effect of the rock mass type. This phenomenon could be explained by the possible movements of rock mass and the geometrical shape of cavity as depicted in Figure 4.17. Assuming two differently inclined cavities, the movement of rock mass could be possible only in the region between the downward and upward limit lines for a moderately inclined cavity. For a highly inclined cavity, however, the additional movement might be induced in the lower region of the cavity. In addition, the downward limit angle might be increased in a highly inclined cavity because a perpendicular vector of cavity is extended toward the surface.

Finally, the downward limit angle is affected by the depth of cavity

(D), but the upward limit angle is not. In addition, the effects of other factors, height (H) and thickness (T) of cavity, were not found clearly from the histogram.

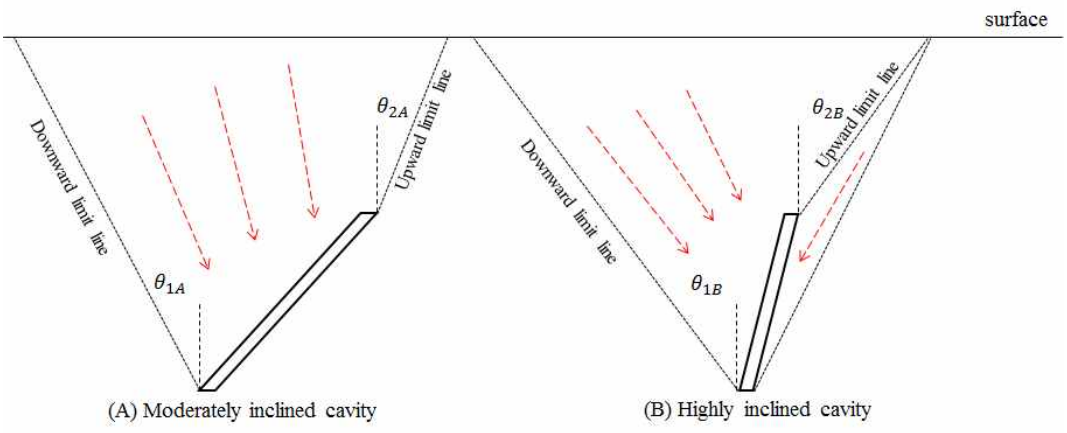

Figure 4.17 Schematic diagram explaining the effect of the inclination of cavity.

Table 4.11 Correlation coefficient between limit angles and influence factors.

Variables	Pearson correlation coefficient						
	1	2	3	4	5	6	7
1. Rock mass type	1	.000	.000	.000	.000	.732*	.516*
2. Depth of cavity		1	.000	.000	.000	-.355*	.028
3. Height of cavity			1	.000	.000	.068	-.016
4. Thickness of cavity				1	.000	-.046	-.043
5. Inclination of cavity					1	.154*	.590*
6. Limit angle 1						1	.546*
7. Limit angle 2							1

*Correlation is significant at the 0.01 level (2-tailed)

In order to assess the effect of the influence factors, the regression analysis was carried out. Similarly to the previous analysis explained in Section 4.1.2, the correlation analysis was performed, and each correlation coefficient is listed in Table 4.11. As a result, it was found that the downward limit angle (θ_1) is related with the rock mass type (R), depth (D), and inclination (I) of cavity at the significant level of 0.01. Meanwhile, the upward limit angle (θ_2) is related with the rock mass (R) and inclination (I) of cavity at the significant level of 0.001. In addition, the two limit angles are correlated with one another. Therefore, two basic formulae for the limit angles could be set up as follows:

$$\theta_1 = f(R, D, I) \tag{4.5}$$

$$\theta_2 = f(R, I, \theta_1) \tag{4.6}$$

A non-linear regression model for the downward limit angle (θ_1) is expressed as equation (4.7), and the coefficient of determination was calculated as 0.734. Meanwhile, the upward limit angle (θ_2) is expressed as equation (4.8), and the coefficient of determination was calculated as 0.642. Tables 4.12 and 4.13 show the estimated coefficients of the regression model for the downward and upward limit angles.

$$\theta_1 = c_0 R^{c_1} \exp(c_2 D) + c_3 I^{c_4} \tag{4.7}$$

$$\theta_2 = c_0 R^{c_1} \theta_1^{c_2} + c_3 I^{c_4} \tag{4.8}$$

Table 4.12 Estimated coefficients of non-linear regression model for the downward limit angle.

Coefficient	Estimated value	Std. Error	95% Confidence Interval	
			Lower bound	Upper bound
c0	4.242	0.576	3.113	5.372
c1	1.388	0.095	1.202	1.573
c2	-0.025	0.001	-0.028	-0.022
c3	15.953	1.105	13.785	18.122
c4	0.146	0.015	0.116	0.176

Table 4.13 Estimated coefficients of non-linear regression model for the upward limit angle.

Coefficient	Estimated value	Std. Error	95% Confidence Interval	
			Lower bound	Upper bound
c0	0.081	0.063	-0.042	0.204
c1	0.900	0.154	0.598	1.201
c2	1.219	0.180	0.866	1.573
c3	0.002	0.002	-0.002	0.007
c4	2.127	0.217	1.701	2.553

4.3 Consideration of multi-cavity effect

In previous sections, the methodologies for estimation of SRL and determination of subsidence hazard area have been explained when a single cavity exists only. However, there may be many cavities with different shapes and locations in the real field. In this condition, the subsidence phenomenon is influenced by multiple cavities; therefore, an assessment of interaction between cavities should be taken into account. The simplest way to evaluate multi-cavity interaction is the superposition theorem in the conventional subsidence prediction model because it estimates the mechanical behavior of ground surface, such as displacement and strain. However, the superposition is no longer effective when the risk is mainly concerned, so an additional evaluating method is needed.

4.3.1 Multi-cavity model

Additional numerical models having more than two cavities were generated. Because the main purpose of this simulation is to assess the effects of multiple cavities on each other, the spatial distribution feature of cavities is considered as major parameter. In order to represent this feature, the rock mass type (R) and the inclination of cavity (I) were set as changing variables, while the height (H) and thickness (T) of cavities were fixed as 5m and 2m, respectively. Meanwhile, the four different depths (i.e. 10m, 20m, 30m, and 40m) were configured, and the number of cavities was added as a new variable, denoted by M and expressed in binary digit, which substitutes the depth of cavity (D) used in the previous simulation.

For example, if the value of M is equal to 1010, the multi-cavity model consists of two cavities located at 10m and 30m in depth, respectively. Therefore, the variable M consists of 11 cases when considering the combination of number of cavities as shown in Figure 4.18. In total, 176 multi-cavity models (=11×4×4) were generated, and the FOS was evaluated by using the strength reduction method.

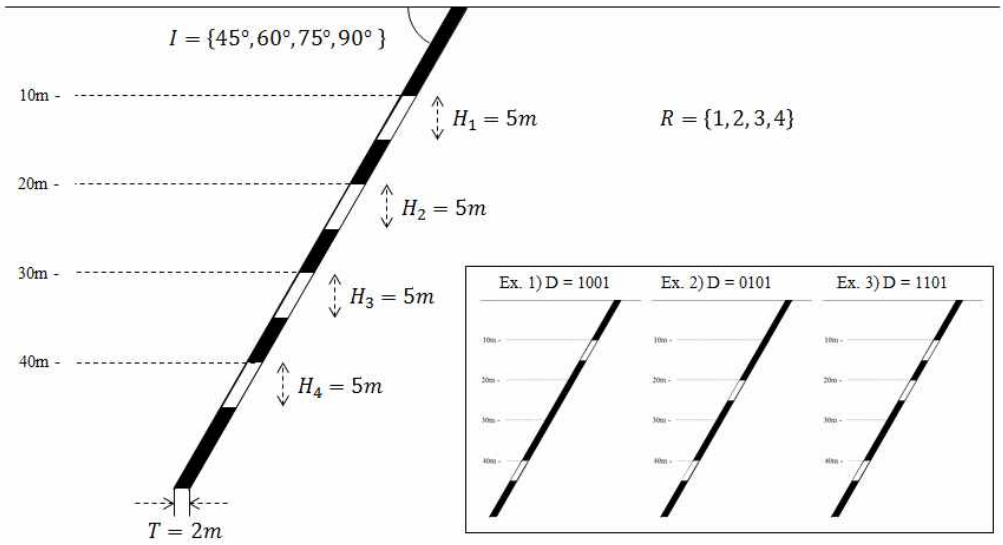

Figure 4.18 Conceptual diagram for multi-cavity simulation model.

4.3.2 Results and analysis

Table 4.14 shows the calculated FOS from 176 cases of multi-cavity models. From the results, the cases can be divided into two groups by comparing the FOS with the results of the single cavity models performed previously. One is a set of cases whose FOS is lower than individual cavities, and the other is a set of cases whose FOS is equal to that of the uppermost cavity only. In addition, the group which has no reduction of the FOS could be subdivided into two groups by considering the effecting range on surface and subsurface. In other words, even if the FOS is not changed, an interaction between adjacent cavities could occur. Consequently, there are three groups, divided by consideration both of the reduction of FOS and the connectivity of the affected area.

In group A, 41 cases are included, in which it can be positively determined that an interaction between cavities occurs. Figure 4.19 shows the normalized displacement of all cases belonging to this group. The interaction arises in adjacent cavities and reduces the FOS to about 88 percent on average compared with a single-cavity model.

Meanwhile, 30 cases are included in group B. As shown in Figure 4.20, the affected region in the surrounding rock mass is enlarged to the lower cavity, but the FOS is equal to that of a single top cavity case exists only.

Group C includes the cases that have no interaction between cavities (Figure 4.21). When the variable M are 1011, 1001, 0101, or 1011, a cavity located on the top dominates the overall behaviour. The reason for this phenomenon can be explained by distance between the first and second cavities. In other words, if the vertical spacing between two adjacent cavities

is larger than 15m, no interaction occurs in these simulations.

Although the interaction between the cavities could be analyzed qualitatively by dividing them into three groups which have different features, it was difficult to define a critical condition by which to judge the occurrence of the interaction. In this study, it was assumed that the interaction occurred in all overlapped influence areas on the surface. This assumption means that the influence areas caused by each cavity are determined individually, and each of the FOS is calculated by equation (4.4) derived from the regression analysis. Then, the FOS in the overlapping areas is recalculated by reducing to 90 percent of the lowest value among the respective FOS.

Table 4.14 FOS calculated from numerical simulations for multi-cavity model.

M	R=1				R=2				R=3				R=4			
	I=45°	I=60°	I=75°	I=90°	I=45°	I=60°	I=75°	I=90°	I=45°	I=60°	I=75°	I=90°	I=45°	I=60°	I=75°	I=90°
1100	2.650	3.425	3.995	4.426	2.051	2.518	2.790	2.936	2.051	**2.392***	2.790	2.936	**1.851***	**2.051***	**2.272***	**2.518***
1010	2.650	3.425	3.995	4.426	2.051	2.518	2.790	2.936	2.051	2.518	2.790	2.936	2.051	2.518	2.790	2.936
1001	2.650	3.425	3.995	4.426	2.051	2.518	2.790	2.936	2.051	2.518	2.790	2.936	2.051	2.518	2.790	2.936
0110	6.338	**7.392***	**8.191***	9.076	3.425	3.995	4.205	4.205	2.650	**2.936***	**3.254***	**3.425***	2.272	2.518	2.650	2.650
0101	6.338	7.781	8.622	9.076	3.425	3.995	4.205	4.205	2.650	3.091	3.425	3.605	2.272	2.518	2.650	2.650
0011	**7.023***	**8.191***	**9.076***	**9.076***	4.659	5.162	5.434	5.434	**3.254***	**3.605***	3.795	3.995	**2.650***	**2.936***	**3.254***	**3.254***
1110	2.650	3.425	3.995	4.426	2.051	2.518	2.790	2.936	2.051	**2.392***	2.790	2.936	**1.851***	**2.051***	**2.272***	**2.518***
1101	2.650	3.425	3.995	4.426	2.051	2.518	2.790	2.936	2.051	**2.392***	2.790	2.936	**1.851***	**2.051***	**2.272***	**2.518***
1011	2.650	3.425	3.995	4.426	2.051	2.518	2.790	2.936	2.051	2.518	2.790	2.936	2.051	2.518	2.790	2.936
0111	6.338	**6.672***	**7.392***	**8.191***	3.425	3.995	4.205	4.205	2.650	**2.936***	**3.254***	**3.425***	2.272	2.518	2.650	2.650
1111	2.650	3.425	3.995	4.426	2.051	2.518	2.790	2.936	2.051	**2.392***	2.790	2.936	**1.851***	**2.051***	**2.272***	**2.518***

*Calculated FOS is lowered when compared to a single cavity model.

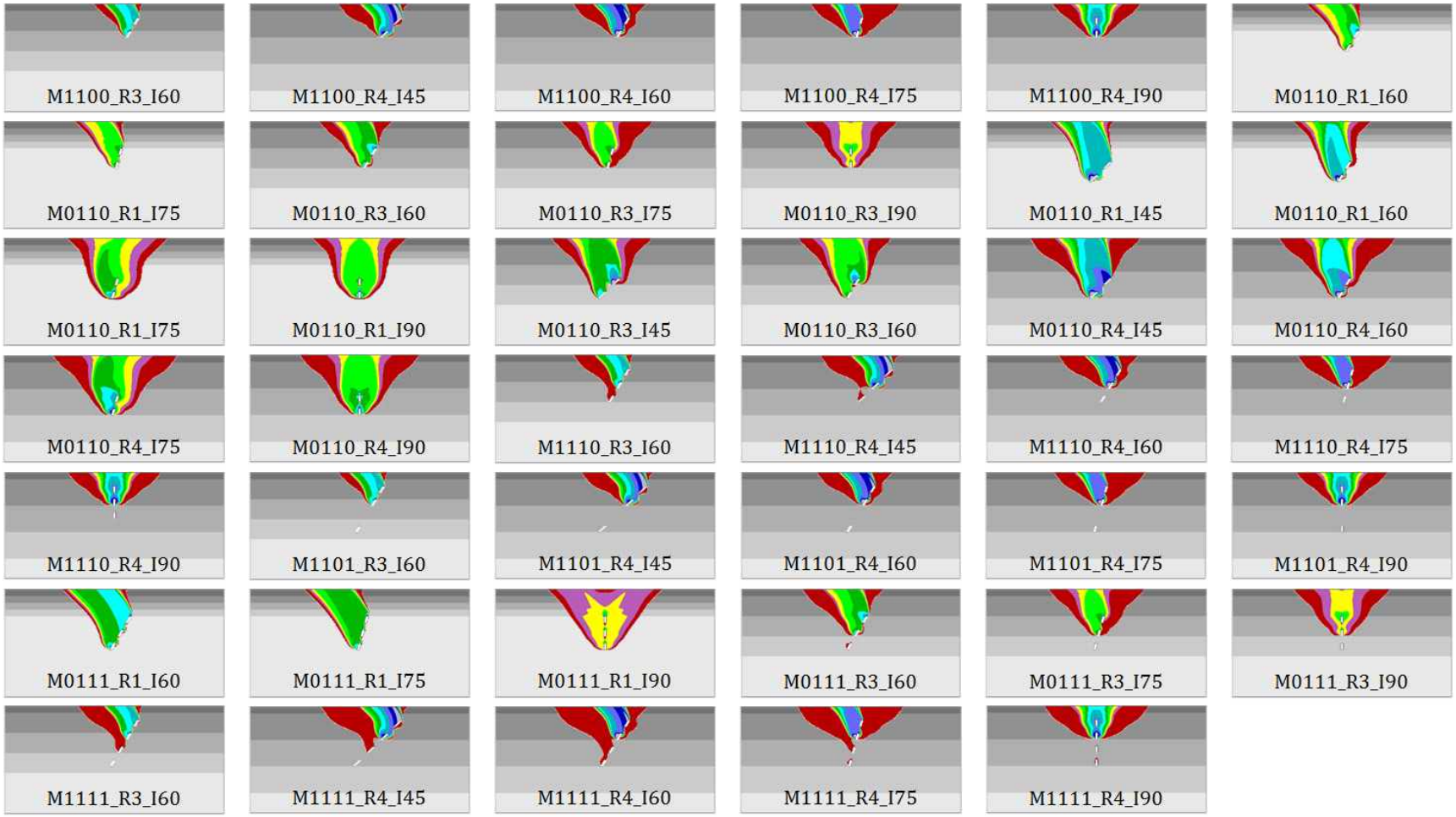

Figure 4.19 Distribution of normalized displacement obtained from multi-cavity simulation for Group A.

Figure 4.20 Distribution of normalized displacement obtained from multi-cavity simulation for Group B.

Figure 4.21 Distribution of normalized displacement obtained from multi-cavity simulation for Group C.

5. Application

5.1 Methodology

The newly developed assessment technique consists of three primary processes. One is the evaluation of the factor of safety (FOS) and the subsidence risk level (SRL) for each cavity, another is the prediction of subsidence risk area on the ground surface, and the other is the recalculation of the FOS and SRL at overlapped influence areas considering the effect of multi-cavity. The following equations are available to fulfill each process:

For calculation of FOS,

$$FOS = 1.905 \times R^{-0.679} \times \left(\frac{D}{L}\right)^{0.347} \times \left(\frac{D}{S}\right)^{0.211} \times \exp(0.006I) \qquad (5.1)$$

For determination of influence area,

$$\theta_1 = 4.242R^{1.388}\exp(-0.025D) + 15.953I^{0.146} \qquad (5.2)$$

$$\theta_2 = 0.081R^{0.900}\theta_1^{1.219} + 0.002I^{2.127} \qquad (5.3)$$

For consideration of multi-cavity,

$$FOS_m = 0.9 \times MIN(FOS_1, FOS_2, \cdots, FOS_n) \qquad (5.4)$$

where R is the rock mass type defined in this study; D is the depth of cavity in meters; L is the length of major axis of cavity in meters; S is the length of minor axis of cavity in meters, I is the inclination of cavity in degrees; FOS_m is the factor of safety at overlapped area, and FOS_i is the factor of safety of i^{th} cavity.

Table 5.1 Empirical correlations between the in-situ deformation modulus (E_m) and the RMR.

Correlations	Unit	References
$E_m = 10^{(RMR-10)/40}$	GPa	Serafim and Pereira (1983)
$E_m = 0.0097 RMR^{3.54}$	MPa	Aydan (1997)
$E_m = 0.1(RMR/10)^3$	GPa	Read et al. (1999)
$E_m = 3\times10^{-5}\times RMR^{3.2388}$	GPa	Miranda (2007)
$E_m = 1.332\exp(0.0364 RMR)$	GPa	Chun et al. (2008)

Table 5.2 Estimated RMR corresponding to each layer of the rock mass models.

Layer	Young's modulus† (Pa)	Estimated RMR					
		Chun et al. (2008)	Miranda (2007)	Read et al. (1999)	Aydan (1997)	Serafim and Pereira (1983)	Average
Soil	1.98×10^7	0	7	6	9	0	4
Weathered rock	2.17×10^8	0	16	13	17	0	9
Weak rock	2.35×10^9	16	32	29	33	25	26
Fair rock	3.50×10^9	27	37	33	37	32	32
Hard rock	9.14×10^9	53	49	45	49	48	48

The value of R can be determined by comparing the field condition of rock mass with the rock mass model introduced in Subsection 3.3.3. However, it may be a little difficult to obtain specific logging data of mining area or match the data to the rock mass model. In order to improve the applicability of this technique, an additional equation, related to the determination of the rock mass type (R), was derived.

The value of R, assumed and used in this study, can be converted to an average value of RMR (rock mass rating). The rock mass model consists of five different types of layers, and the thickness of each layer is also different. In addition, the RMR corresponding to each layer can be estimated from the empirical correlations between the in-situ deformation modulus and the RMR, such as listed in Tables 5.1 and 5.2.

The weighted average value of RMR for each rock mass model can be calculated considering the estimated RMR and the thickness of each layer, such as equation (5.5).

$$RMR = \frac{\sum (TL_i \times RMR_i)}{\sum TL_{total}} \tag{5.5}$$

where TL_i and RMR_i are the thickness and RMR of each layer, respectively. TL_{total} is the total thickness of the rock mass model, which is 80m in this study.

From equation (5.5), The weighted average values of RMR were calculated as 40, 36, 31, and 26 for corresponding to each rock mass

model, which is varying 1 to 4, respectively. Consequently, the rock mass type (R) can be easily determined from the RMR, such as equation (5.6).

$$R = \left(\frac{42}{RMR} \right)^{3.3} \tag{5.6}$$

where RMR is obtained from field conditions of rock mass in mining area, and R is the value used to determine the FOS and influence area such as equations (5.1), (5.2), and (5.3).

Figure 5.1 shows an arbitrary example case having three cavities that vary in location and depth. The subsidence risk area on the ground surface could be divided into five areas by the affecting cavities such as shown in Figure 5.1(a). When considering the three-dimensional shape of cavities, the surface can be divided into seven risk regions as many as possible. Figure 5.1(b) depicts the plane view of subsidence risk areas on the ground surface.

However, the actual ground surface is not perfectly flat, but has bumpy ground conditions. Especially, substantial underground mining operations in Korea have been performed in mountainous terrains. In spite of the significant sloping of the surface, the simulations in this study have been just focused on the flat and horizontal ground surface. Therefore, the method of projecting subsidence profile on to the sloping surface was used such as shown in Figure 5.2.

In order to apply the assessment technique for prediction and evaluation of subsidence risk, obtaining information of topography and cavities is

essential. The topography can be easily obtained by purchasing a map from National Geographic Information Institute. Unfortunately, the geometrical feature of cavities, such as size, shape, and location, should be assumed from the mining conditions which include the gangways, nature of ore-body, and mining methods.

Finally, it is preferred to apply the technique through the following procedure:

Step 1: Prepare a topographic map including the whole of the mining area.

Step 2: Extract spatial data of cavity such as shape, size, and location.

Step 3: Determine the rock mass type (R) of the evaluating region.

Step 4: Estimate the influence areas individually by using the two limit angles.

Step 5: Calculate the FOS and SRL in that areas by using the non-linear regression model.

Step 6: Recalculate the FOS and SRL in any overlapped influence areas by reducing to 90% of the lowest FOS.

Step 7: Draw subsidence risk map.

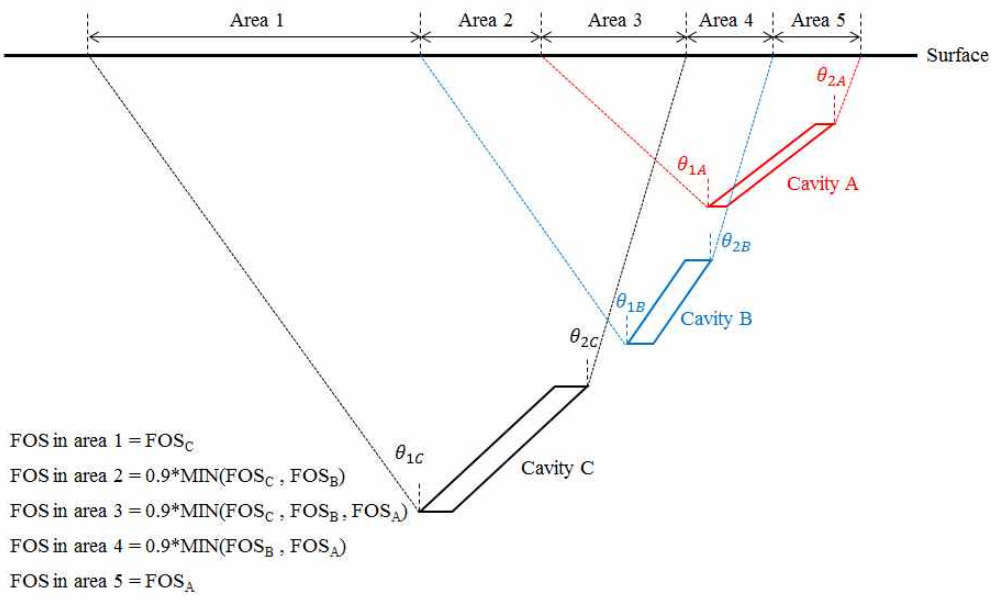

(a) Vertical section view

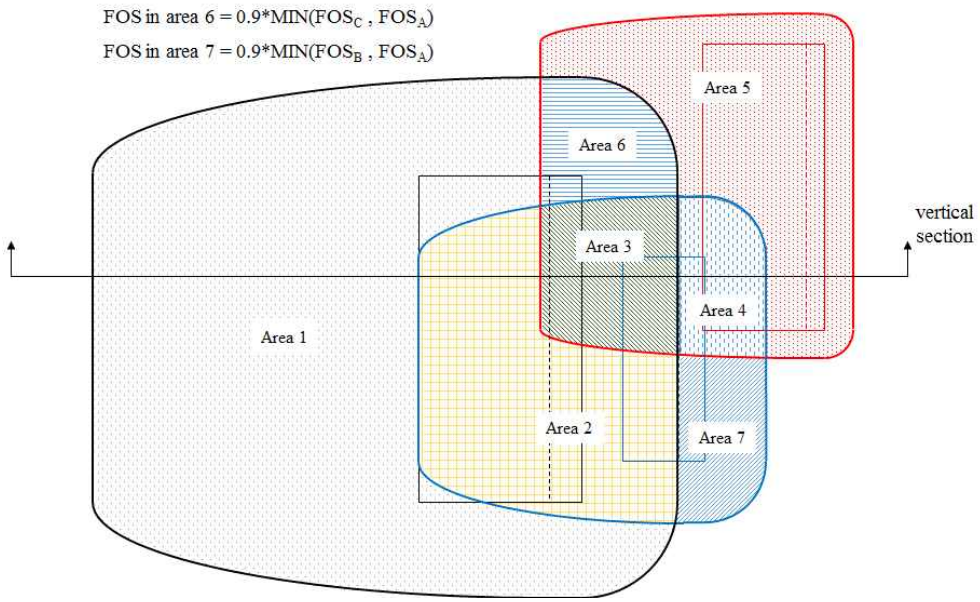

(b) Plane view

Figure 5.1 Conceptual diagram for evaluating the subsidence risk on horizontal ground surface using the developed assessment technique.

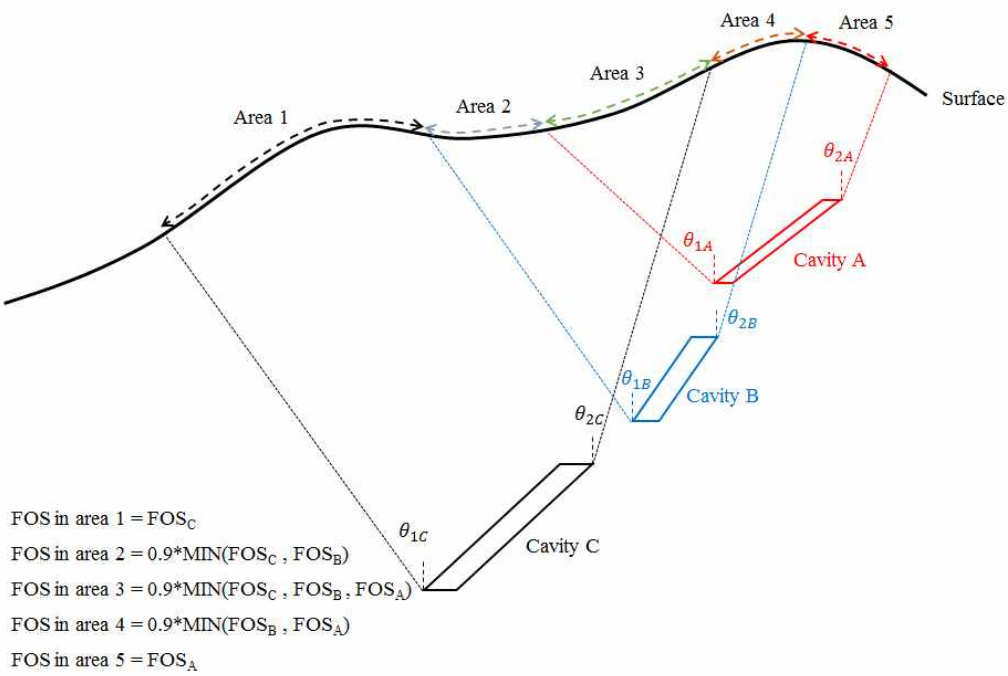

Figure 5.2 Conceptual diagram for evaluating the subsidence risk on bumpy ground surface using the developed assessment technique.

5.2 Results

5.2.1 Mining site #1 (Daerueng Coal Mine)

a. Overview

Daerueng Coal Mine in Boryong Province, an abandoned coal mine in Korea, was chosen to evaluate the subsidence risk. This mine had been actively operated since 1983 and produced 18,000 tons of coal annually till it was closed in 1989 (MIRECO, 2006). Figure 5.3 shows the location and topography of the mining region, which is placed in a mountainous terrain.

According to the investigation report of this area, a total of 18 traces of subsidence were observed, and their type were conical sinkhole or ellipse trough, as shown in Figure 5.4. Most of the subsidence traces were caused by the mined cavities located in various depths, except one case (#1) that occurred in the vicinity of the gangway, in which there is no cavity.

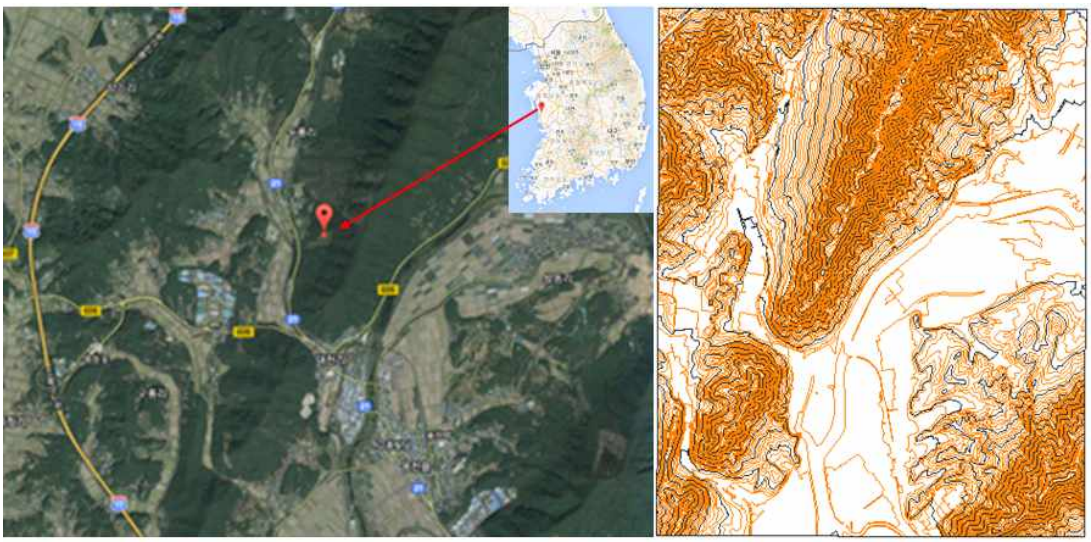

Figure 5.3 A satellite photograph and contour map of Daerueng Coal Mine.

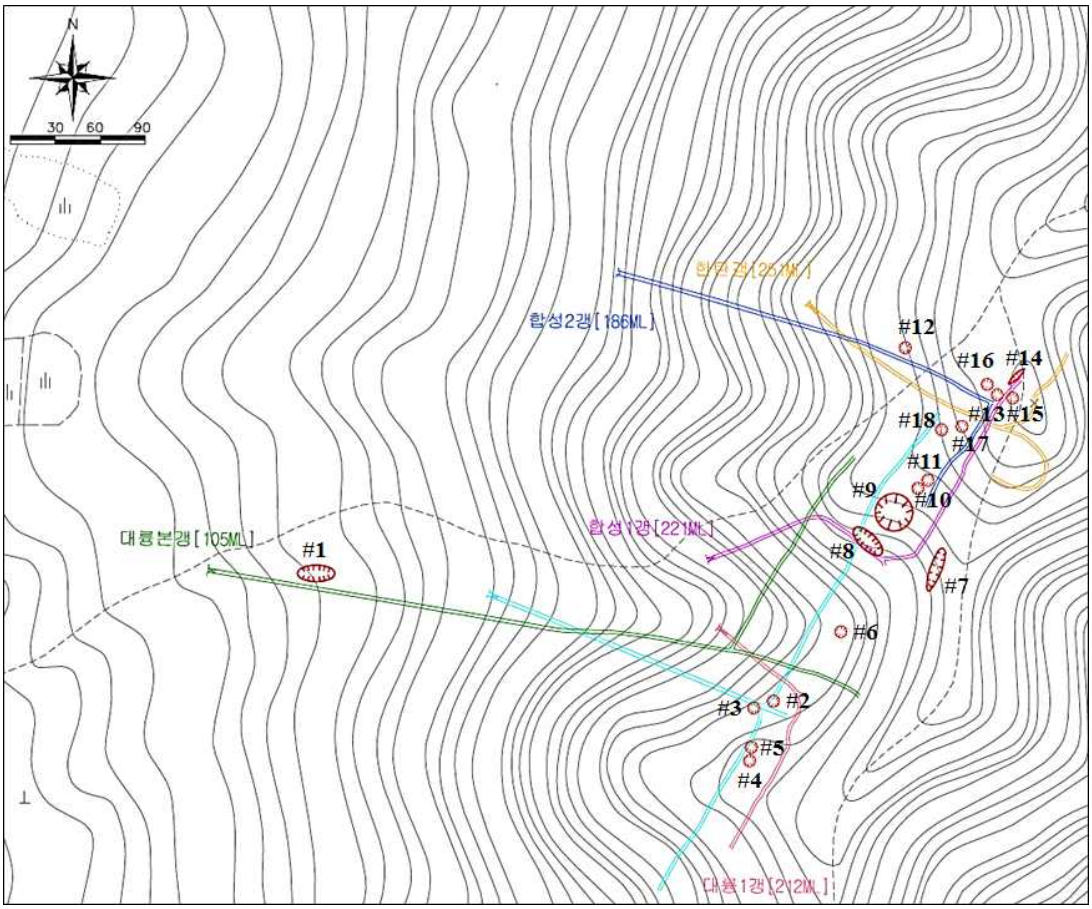

Figure 5.4 Subsidence traces observed in Daerueng Coal Mine region (after MIRECO, 2006).

b. Information of cavity

In this site, it was difficult to obtain the information about the mined cavities directly from the survey report. Therefore, the data should be extracted from the schematic diagram of developing process, gangway map, cross-sectional diagram, and topography as shown in Figure 5.5. The height (H) and width (W) of the cavities could be obtained and assumed from the schematic diagram, which outlines the excavated area and developed levels

(Figure 5.5(a)). The gangway map, shown in Figure 5.5(b), was used to determine the dip-direction (DD) and location (i.e., x, y, and z coordinate) of the cavities. The thickness (T) and inclination (I) of the cavities could be estimated from the cross-sectional diagram (Figure 5.5(c)), which represents the cavities in detail. In addition, the depths (D) of cavities were obtained by calculating the distance between the cavities and surface. As a result, a total of six cavities were obtained by combining these survey data. Table 5.3 presents the information of cavities.

Table 5.3 Information of cavities obtained from Daerueng Coal Mine.

Cavity ID	Location			Shape							Depth (m)
	x (m)	y (m)	z (m)	H (m)	T (m)	I (°)	W (m)	DD (°)	L (m)	S (m)	
C1	717.4	469.5	251.0	15.0	0.5	68.8	30.0	300	16.1	0.5	62.7
C2	674.9	249.3	221.0	22.0	1.5	65.3	112.5	300	24.2	1.4	73.1
C3	643.3	447.8	166.0	34.3	2.0	50.1	37.8	308	44.7	1.5	111.7
C4	587.1	393.6	135.0	56.0	2.0	58.2	37.3	298	65.9	1.7	92.6
C5	542.1	224.6	212.0	10.0	0.5	44.0	75.2	296	14.4	0.3	43.3
C6	540.5	269.0	166.0	12.4	0.5	61.0	150.0	299	14.2	0.4	72.5

x, y, and z is the coordinate of bottom of cavity.
H, T, I, and W are the height, thickness, inclination, and width of each cavity.
L and S are the length of major and minor axes of the cavity.
DD is dip-direction of cavity.

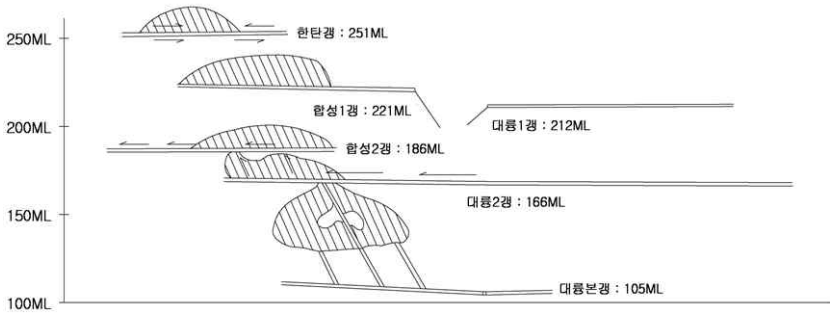

(a) Schematic diagram of developing process

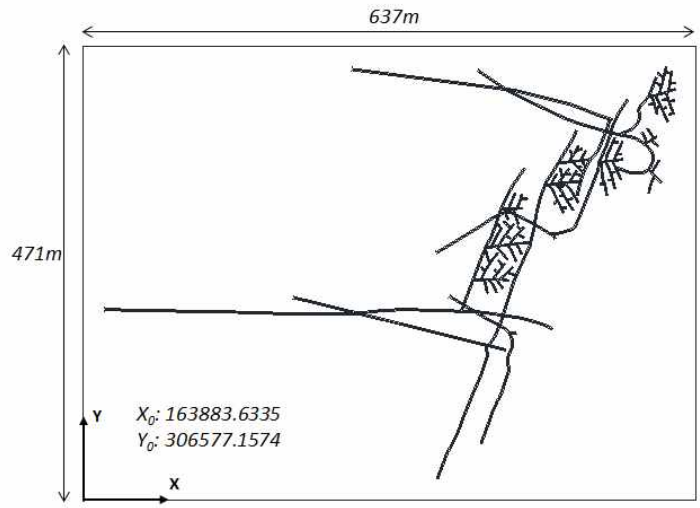

(b) Gangway map in plan view

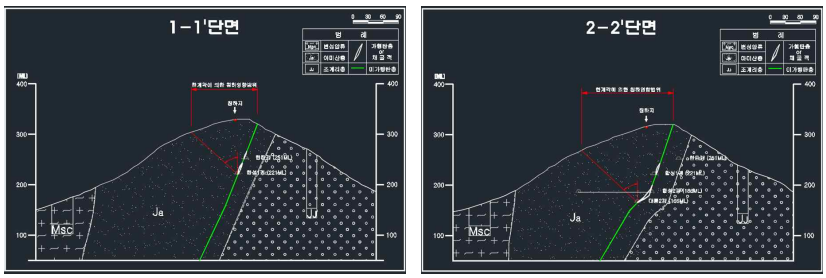

(c) Cross-sectional diagram

Figure 5.5 Available survey data used for estimating the mined cavities in Daerueng Coal Mine.

c. Rock mass type

It is essential to decide the rock mass type (R) for performing risk assessment of given mine. According to the assessment technique proposed in this study, it is desirable to determine input variables based on in-situ data. However, the data were insufficient in this area, so the rock mass type was assumed. In this region, the average value of RMR was assumed as 30, then the value of R was calculated as 3.035 by using equation 5.6.

d. Estimation of influence area and evaluation of SRL

The FOS for each cavity is calculated from Equation (5.1), and the two limit angles are estimated from Equations (5.2) and (5.3). Tables 5.2 and 5.3 summarize the calculated values. Besides, the FOS in overlapped hazard areas is recalculated by using the Equation (5.4).

Table 5.4 FOS, SRL, and limit angles calculated from observed data in Daerueng Coal Mine.

Cavity ID	FOS	SRL(%)	Downward limit angle (θ_1)	Upward limit angle (θ_2)
C1	6.11	16.37	33.72	32.23
C2	4.51	22.18	32.55	29.86
C3	4.11	24.33	29.46	21.85
C4	3.32	30.08	30.83	25.72
C5	4.73	21.12	34.43	22.71
C6	6.69	14.94	32.31	27.76

e. Draw subsidence risk map

From the previous procedure, a subsidence risk map could be made as shown in Figure 5.6. In addition, the validation of this assessment technique could be carried out by comparing the estimated subsidence risk area with the subsidence traces observed in the field survey as shown in Figure 5.7.

f. Conclusion

It could be concluded that the assessment technique developed in this study is useful to estimate and evaluate the subsidence risk through this application. The estimated subsidence risk area included most of the field data of subsidence traces. Table 5.5 shows the subsidence risk level corresponding to each subsidence trace.

Table 5.5 Estimated SRL for observed subsidence traces in Daerueng Coal Mine.

Subsidence trace	SRL(%)	Subsidence trace	SRL(%)
#1	-	#10	33.4
#2	14.9	#11	33.4
#3	14.9	#12	24.3
#4	23.5	#13	27.0
#5	23.5	#14	27.0
#6	14.9	#15	27.0
#7	33.4	#16	27.0
#8	33.4	#17	27.0
#9	33.4	#18	27.0

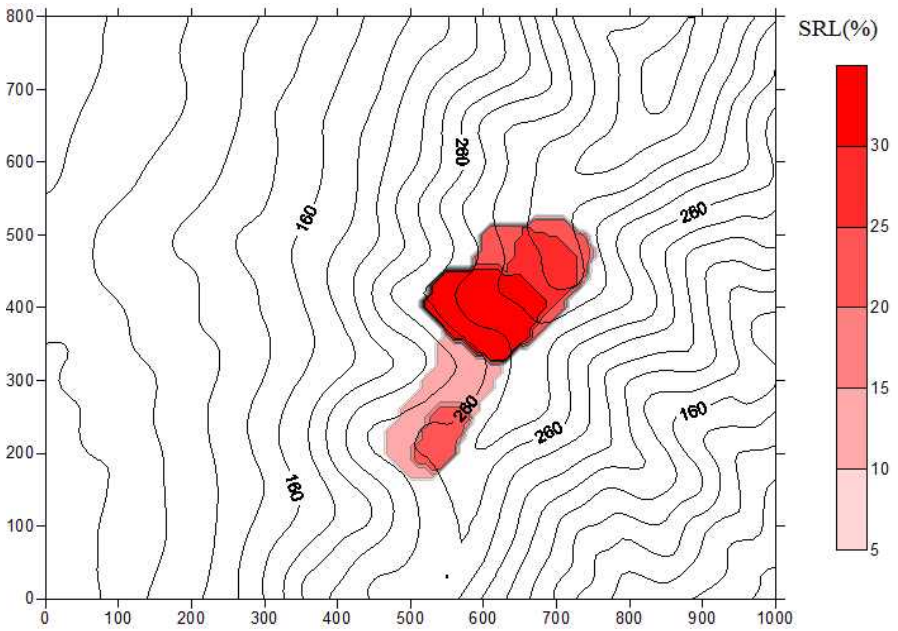

(a) plane view

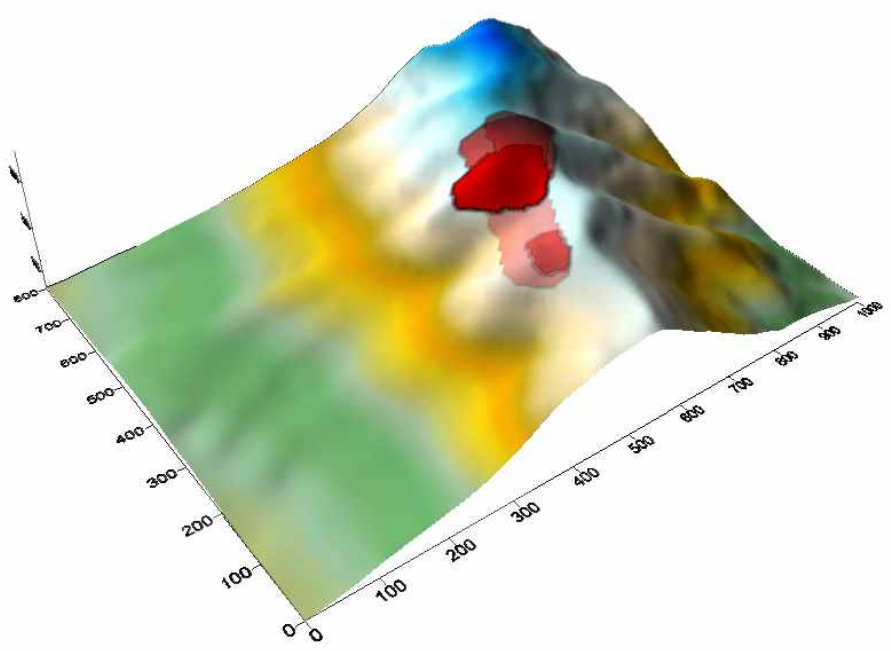

(b) 3-D view

Figure 5.6 Subsidence risk map of Daerueng Coal Mine region evaluated from new assessment technique developed in this study.

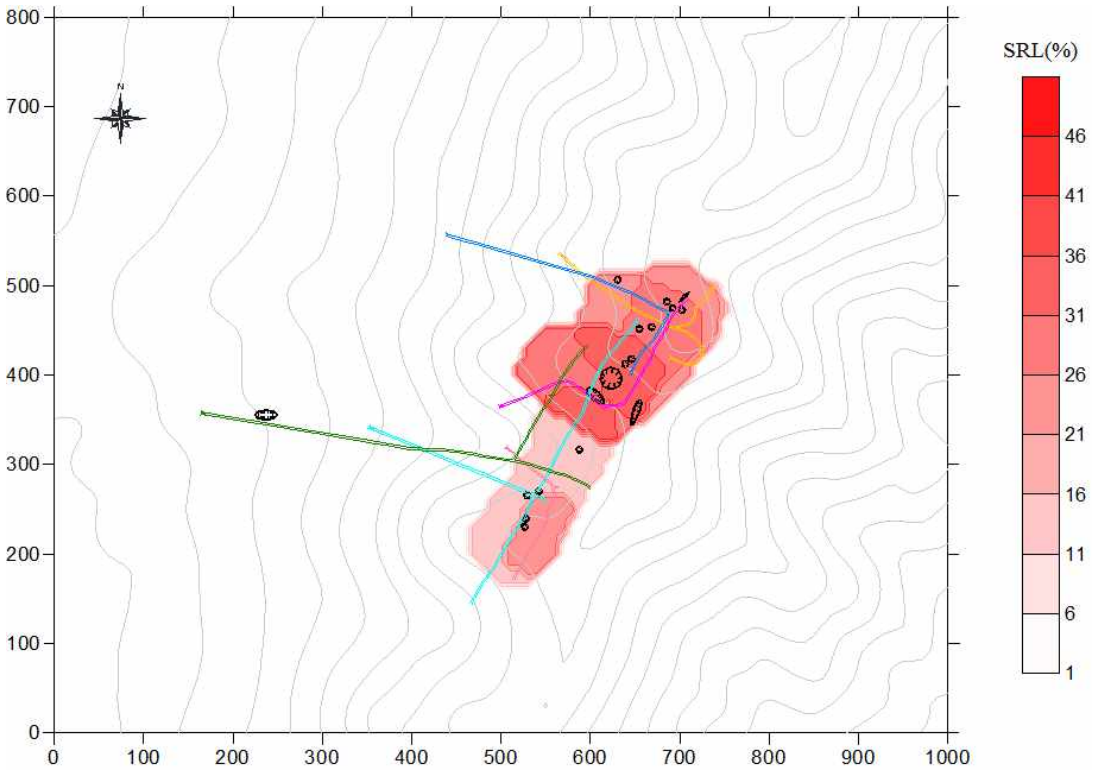

Figure 5.7 Subsidence risk map with observed subsidence traces in Daerueng Coal Mine region.

5.2.2 Mining site #2 (Wolmyung Coal Mine)

a. Overview

Similar to the previous application, another mine site (Wolmyung Coal Mine) was selected to carry out for verification of this technique. This mine is located in Seocheon Province, Korea, as shown in Figure 5.8. The coal seam in this region is slightly inclined, about 20 degrees, and extraction was performed at shallow depth during 1962 - 1990. According to the investigation report of this area (MIRECO, 2012b), a total of 6 traces of subsidence were observed, and all of them were sinkhole types, such as shown in Figure 5.9.

The most remarkable difference with Daeryung mine is that the cavities in this region are inclined gently, varying from 0° to 30°. In addition, the cavities are located at shallow depth, which might cause the increase of subsidence risk.

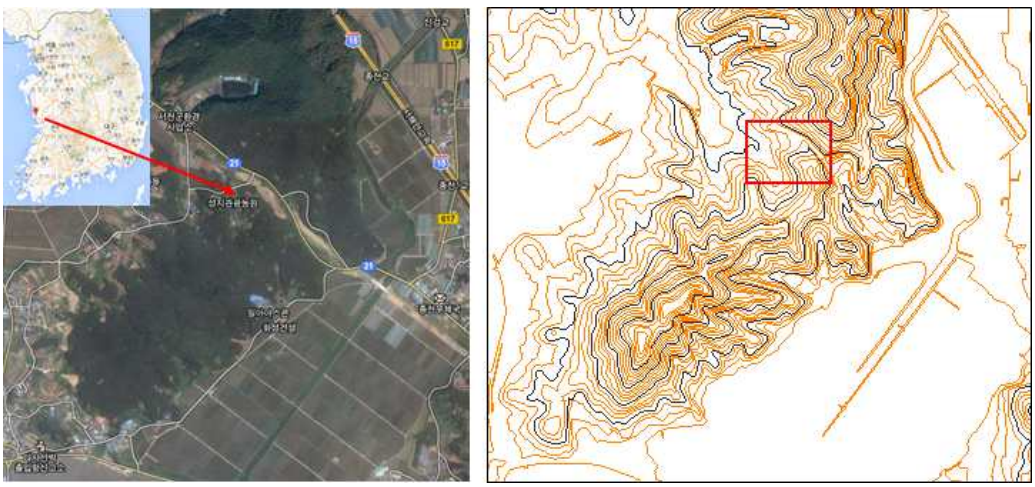

Figure 5.8 A satellite photograph and contour map of Wolmyung Coal Mine region.

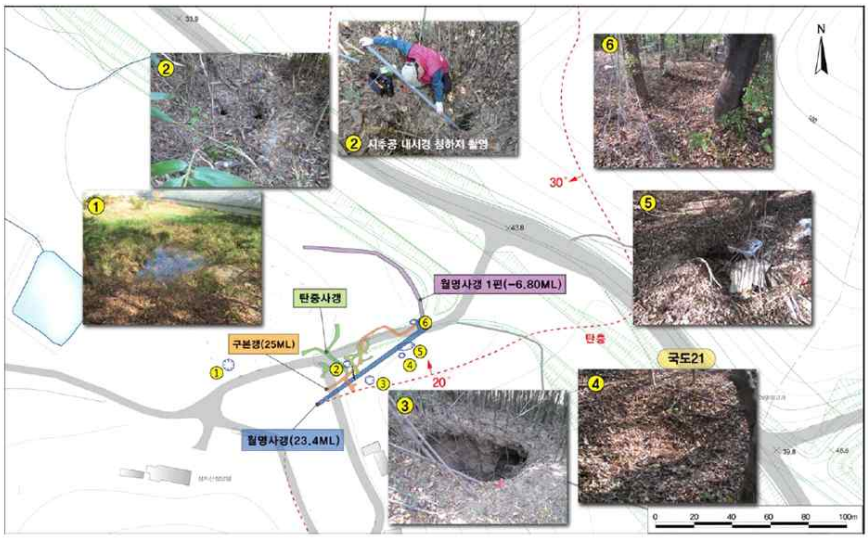

Figure 5.9 Subsidence traces observed in Wolmyung Coal Mine region (MIRECO, 2012b)

b. Information of cavity

Unfortunately, there are no available data which can be used to identify the mined cavities in three-dimensional. Instead, a plane map including the gangways and subsidence traces could be obtained from the survey report, which also provides eleven vertical section maps containing the cavities. In addition, the plane map should be merged with a topographic map to determine the coordinate of a reference point, because the plane map has no spatial information about the horizontal position. Figure 5.10 shows the merged map, which includes the reference point, the distribution of gangways, and the lines for marking the location of the vertical sections. Consequently, the subsidence risk assessment for this region was carried out in each section; then the results were combined. Table 5.6 presents the information of cavities, which was extracted from the cross-sectional diagrams (Figure 5.11).

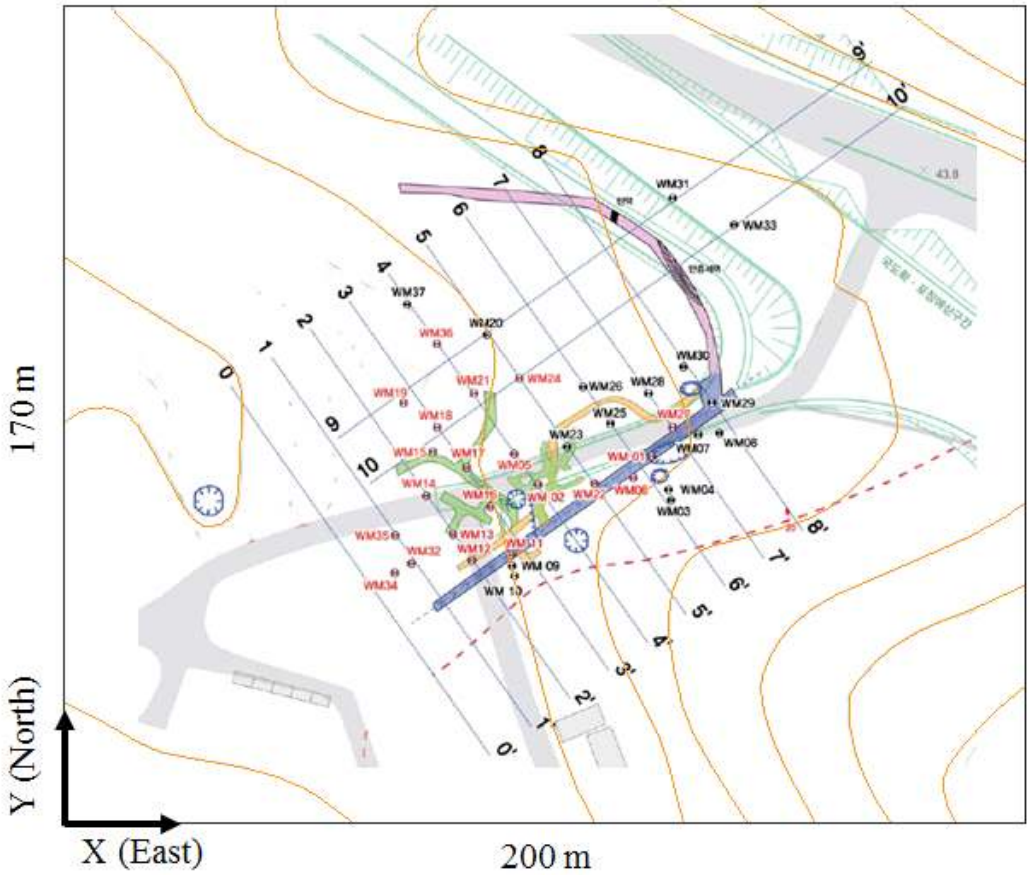

Figure 5.10 Merged map of Wolmyung Coal Mine. This includes the reference point, the distribution of gangways, and the lines for marking the location of the vertical sections.

c. Rock mass type

From the cross-sectional diagram, the rock mass condition over the cavity is very poor, and it mainly consists of the weak rock and soil layer with significant thickness. The average thickness was calculated as 4 m for the soil layer, and the rest of the rock mass layer consists of weak rock. Therefore, the average RMR of this region was assumed as 26 (Table 5.2), then the value of R was calculated as 4.8 by using equation 5.6.

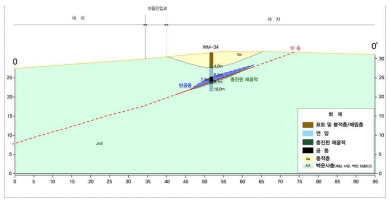

(a) section 0-0’

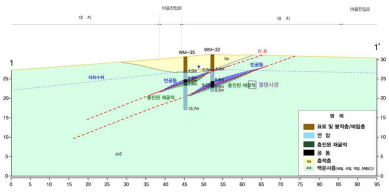

(b) section 1-1’

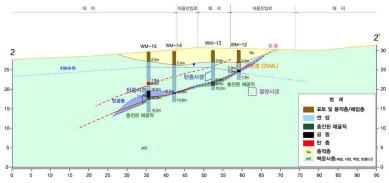

(c) section 2-2’

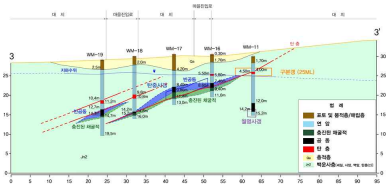

(d) section 3-3’

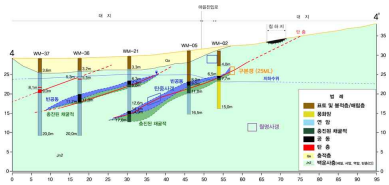

(e) section 4-4’

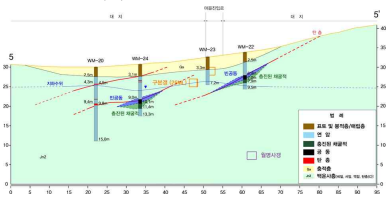

(f) section 5-5’

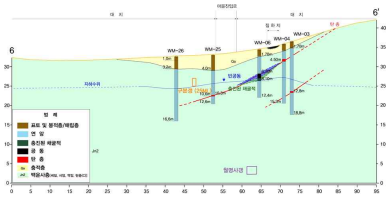

(g) section 6-6’

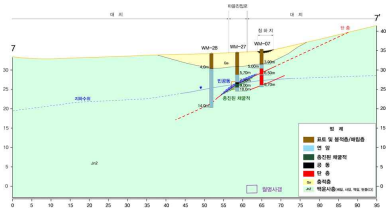

(h) section 7-7’

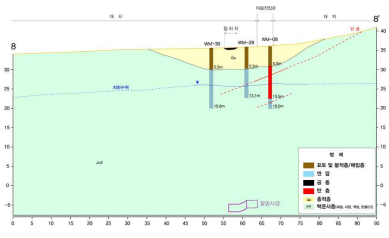

(i) section 8-8’

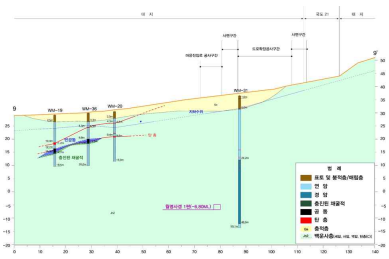

(j) section 9-9’

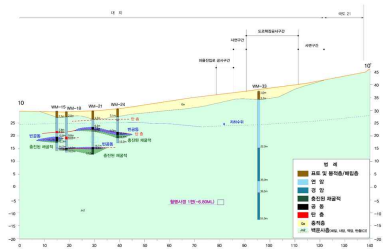

(k) section 10-10’

Figure 5.11 Vertical section diagram of Wolmyung Coal Mine.

d. Estimation of hazard area and evaluation of SRL

The FOS and two limit angles are estimated from Equations (5.1), (5.2) and (5.3). Tables 5.6 summarizes the calculated values of each cavity. The SRL was very high, because the cavities are located at shallow depth and the rock mass condition is weak.

Table 5.6 Information of cavities obtained from survey report and results calculated by the developed technique for Wolmyung Coal Mine.

Cross section	Cavity ID	D (m)	L (m)	S (m)	I (°)	R	FOS	SRL (%)	θ_1 (°)	θ_2 (°)
0-0’	0-1	3.4	18.3	1.1	20.9	4	0.52	100	59.2	49.4
1-1’	1-1	4.4	13.8	0.7	22.6	4	0.74	100	58.7	49.1
	1-2	3.4	19.4	1.3	21.5	4	0.50	100	59.3	49.6
2-2’	2-1	11.6	10.2	1.6	24.1	4	1.21	82.4	53.4	44.1
	2-2	11.1	6.7	1.0	3.1	4	1.32	75.5	47.2	36.5
	2-3	8.7	10.4	0.3	15.8	4	1.39	71.8	54.0	43.7
	2-4	5.8	7.3	0.3	22.7	4	1.32	75.7	57.5	48.0
	2-5	1.5	7.9	0.8	31.2	4	0.51	100	62.4	54.3
3-3’	3-1	11.2	14.7	1.5	22.2	4	1.05	95.6	53.4	43.8
	3-2	13.8	7.2	0.4	22.5	4	2.02	49.5	51.6	42.2
	3-3	8.6	11.8	1.2	29.5	4	1.06	94.3	56.3	47.9
	3-4	7.6	10.0	1.4	6.0	4	0.89	100	51.7	40.8
	3-5	5.6	7.8	1.1	18.6	4	0.92	100	57.0	46.9
4-4’	4-1	5.2	30.5	1.0	17.5	4	0.56	100	57.1	46.9
	4-2	7.6	29.0	0.9	21.6	4	0.73	100	55.9	46.3
5-5’	5-1	7.2	12.4	0.8	19.6	4	0.96	100	55.9	46.0
	5-2	3.7	16.7	1.0	26.9	4	0.61	100	59.9	51.0
6-6’	6-1	4.6	12.6	1.3	27.7	4	0.71	100	59.3	50.5
7-7’	7-1	5.8	10.9	0.3	30.1	4	1.22	82.2	58.6	50.3
8-8’	None									
9-9’	9-1	10.2	25.0	1.4	15.7	4	0.80	100	52.8	42.6
10-10’	10-1	10.2	10.8	1.7	4.9	4	0.97	100	49.1	38.4
	10-2	14.3	19.4	0.8	0.0	4	1.09	92.1	26.2	26.2
	10-3	6.2	22.9	1.0	7.0	4	0.64	100	53.2	42.4

L and S are the length of major and minor axes of the cavity.
D and I are the depth and inclination cavity.
R is the rock mass type.
θ_1 and θ_2 are the downward and upward limit angles.
*Upward limit angle is replaced with downward limit angle, because the inclination of the cavity is zero.

e. Draw subsidence risk map

Because the assessment for subsidence risk in this area was carried out in two-dimensional, the risk map could be made by using an interpolation method, as shown in Figure 5.12.

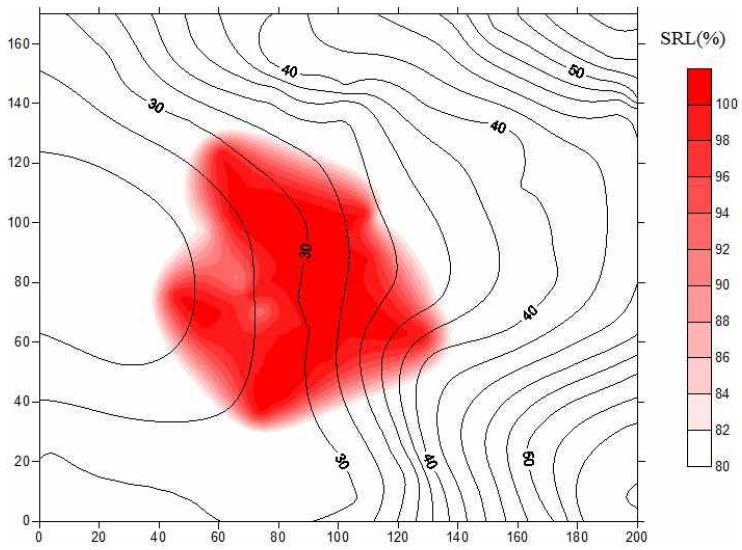

(a) plane view

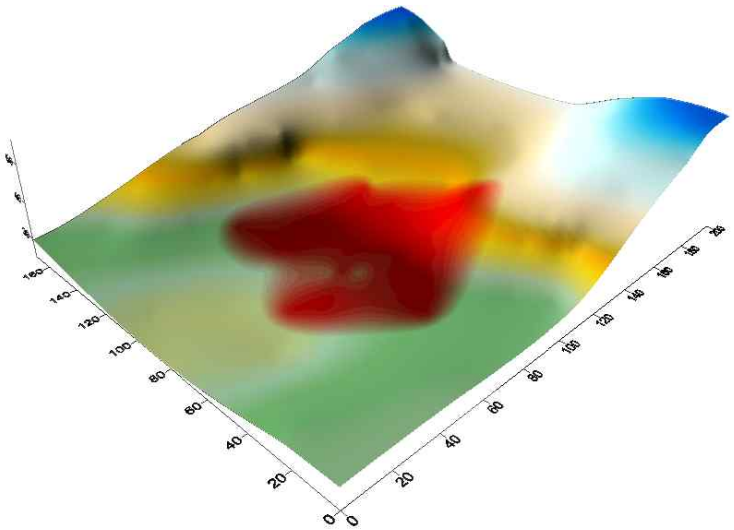

(b) 3-D view

Figure 5.12 Subsidence risk map of Wolmyung Coal Mine region evaluated from new assessment technique developed in this study.

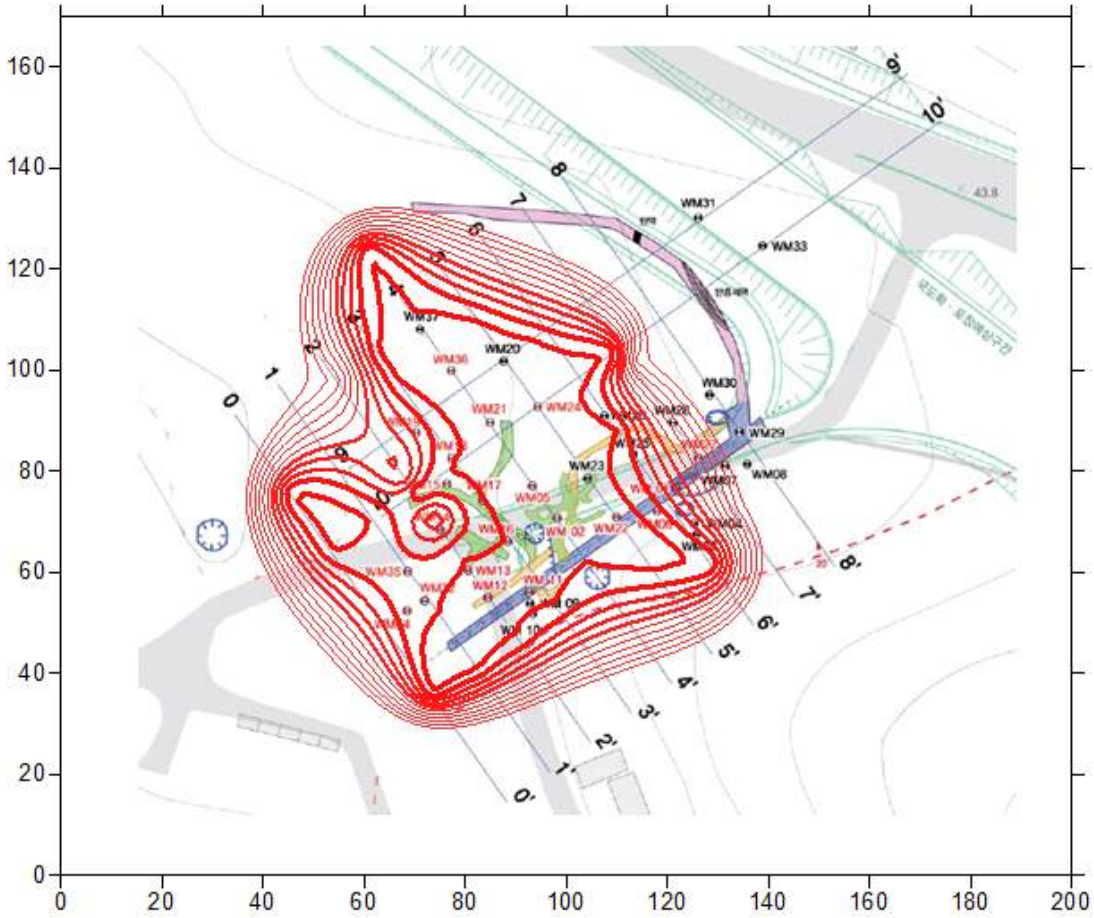

Figure 5.13 Subsidence risk map with observed subsidence trace in Wolmyung coal mine areas.

f. Conclusion

In this application, applicability of the developed technique was verified. Especially, it was found that this technique is applicable for gently as well as steeply inclined cavities. The subsidence risk level was calculated as more than 90%, and this high-risk area contains most of the subsidence traces observed from field investigation (Figure 5.13).

5.2.3 Mining site #3 (Mugeuk Gold Mine)

a. Overview

A risk assessment of subsidence in Mugeuk Gold Mine region was performed to verify this technique. This mine is located in Eumseong Province, Korea, as shown in Figure 5.14(a). In this area, a significant subsidence occurred in 2008 and became the social issue, because a residential building collapsed due to the subsidence (Figure 5.14(b)). The type of subsidence was sinkhole, and the extent of that was about 10m in diameter.

(a) Location (b) Subsidence

Figure 5.14 Location and subsidence accident of Mugeuk Gold Mine (MIRECO, 2008b).

b. Information of cavity

Due to the serious damage in the structure, the feature of cavity was scrutinized as shown in Figure 5.15. The depth (D), height (H), thickness (T), inclination (I), and width (W) were investigated as 15m, 28m, 3m, 80°, and 45m, respectively.

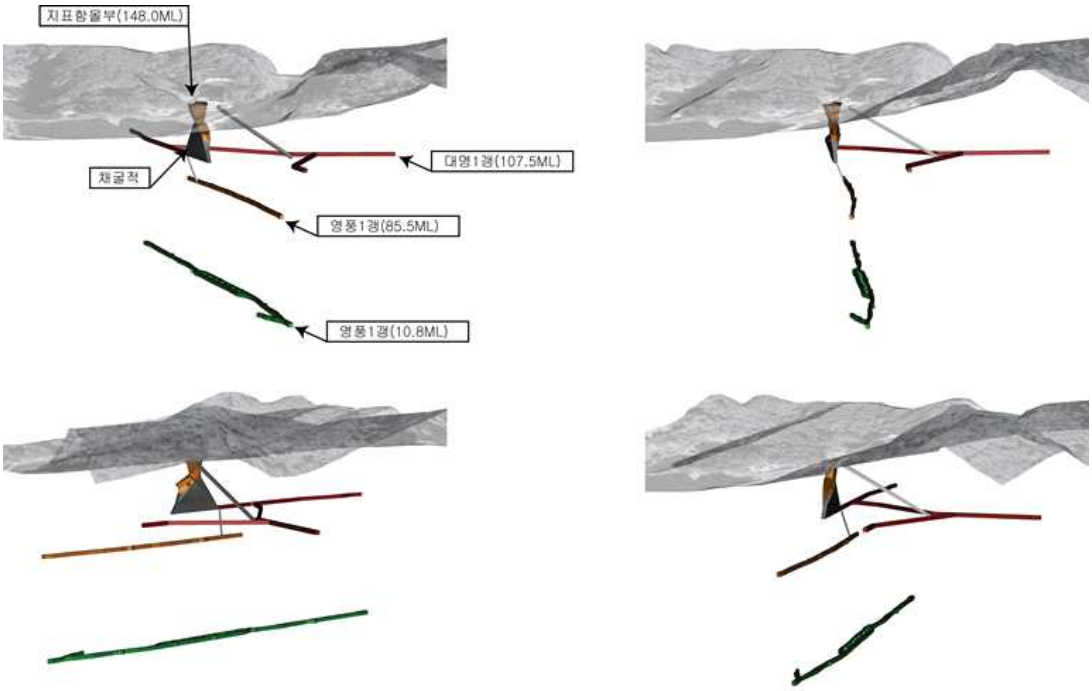

Figure 5.15 Three dimensional view of gangways and cavity in Mugeuk Gold Mine (MIRECO, 2008b).

c. Rock mass type

From the logging data, it was found that the rock mass in this region is classified as the grade Ⅳ or Ⅲ of RMR. Therefore, the average value of RMR was assumed to 40, then the value of the rock mass type (R) was calculated as 1.2 by using equation 5.6.

d. Estimation of influence area and evaluation of SRL

Similar to the previous two applications, the FOS, SRL, and limit angles could be estimated by equations (5.1), (5.2), and (5.3), such as listed in Table 5.7. The SRL was calculated as 32.56%, but the estimation of influence area was skipped because the surface is nearly flat and the

subsidence occurred directly above the cavity. In this application, it could be concluded that the assessment technique developed in this study can be applied to the simple case, which has a single cavity.

Table 5.7 Information of cavities obtained from survey report and results calculated by the developed technique for Mugeuk Gold Mine.

Cavity ID	D (m)	L (m)	S (m)	I (°)	R	FOS	SRL (%)	θ_1 (°)	θ_2 (°)
C1	15	28.43	2.95	80	1.2	3.07	32.56	34.0	29.36

L and S are the length of major and minor axes of the cavity.
D and I are the depth and inclination cavity.
R is the rock mass type.
θ_1 and θ_2 are the downward and upward limit angles.

5.2.4 Conclusion of application

The three application results confirm that the assessment technique is suitable to evaluate the subsidence risk and estimate the risk areas on the ground surface. Although this approach was developed under the flat and horizontal surface situation, it could be applied to an inclined surface such as mountainous terrain. In addition, this technique could be applied to various conditions of mined cavity, such as horizontal and vertical inclined cavities. However, this technique has a limitation that the estimated SRL is insufficient to determine whether or not the subsidence is occurring obviously. In these applications, the values of SRL in the subsidence traces range widely from 15 to 100.

6. Conclusions and discussion

6.1 Conclusions

In this study, a new assessment technique for prediction and evaluation of ground subsidence risk in mining areas was developed using numerical and statistical analysis.

To estimate the subsidence risk, SRL was defined and suggested as an indicator that represents the probability of subsidence in mining areas. The value of SRL was calculated as the reciprocal of FOS in the analyzing area and expressed in percentage terms.

For representation and investigation of a phenomenon of mining subsidence, numerical simulation was carried out. The numerical approach has been successfully applied for prediction of subsidence by generating various situations reflecting the field conditions of mining areas. In this study, FLAC2D, a commercial analysis software based on finite distinct method, was used.

Furthermore, the strength reduction method (SRM) was implemented to identify the FOS in given conditions of the mining areas. The SRM has been widely used for evaluating the stability of various types of geotechnical structures. A remarkable advantage of using SRM is that the critical failure surface can be found automatically without any assumptions.

To build the assessment technique, a statistical analysis was performed for the results of numerical simulation. The relations of the SRL and affecting parameters (i.e., the rock mass type and geometric features of the

cavity) were derived from the correlation and non-linear regression analyses. The two limit angles, downward and upward angle in an inclined cavity, were figured out from the non-linear regression analysis. Moreover, the interaction between cavities was evaluated by considering the spatial distribution of the multiple cavities. Therefore, the assessment technique consists of three sub-models: the calculation of FOS and SRL, the estimation of influence areas on the surface, and the consideration of multi-cavity.

Finally, the developed technique was applied to three abandoned mine areas; then, validation was made by comparing the estimated hazard areas with subsidence traces obtained from field survey reports. The following conclusions were drawn.

1) The strength reduction method was successfully applied to numerical simulation for subsidence risk analysis. Because the modified simple approach for applying the reducing strength process was adopted, the progressive failure of surrounding rock mass above the cavity could be identified. The failure of rock mass initiates at the vicinity of the cavity and propagates through the rock mass, and eventually reaches to the surface.

2) From the correlation analysis, it was revealed that the SRL is reduced when the cavity is located in depth and inclined steeply, whereas the SRL increases when the rock mass condition is poor and the area of extracted cavity is enlarged. The effects of the four

parameters, R, D, H, and T, were understandable intuitively, but that of the inclination of cavity was not clear. The relations of SRL and I could be explained from the vertically projected area on the surface of a given cavity being decreased when the cavity is more inclined.

3) The downward and upward limit angles could be estimated from numerical simulation using SRM. The surface area of subsidence risk induced by the mined cavity was estimated from the two limit angles. In addition, the equations to calculate the limit angles were derived as a function of affecting parameters.

4) From the numerical simulation, the interaction between multiple cavities was assessed. It was found that the interaction is affected by a distance between the adjacent cavities and rock mass conditions. Especially, the FOS in the interaction area reduced to about 90 percent on average when compared to the results of single cavity models.

5) The proposed technique was verified by applying it to three abandoned mine sites. The subsidence risk areas estimated from the new technique includes most of the subsidence traces observed from field data in the applications, which means that this approach is appropriate to estimate the risk areas.

6.2 Discussion

There are several limitations for application of the new assessment technique. Firstly, the value of SRL calculated from this approach cannot be simply used to determine whether or not the subsidence will occur. The estimated SRL just indicates the relative potential levels of subsidence occurrence so that the results can be used to decide which area is more prone to subside.

Secondly, further application with additional case studies should be carried out to validate this technique. In the present study, three applications were performed in abandoned mine areas; two for coal mines and one for gold mine. The proposed technique may not be applicable in the same manner to other mines with different types of minerals or operation by different mining methods.

Thirdly, this technique was developed from two-dimensional models which generally provide conservative results. Although three-dimensional simulation might result in more accurate outputs, the computation time would significantly increase, especially when lots of cases, i.e. 1,200 cases in this study, need to be simulated.

Fourthly, there are other influencing factors related to the mine subsidence. In this assessment technique, the rock mass condition and geological feature of mined cavities were considered. However, structural discontinuities such as fault and joint as well as ground water level will also highly affect the subsidence.

Finally, this technique does not differ in the types of subsidence:

continuous (i.e., trough type) and discontinuous (i.e., sinkhole type). Because the two types of subsidence are formed by different mechanisms, it should be carefully used to estimate the type and extent of the subsidence.

In spite of the limitations listed above, the new assessment technique can be restrictively used for prediction and evaluation of subsidence risk. Especially, it is expected that this technique could be helpful to determine the relatively high-risk areas in the ground stabilization projects.

References

Alejano, L.R., Ramirez-Oyanguren, P., Taboada, J., (1999) FDM predictive methodology for subsidence due to flat and inclined coal seam mining. International Journal of Rock Mechanics and Mining Sciences 36(4), pp. 475-491.

Asadi, A., Shakhriar, K., Goshtasbi, K., (2004) Profiling function for surface subsidence prediction in mining inclined coal seams. Journal of mining science 40(2), pp. 142-146.

Asadi, A., Shahriar, K., Goshtasbi, K., Najm, K., (2005) Development of a new mathematical model for prediction of surface subsidence due to inclined coal-seam mining. Journal of the South African Institute of Mining and Metallurgy 105(1), pp. 15-20.

Bekendam, R.F., (2004) Stability and subsidence assessment over shallow abandoned room and pillar limestone mines. In Engineering Geology for Infrastructure Planning in Europe, pp. 657-670.

Brady, B.H.G., Brown, E.T., (2004) Rock mechanics: for underground mining. 3rd edn. Kluwer Academic Publishers. pp. 484-517..

Cai, F., Ugai, K., (2000) Numerical analysis of the stability of a slope reinforced with piles. Soils and Foundations 40(1), pp. 73-84.

Caudron, M., Emeriault, F., Kastner, R., Al Heib, M.. (2006) Numerical modeling of the soil structure interaction during sinkholes. Numerical Methods in Geotechnical Engineering, Graz: pp. 267-273.

Chakraborti, S., Konietzky, H., Walter, K., (2012) A comparative study of different approaches for factor of safety calculations by shear strength reduction technique for non-linear Hoek−Brown failure criterion. Geotechnical and Geological Engineering 30(4), pp. 925-934.

Cheng, Y.M., Lansivaara, T., Wei, W.B., (2007) Two-dimensional slope stability analysis by limit equilibrium and strength reduction methods. Computers and Geotechnics 34(3), pp. 137-150.

Choi, J.K., Kim, K.D., (2007) Extract the main factors related to ground subsidence near abandoned underground coal mine using PCA. Proceedings of the KSRS spring conference, pp. 301-304.

Choi, S.O., Kim, K.S., (2003) Ground stability analysis on the limestone region. Geosystem Engineering 6(2), pp. 33-39.

Choi, S.O., Kim, J., Choi, G., (2009) Application of fuzzy reasoning method for prediction of subsidence occurrences in abandoned mine area. Journal of Korean Society for Rock Mechanics 19(5), pp. 463-472.

Chun, B.S., Ryu, W.R., Sagong, M., Do, J.N., (2009) Indirect estimation of the rock deformation modulus based on polynomial and multiple regression analyses of the RMR system. International Journal of Rock Mechanics and Mining Sciences 46(3): pp. 649-658.

Dawson, E.M., Roth, W.H., Drescher A., (1999) Slope stability analysis by strength reduction. Geotechnique 49(6), pp. 835-840.

Dawson E., You, K., Park, Y., (2000) Strength-reduction stability analysis of rock slopes using the Hoek-Brown failure criterion. In: Labuz JF, Glaser SD, Dawson E, editors, Trends in rock mechanics, proceedings of sessions of Geo-Denver 2000, Denver, Colorado, August 2000. Geotechnical Special Publication No. 102, Reston, ASCE, Virginia, pp. 65-77.

Diez, R.R., Alvarez, J.T., (2000) Hypothesis of the multiple subsidence trough related to very steep and vertical coal seams and its prediction through profile functions. Geotechnical & Geological Engineering 18(4), pp. 289-311.

Fu, W., Liao, Y., (2010) Non-linear shear strength reduction technique in slope stability calculation. Computers and Geotechnics 37(3), pp. 288-298.

Griffiths, D.V., Lane, P.A., (1999) Slope stability analysis by finite elements. Geotechnique 49(3), pp. 387-403.

Hammah, R.E., Yacoub, T.E., Corkum B.C., Curran, J.H., (2005) The shear strength reduction method for the generalized Hoek-Brown criterion. In Alaska Rocks 2005, The 40th US Symposium on Rock Mechanics (USRMS). American Rock Mechanics Association.

Han, K., Cheon, D., Ryu, D., Park, S., (2007) Analysis of ground subsidence on Gyochon residential region of Muan City. Journal of Korean Society for Rock Mechanics 17(1), pp. 66-74.

Harrison, J.P., (2011) Mine subsidence. In: Darling, P. (ed) SME mining engineering handbook, 3rd edn. SME, pp. 627-644.

Huang, F., Zhang, D.B., Sun, Z.B., Jin, Q.Y., (2012) Upper bound solutions of stability factor of shallow tunnels in saturated soil based on strength reduction technique. Journal of Central South University 19, pp. 2008-2015.

ITASCA, (2011) Fast Lagrangian Analysis of Continua: Factor of Safety. Itasca Consulting Group Inc. Minneapolis, Minnesota, USA.

Jeon, B., Jeon, S., Kim, J., Kim, T.H., (2012) Numerical evaluation of affecting parameters of surface subsidence in abandoned mine areas. Geosystem Engineering 15(4), pp. 299-304.

Jeon, S., Jeon, B., (2014) Review on the prevention and reclamation of mining induced subsidence in abandoned mine areas in the Republic of Korea. Journal of the Korean Society of Mineral and Energy Resources Engineers 51(1), pp. 141-150.

Jung, Y.B., Kim, T.H., Song, W.K., Choi, G.S., Kwon, H.H., (2010) Development of mine subsidence hazard estimation method through the analysis of influential factors on subsidence. Journal of the Korean Society of Mineral and Energy Resources Engineers 47(3), pp. 324-338.

Jung, Y.B., Song, W.K., Cheon, D.S., Lee, D.K., Park, J.Y., (2014) Simple method for the identification of subsidence susceptibility above underground coal mines in Korea. Engineering Geology 178, pp. 121-131.

Keilich, W., Seedsman, R., Aziz, N.H., (2006) Numerical modelling of mining induced subsidence. In Coal Operators' Conference, pp. 313-326.

Kim, K.D., Lee, S., Oh, H.J., Choi, J.K., Won, J.S., (2006) Assessment of ground subsidence hazard near an abandoned underground coal mine using GIS. Environmental Geology 50(8), pp. 1183-1191.

KOSIS, (2015) Number of metal and non-metal operating mines by the annul sales scale. Available at http://kosis.kr.

Lee, S.J., Choi, S.O., (2011) A study on theoretical consdieration and numerical analysis according the dip angle of joint for volumetric expansion ratio of rock mass. Geosystem Engineering 14(1), pp. 1-8.

Lee, Y.S., Park, D.H., SunWoo, C., Kim, G.W., Kang, J.S., (2012) Numerical design approach to determining the dimension of large-scale underground mine structures. Journal of Korean Society for Rock Mechanics 22(2), pp. 120-129.

Lin, S., Whittaker, B.N., Reddish, D.J., (1992) Application of asymmetrical influence functions for subsidence prediction of gently inclined seam extractions. International journal of rock mechanics and mining sciences & geomechanics abstracts 29(5), pp. 479-490.

Lloyd, P.W., Mohammad, N., Reddish, D.J., (1997) Surface subsidence prediction techniques for UK coalfields-an innovative numerical modelling approach. In Proceeding of the 15th Mining Congress of Turkey, Ankara, May, pp. 111-124.

Martins, F.F., Miranda, T.F., (2012) Estimation of the rock deformation modulus and RMR based on Data Mining techniques. Geotechnical and Geological Engineering 30(4): pp. 787-801.

Malinowska, A., Hejmanowski, R., (2010) Building damage risk assessment on mining terrains in Poland with GIS application. International Journal of Rock Mechanics and Mining Sciences 47(2), pp. 238-245.

Matsui T, San K.C., (1992) Finite element slope stability analysis by shear strength reduction technique. Soils and Foundations 32(1), pp. 59-70.

Ministry of Environment, (2009) 18th-19th Session of the commission on sustainable development (CSD): National report. Available at https://sustainabledevelopment.un.org/intergovernmental/csd19.

MIRECO, (2006) Investigation report of Boryong and Woongchun province. Mine Reclamtion Corporation.

MIRECO, (2007) Yearbook of MIRECO Statistics. Mine Reclamation Corporation. Available at http://www.nanet.go.kr.

MIRECO, (2008a) Yearbook of MIRECO Statistics. Mine Reclamation Corporation. Available at http://www.nanet.go.kr.

MIRECO, (2008b) Investigation report of Mugeuk Mine areas. Mine Reclamation Corporation.

MIRECO, (2009) Yearbook of MIRECO Statistics. Mine Reclamation Corporation. Available at http://www.mireco.or.kr.

MIRECO, (2010) Yearbook of MIRECO Statistics. Mine Reclamation Corporation. Available at http://www.mireco.or.kr.

MIRECO, (2011) Yearbook of MIRECO Statistics. Mine Reclamtaion Corporation. Available at http://www.mireco.or.kr.

MIRECO, (2012a) Yearbook of MIRECO Statistics. Mine Reclamation Corporation. Available at http://www.mireco.or.kr.

MIRECO, (2012b) Investigation report of Wolmyung Mine areas. Mine Reclamation Corporation.

MIRECO, (2013) Yearbook of MIRECO Statistics. Mine Reclamation Corporation. Available at http://www.mireco.or.kr.

MIRECO, (2014) Yearbook of MIRECO Statistics. Mine Reclamation Corporation. Available at http://www.mireco.or.kr.

National Coal Board, (1975) Subsidence Engineer's Handbook, National Coal Board, London.

Ren, G., Reddish, D.J., Whittaker, B.N., (1987) Mining subsidence and displacement prediction using influence function methods. Mining Science and Technology 5(1), pp. 89-104.

Ren, G., Whittaker, B.N., Reddish, D.J., (1989) Mining subsidence and displacement prediction using influence function methods for steep seams. Mining Science and Technology 8(3), pp. 235-251.

Ren, G., Li, J., (2008). A study of angle of draw in mining subsidence using numerical modeling techniques. Electronic Journal of Geotechnical Engineering 13, pp. 1-14.

Ren, G., Li, J., Buckeridge, J., (2010) Calculation of mining subsidence and ground principal strains using generalised influence function method. Mining Technology 119(1), pp. 34-41.

Ren, G., Li, G., Kulessa, M., (2014) Application of a generalised influence function method for subsidence prediction in multi-seam longwall extraction. Geotechnical and Geological Engineering 32(4), pp. 1123-1131.

Ryu, D.W., Synn, J.H., Song, W.K., Kim, T.K., Park, J.Y., (2007) A study on the evaluation method of subsidence hazard by a diffusion equation and its application. Journal of Korean Society for Rock Mechanics 17(5), pp. 372-380.

Shahriar, K., Amoushahi, S., Arabzadeh, M., (2009) Prediction of surface subsidence due to inclined very shallow coal seam mining using FDM. In Coal Operators' Conference, pp. 130-139.

Sutherland, H.J., Munson, D.E., (1984) Prediction of subsidence using complementary influence functions. International Journal of Rock Mechanics and Mining Sciences & Geomechanics Abstracts 21(4), pp. 195-202.

Torano, J., Rodrıguez, R., Ramırez-Oyanguren, P., (2000) Probabilistic analysis of subsidence-induced strains at the surface above steep seam mining. International Journal of Rock Mechanics and Mining Sciences 37(7), pp. 1161-1167.

UN/International Strategy for Disaster Reduction. (2004). Living with risk: a global review of disaster reduction initiatives (Vol. 1). United Nations Publications.

Ugai, K., Leshchinsky. D., (1995) Three-dimensional limit equilibrium and finite element analysis: A comparison of results. Soils and Foundations 35(4), pp. 1-7.

Vyazmensky, A., Elmo, D., Stead, D., Rance, J., (2007) Combined finite-discrete element modelling of surface subsidence associated with block caving mining. In Proceedings of 1st Canada-US Rock Mechanics Symposium, pp. 467-475.

Vyazmensky, A., Elmo, D., Stead, D., (2010) Role of rock mass fabric and faulting in the development of block caving induced surface subsidence. Rock mechanics and rock engineering 43(5), pp. 533-556.

Whittaker, B.N., Reddish, D.J., (1989) Subsidence: occurrence, prediction and control. Elsevier 1989.

Xu, N., Kulatilake, P.H., Tian, H., Wu, X., Nan, Y., Wei, T., (2013) Surface subsidence prediction for the WUTONG mine using a 3-D finite difference method. Computers and Geotechnics 48, pp. 134-145.

Yang, X.L., Huang, F., (2009) Stability analysis of shallow tunnels subjected to seepage with strength reduction theory. Journal of Central South University of Technology 16, pp. 1001-1005.

Yao, X.L., Reddish, D.J., Whittaker, B.N., (1993) Non-linear finite element analysis of surface subsidence arising from inclined seam extraction. International Journal of Rock Mechanics and Mining Sciences & Geomechanics Abstracts 30(4), pp. 431-441.

Yi, L.U.O., Cheng, J.W., (2009) An influence function method based subsidence prediction program for longwall mining operations in inclined coal seams. Mining Science and Technology 19(5), pp. 592-598.

Zeinkiewicz, O.C., Humpheson, C., Lewis, R.W. (1975) Associated and non-associated visco-plasticity in soils mechanics. Geotechnique 25(4), pp. 671-689.

초 록

광산개발에 의해 발생되는 다양한 형태의 광해 중에서 지반침하는 사회적·경제적으로 큰 문제를 야기한다. 특히, 광산지역 지반침하는 그 발생 시기, 규모, 위치를 명확히 예측하기 어렵다는 특징이 있으며, 광산개발이 종료된 이후에도 지속적으로 발생하기 때문에 큰 위험요소로 작용하게 된다. 이러한 지반침하를 예측하기 위한 다양한 기법들은 유럽을 포함한 국외에서 수십 년간 꾸준히 연구되어 왔으나, 국내 광산지역의 복잡한 광체특성을 고려할 때, 이 기법들을 그대로 적용하기에는 한계가 있다. 한편, 국내 폐광지역에 대한 지반침하 방지 및 복구 사업을 수행함에 있어서, 한정된 예산을 효율적으로 집행하기 위해서는 지반침하 위험도를 평가할 수 있는 방법이 필요하다.

본 연구에서는 광산지역 지반침하에 대해서 그 위험도를 평가하고, 해당 지역에 대한 위험지도를 작성할 수 있는 기법을 개발하였다. 지반침하가 발생할 가능성을 안전율 개념을 도입하여 평가하였으며, 지반침하 위험지수를 정의하여 광산지역 전반에 걸친 위험수준을 정량적으로 분석하였다. 지반침하 위험지수를 산정하기 위해서 광산지역 지반침하에 영향을 미치는 다양한 요인 중, 채굴적 특성과 암반조건을 주요 영향인자로 선정하였으며, 수치해석 기법을 활용하여 각 영향인자가 지반침하에 미치는 영향을 정량적으로 평가하였다. 특히, 사면이나 지하구조물의 안정성 해석에 주로 사용되는 강도감소법을 지반침하 해석에 효과적으로 적용할 수 있었으며, 수치해석 결과를 바탕으로 각 영향인자와 안전율 사이의 관계를 비선형 회귀분석을 통해 분석하고, 지반침하 위험지수 계산을 위한 회귀모형식을 제안하였다. 개발된 기법의 현장 적용성을 검증하기 위해서 실제로 침하가 발생한 광산지역을 대상으로 지반침하 위험

도 분석을 수행하였다. 그 결과, 이 연구에서 개발된 기법으로 예측한 위험지역 내에 대부분의 침하지가 위치하는 것을 확인할 수 있었다. 최종적으로 개발된 기법을 지반침하 방지 및 복구 사업과 같은 실무에서 유용하게 활용될 수 있을 것으로 기대된다.

주요어: 광산지역 지반침하, 위험도 분석, 수치해석, FLAC2D, 강도감소법, 회귀분석

학 번: 2007-30285